REPUBLIQUE DU CAMEROUN
Paix-Travail-Patrie

UNIVERSITE DE YAOUNDE I

CENTRE DE RECHERCHE ET DE FORMATION DOCTORALE EN SCIENCES, TECHNOLOGIES ET GEOSCIENCES

UNITE DE RECHERCHE ET DE FORMATION DOCTORALE EN PHYSIQUES ET APPLICATIONS

B.P 812 Yaoundé
Email: crfd_stg@uy1.uninet.cm

REPUBLIC OF CAMEROON
Peace-Work-Fatherland

THE UNIVERSITY OF YAOUNDE I

POSTGRADUATE SCHOOL OF SCIENCES, TECHNOLOGY AND GEOSCIENCES

RESEARCH AND POSTGRADUATE TRAINING UNIT FOR PHYSICS AND APPLICATIONS

P.O. Box 812 Yaoundé
Email: crfd_stg@uy1.uninet.cm

Laboratoire de Mécanique, Matériaux et Structures

Laboratory of Mechanics, Materials and Structures

PHASE TRANSITIONS IN QUANTUM TUNNELING, EXACT STATISTICAL MECHANICS AND OSCILLONS IN ONE-DIMENSIONAL SYSTEMS WITH DEFORMABLE DOUBLE-WELL ENERGY LANDSCAPES

Thesis submitted in partial fulfillment of the requirements for the award of The degree of Doctor of Philosophy (Ph.D.) in Physics,

Specialty: **Fundamental Mechanics and Complex Systems**

By

NAHA NZOUPE Fernand

Registration Number: **10W1519**

Master of Science in Physics

Under the Supervision of

DIKANDE Alain Moise
Professor
University of Buea

TCHAWOUA Clément
Professor
University of Yaoundé I

2022

UNIVERSITÉ DE YAOUNDÉ
THE UNIVERSITY OF YAOUNDE I

FACULTÉ DES SCIENCES
FACULTY OF SCIENCES

DÉPARTEMENT DE PHYSIQUE
DEPARTMENT OF PHYSICS

ATTESTATION DE CORRECTION DE LA THÈSE DE DOCTORAT/Ph.D

Nous, Professeur **ZEKENG Serge Sylvain** et Professeur **ESSIMBI ZOBO Bernard**, respectivement Examinateur et Président du jury de la Thèse de Doctorat/PhD de Monsieur **NAHA NZOUPE Fernand**, Matricule **10W1519**, préparée sous la direction des Professeurs **DIKANDE Alain Moise** (Université de Buéa) et **TCHAWOUA Clément** (Université de Yaoundé 1), intitulée : « **PHASE TRANSITIONS IN QUANTUM TUNNELING , EXACT STATISTICAL MECHANICS AND OSCILLONS IN ONE-DIMENSIONAL SYSTEMS WITH DEFORMABLE DOUBLE-WELL ENERGY LANDSCAPES** », soutenue le Jeudi, **29 Juillet 2022**, en vue de l'obtention du grade de Docteur/PhD en Physique, Spécialité **Mécanique, Matériaux et Structures,** option **Mécanique Fondamentale et Systèmes Complexes** attestons que toutes les corrections demandées par le jury de soutenance ont été effectuées.

En foi de quoi, la présente attestation lui est délivrée pour servir et valoir ce que de droit.

Fait à Yaoundé, le 17 OCT 2022

Examinateur	Le Président du jury	Le Chef de Département de Physique
Pr. ZEKENG Serge Sylvain	Pr. ESSIMBI ZOBO Bernard	Pr. NDJAKA Jean-Marie

UNIVERSITE DE YAOUNDE I ★ FACULTE DES SCIENCES ★ DEPARTEMENT DE PHYSIQUE
Le Chef de Département

University of Yaoundé I

Faculty of Sciences

Department of Physics

Phase transitions in quantum tunneling, exact statistical mechanics and oscillons in one-dimensional systems with deformable double-well energy landscapes

Submitted and defended in Fulfillment of the Requirements for the Degree of Doctor of Philosophy/PhD in Physics

Option: Fundamental Mechanics and Complex Systems

By

NAHA NZOUPE Fernand

Registration number: 10W1519

Master in Physics

Director

Prof. DIKANDÉ Alain Moïse

Professor, University of Buea (Cameroon)

Supervisor

Prof. TCHAWOUA Clément

Professor, University of Yaoundé I (Cameroon)

Laboratory of Mechanics, Materials and Structures

Dedication

To almighty God and my family.

Acknowledgements

The accomplishment of this thesis would not have been possible without the assistance and the help of numerous individuals and institutions.

• First of all, I would like to express my deepest thankfulness to my supervisor, Professor **TCHAWOUA Clément**, for giving me the opportunity to complete successfully this thesis. His expertise, his vast knowledge in both nonequilibrium physics and coherent structures and his unique scientific feeling considerably shaped my current interest and experience in theoretical physics.

• A very special acknowledgment goes out to my director, Professor **DIKANDÉ Alain Moïse** for his guidance and help during the entire course of this work. His tremendous insight in physics and unreserved willingness to share his understanding of physics with others have made this project very enjoyable and instructive. I owe him a debt of gratitude and respect.

• I would also like to express my thanks to the President of the Jury, Professor **ESSIMBI ZOBO Bernard**, and to the members of the jury, Professors **ZEKENG Serge Sylvain**, **NGUE-NANG Jean Pierre** and Professor **BODO Bertrand**, who accepted to participate to my thesis defence.

• I would like to acknowledge Professor **NDJAKA Jean-Marie Bienvenu**, the head of Department of Physics at the Faculty of Science at the University of Yaoundé I, for receiving me in his Department.

• It would be very pleasing to recognize trade and constructive discussions combined with great moments of sharing with all the teachers of the Department of Physics in general and of the laboratory of Mechanics, Materials and Structures in particular. I have named Professor **KO-FANÉ Timoléon Crépin**, Professor **BOUETOU Thomas** and Dr. **WOULACHÉ Rosalie Laure**.

• I would also like to express my gratitude for the support of the members of the Laboratory of Research on Advanced Materials and Nonlinear Sciences (LARAMANS) of the University of Buea, in particular Professor **MOUKAM KAKMENI François** and Professor **MKAM TCHOUOBIAP Serge** for their guidance.

• Special thanks to Dr. **NDJOMATCHOUA Thomas Frank**, Dr. **DJOMO MBONG Thierry Landry Michel**, Dr. **TEMGOUA Diane Estelle**, Dr. **ISSOKOLO Rémi Jean Noumana**, Dr. **METSOBO Jules**, Dr. **KEPNANG PEBEU Maxime** , Dr. **WADOP NGOUONGO Yannick Joel**, Dr. **BITANG A ZIEM Cassidy**, **Mr. GNINZANLONG Carlos**, for the multitude exchanges and help.

• A deep gratitude goes to **Dr. ZANGA Dieudonné** for his great support during the period of completion of this thesis.

• I express my eternal gratefulness to my parents, Mr. **NZOUPE Jean Pierre** and Mrs. **DONGUE Régine**, without whose support and love throughout my entire life, I would not have started and finished this thesis.

• I also thank the permanent support provided by my dear and lovely wife Mrs. **ONONINO Emilienne**.

• I am feelingly grateful to members of my familly, for the crucial role they have played in my life through their love, patience and all the great moments that we have shared during this time.

• I cannot finish without thank the **International Center for Theoretical Physics** (ICTP), and the Laboratory of Research on Advanced Materials and Nonlinear Sciences (LARAMANS) that offered me participation to numerous schools and seminars which has contributed to improve my level in physics, allowing me to feel comfortable when treating my subject.

• My sincere thanks go to the official editors and referees of **Mathematical Methods in the Applied Sciences**, and **Modern Physics Letters A**, for their detailed review, constructive criticism and excellent advice during the preparation of my different publications.

• Thanks to all unmentioned persons who have contributed even a little to this work.

Contents

List of Figures

List of Tables

List of Abbreviations

DK: **D**ikandé-**K**ofané
DSHG: **D**ouble **S**in**H** **G**ordon
DW: **D**ouble-**W**ell
DWP: **D**ouble-**W**ell **P**otential
NKG : **N**onlinear **K**lein **G**ordon
RK4 : **F**ourth-order **R**unge-**K**utta
SHH: **S**onic-**H**edge**H**og

Abstract

In this thesis we study phase transitions in quantum tunneling, kink-antikink scattering-induced oscillons, and the exact statistical mechanics of bistable systems with deformable energy landscapes.

To start we examine the nature of the phase transition, characterized by a crossover from temperature-assisted tunneling to thermal activation across a potential barrier. This potential barrier is associated with a family of parametrized one-body double-well potentials, whose barrier height, position of the degenerate minima, and curvature of the barrier, can be varied as a function of a deformability parameter μ, and which reduces to the ϕ^4 potential as μ tends to zero. It is found that unlike bistable models involving the standard ϕ^4 field, for which the transition in quantum tunneling is known to be strictly of second-order, the parametrization of the double-well potential favors the second-order transition as well as a first-order transition, occurring above some universal critical value of the deformability parameter μ_c. This critical value turns out to be the same for all members of the family of generic potentials considered in this study. In particular, we find that systems with steep walls and flat barrier tops are relevant candidates for first-order transitions in quantum tunneling.

Next, by expressing the statistical-mechanical problem of the model with the use of the transfer-operator formalism, the corresponding classical partition function can be mapped onto a Schrödinger-like eigenvalue problem with a scattering potential corresponding to each member of the family of parametrized double-well potentials. The condition for exact integrability of the partition function is formulated in terms of a constraint between the thermodynamic temperature and the shape deformability parameter. For this condition, the exact eigenfunctions and energy eigenvalues of the transfer-operator eigenvalue problem are derived. The dependence of the ground states on the shape deformability parameter is highlighted.

Finally, kink scatterings are investigated for one particular member of the family of potentials, with a focus on the formation of long-lived low-amplitude almost harmonic oscillations of the scalar field around a vacuum, so-called oscillons. The particular deformable model considered is characterized by a double-well potential, for which the shape deformability parameter changes only the steepness of the potential walls, and hence the flatness of the barrier hump leaving unaffected the two degenerate minima and the barrier height. It is found that the variation of the deformability parameter promotes several additional vibrational modes in the kink-phonon scattering potential, leading to suppression of the two-bounce windows in kink-antikink scatterings and production of oscillons. Numerical results suggest that a curvature shape of the potential barrier characterized by a flat barrier hump is the leading factor for the production of oscillons in double-well systems.

Keywords: Bistable systems; instantons; kink-antikink collision; oscillons; quantum-classical transition; related classical field theories; quasi-exact solvability; deformable potentials.

Résumé

Dans cette thèse nous étudions la transition du regime de tunnel quantique au regime d'évasion classique, la formation de modes liés appelés oscillons lors de collisions kink-antikink, ainsi que la mécanique statistique exacte des systèmes bistables présentant des profils énergétiques déformables.

Pour commencer, nous examinons la nature de la transition de l'évasion d'une particule d'un puits de potentiel par tunnel quantique à une évasion purement classique caractérisée par un saut de barrière. Pour cette étude, nous considérons une classe de potentiels double-puits dont la hauteur de la barrière, la position des minima, et même la courbure de la barrière peut varier en fonction d'un paramètre de déformabilité μ, tout en admettant le potentiel ϕ^4 comme limite quand $\mu \to 0$. Nous montrons que contrairement aux modèles bistables faisant intervenir le champ ϕ^4 standard, pour lesquels la transition du régime de tunnel quantique au régime classique est strictement de second ordre, la paramétrisation de la classe de potentiels considérée favorise les transitions de second ordre et ensuite de premier ordre, survenant au-dessus d'une certaine valeur critique μ_c. De plus, cette valeur critique s'avère la même pour tous les cas de la classe de potentiels. En particulier, nous constatons que les potentiels avec des parois abruptes et un sommet de barrière plat sont des candidats ideaux pour les transitions quantique-classique de premier ordre.

Ensuite, en exprimant la mécanique statistique du modèle via le formalisme de l'opérateur de transfert, la fonction de partition classique correspondante se ramène à un problème aux valeurs propres du type Schrödinger, avec un potentiel de diffusion correspondant à chaque cas de la classe de potentiels. La condition d'intégrabilité exacte de la fonction de partition est alors formulée en termes d'une relation de contrainte entre la température thermodynamique et le paramètre de déformabilité. Pour cette condition, les expressions exactes des fonctions propres et des énergies propres des niveaux d'énergie fondamentales de l'opérateur de transfert sont obtenues.

Enfin, les collisions kink-antikink sont étudiées pour un cas particulier de la classe de potentiels bistables, en mettant l'accent sur la formation d'oscillations quasi-harmoniques de faibles amplitudes mais de longue durée de vie du champ scalaire, appelées oscillons. Le modèle déformable particulier considéré est caractérisé par un potentiel double-puits pour lequel le paramètre de déformabilité ne modifie que la pente des parois du potentiel. Autrement dit seule la planéité de la bosse de la barrière est affectée par la déformabilité, laissant intacts les deux minima dégénérés et la hauteur de la barrière de potentiel. Nous observons que la variation du paramètre de déformabilité favorise plusieurs modes vibrationnels supplémentaires dans le spectre de fréquences lié au potentiel de diffusion, conduisant à la suppression des fenêtres à

deux "rebonds" dans les diffusions kink-antikink et à la production d'oscillons. Les simulations numériques suggèrent que la planéité de la courbure de la barrière de potentiel est le principal facteur de production d'oscillons dans les systèmes à double-puits.

Mots clés: Systèmes bistables, instantons, collision kink-antikink; oscillons, transition quantique-classique, théories des champs classiques associées, résolubilité quasi-exacte, potentiels déformables.

General Introduction

In the absence of a comprehensive theoretical understanding of a physical system or the presence of extremely complex details, the use of different models is necessary for practical applications and further scientific investigation. In modeling physical systems, the notion of potential was introduced to address the energy landscape governing the interactions of the system elements with themselves and/or with their environment. In this respect, several potentials accounting for the stable configurations of the system were proposed. For example, the harmonic potential was used to model the mechanics of harmonic oscillators that, when displaced from its equilibrium position, experience a restoring force proportional to their displacement [**?**]; multistate potentials such as the sine-Gordon potential were used in the framework of the Frenkel-Kontorova model [**?**] to study nucleation in CMP [**?**]; and the double-well (DW) potentials that have been used in quantum theory of molecules as a crude model to describe the motion of a particle in the presence of two centers of force.

DW potentials (DWPs) are an important class of configurations which have been extensively used in many fields of physics and chemistry. Solutions of the Schrödinger equation with DWPs have found applications in the Bose-Einstein condensation [**?**], molecular systems [**?**], quantum tunneling [**?**, **?**], and so forth. For instance, the quantum theory of instantons [**?**] in bistable systems has been a fascinating topic that has attracted considerable interest. This theory possesses applications in quantum-mechanical models, particularly in the area of macroscopic spin systems. In spin systems, it is now known that at temperature closed to zero, decay rates of the metastable state in a DWP are determined by quantum tunneling processes whose dynamics are described by classical configurations such as vacuum bounces or periodic instantons [**?**]. but with increasing the temperature, thermal activation becomes more and more important, and beyond some critical or crossover temperature T_c becomes the decisive mechanism. It has been realized that this crossover can be regarded as a transition from quantum to classical behavior, which in turn can be looked at like a phase transition in, e.g., the thermodynamics of gases [**?**].

DWPs are also interesting given the fact that distinctive features of motion in a DWP model

are reflected in the properties of the low-lying quantum states of the system. So in most of the quantum mechanical problems the complete solvability i.e., the determination of all eigenfunctions from the Schrödinger equation is not important. Some renowed DWPs in the literature are the quartic potential [**?**], the sextic potential [**?**], the Manning potential [**?**], and the Razavy potential [**?**]. In addition, it has been found that with some special constraints on the parameters of these potentials, a finite part of the energy spectrum and corresponding eigenfunctions can be obtained as explicit expression in a closed form. In other words, these systems are quasi-exactly solvable (QES) [**?**, **?**, **?**, **?**, **?**]. DWPs in the framework of QES systems have received a great deal of attention. This is due to the pioneering work of Razavy, who proposed his well-known potential for describing the quantum theory of molecules [**?**]. QES systems can be studied by three main approaches: the analytical approach based on the Sommerfeld method [**?**], on the Bethe ansatz [**?**, **?**, **?**, **?**, **?**, **?**], and the Lie algebraic approach [**?**, **?**, **?**, **?**]. These techniques are of great importance because only a few number of problems in quantum mechanics can be solved exactly. Therefore, these approaches can be applied as accurate and efficient techniques to study and solve the new problems that arise in different areas of physics such as quantum field theory [**?**, **?**, **?**], condensed matter physics [**?**, **?**, **?**], and quantum cosmology [**?**, **?**, **?**, **?**, **?**, **?**]. It happens those areas, exact solutions are hard to obtain or are impossible to find. In the literature, DWPs have been studied by using various techniques such as the Wentzel Kramers Brillouin approximation [**?**, **?**], asymptotic iteration method [**?**], and the Wronskian method [**?**]. On the other hand, it is recognized that the tunnel splitting which is the differences between the adjacent energy levels characterises of the energy spectrum for the DWPs [**?**, **?**, **?**, **?**].

At last, a pertinent feature of DWP models is that they possess a suitable framework for the generation of some localized structures that have shown their importance in nonlinear physics. In low and high energy physics, these localized structures have been studied in several different contexts [**?**, **?**, **?**]. In high energy physics, in particular, nontrivial localized structures appear as kinks, vortices and monopoles in (1, 1), (2, 1) and (3, 1) spacetime dimensions, respectively [**?**]. In the simplest situation, kinks and antikinks appear in scalar field theories described by a single real scalar field. In nonintegrable scalar field theories like the so-called ϕ^4 model [**?**], the existence of kinks and antikinks motivates the study of their scattering, that may sometimes lead to surprisingly rich consequences. For instance, when the collision is analyzed as a function of the initial velocity of the two objects, a complicated structure appears [**?**]. The latter structure

is usually connected with the deformation of the field profile and the emission of radiation. However, for larger initial velocities a simple inelastic scattering occurs and the kink-antikink pair retreats from each other. In the richer case, with sufficiently small initial velocities, the kink and antikink capture one another, forming a trapped bion state that radiates continuously until being completely annihilated. An intriguing aspect of the collision is observed in particular in the ϕ^4 model [**?**, **?**, **?**]. Some windows of intermediate velocities, named two-bounce windows, are observed. In such windows, the scalar field at the center of mass bounces twice before the pair recedes to infinity. These windows appear in sequence with smaller thickness, accumulating in the border of the one-bounce region. The same effect was also verified for higher levels of bounce windows, leading to a fractal structure [**?**]. The study of collisions of kink and antikink has gained further attention recently, with the study of bistable polynomial models with one [**?**, **?**] and two or more [**?**, **?**, **?**] scalar fields, and of bistable nonpolynomial models [**?**, **?**, **?**].

In the early 90^s, Chudnovsky [**?**] discussed the general features of phase transition and the possibilities to observe them in bistable systems. Some years later in 1998, Liang *et al* [**?**] found that within the framework of the famous ϕ^4 model could be observed phase transitions only of the second order. In the same year, Habib *et al* [**?**] studied the classical thermodynamics of the double sinh-Gordon theory in $(1+1)$ dimensions. The model theory has a DWP being the hyperbolic analog of the double sine-Gordon theory [**?**]. They found that under some conditions on the potential parameters, the model holds the QES property allowing the exact formulation of the thermodynamics quantities at a discrete set of temperatures. We recall that the ϕ^4 model does not possess this property. Recently in 2018, Bazeia *et al* [**?**] considered the scattering of kinks of the sinh-deformed ϕ^4 model. In addition to the scattering outcomes already found to appear in the ϕ^4 model, the observed the formation of bound states of oscillons, depending on the initial velocity of colliding kinks. In 2020, Bazeia again with another team of researchers reconsidered the problem of kink scattering, now in the context of two parametrized ϕ^4 potentials [**?**]. After observation of the formation of oscillons, the author proposed the production of the later to be related to the energy of the kink traveling in the system.

From the above cited study, parametric DWPs modeling systems with deformable energy landscapes form a class of interest to address the issues of phase transition in quantum tunneling, the exact solvability for the statistical mechanic, and kink-antikink induced phenomena in bistable systems. Nevertheless, however easily manipulable a parametrized model may be, this

cannot constitute by itself a consistent argument to claim its usefulness with respect to an old one. Its advantage must reside rather on an analytical tractability allowing deep analysis of its dynamical, thermodynamical and other behavior relevant for experiments. Although some of the existing deformable DW potential admit analytical kink solutions, most will certainly remain in their infancy owing to the complexity which prevents one to go far in their theoretical treatments. Sometimes, numerical investigations of relevant aspects as the few mentioned above (i.e. the dynamics and thermodynamics) are carried out but results are not always satisfactory. More important, it is always difficult to appreciate the specific features of a model from simple numerical curves, last numerical results cannot help experimenters to proceed deeply, as for example to test the validity of a given model in a precise physical context. This thesis aims to address the issue of the exact solvability for the statistical mechanics, the kink scattering, and the quantum-classical transition in a particle escape from a potential well, considering one or several cases in a family of parametric bistable potential. This family permits to avoid the situation where the presence of numerous parameters or degree of freedom in other parametric bistable potentials forbids the analysis of a specific potential trend. Indeed, in our context there is a unique shape deformability parameter that can tune one or several potential behaviors, such as, varying only the barrier height, only the potential minima, both the barrier height and the potential minima, and varying only the curvature shape of the barrier leaving the barrier height and minima unchanged. Furthermore, the family of potentials admits the so-called ϕ^4 potential as a particular limit, allowing comparative analysis with theories in the context of the Ginzburg-Landau phenomenological potentials.

In the first chapter, we conducted a review around the theme of bistability. The chapter presents the concept of bistability in real systems, together with several problems to study from dynamics of physical systems modeled by DWPs, after presenting some of the latter potentials. The second chapter focuses on the mathematical modeling of the dynamics of the different models used to contextualize this thesis. The analytical and numerical techniques used for the investigations are presented with details in this chapter. The third chapter is devoted to the presentation of the key obtained results and their discussions. In fact, we show in this chapter that the shape of the potential is the justification for the possibility of the analytical tractability of several processes in DWPs. Particularly, the curvature shape of the barrier hump is a key element to determine the nature of phase transitions in quantum tunneling, but also to favor the generation

of oscillons in bistable systems.

The document ends with a general conclusion summarizing the main findings and provides future directions.

CHAPTER I

LITERATURE REVIEW

I.1 Introduction

In this chapter, we discuss some generalities on bistability in nature and some problems of interest in systems with a bistable energy landscape modeled by a double-well (DW) potential. This chapter is organized as follows: In Section **??**, without being exhaustive, we describe the existence of a bistable configuration in physical systems such as chemical and biological systems, mechanical systems, optical and electronic systems, and also the potential well description of bistability. The concept of soliton in bistable systems is discussed, followed by the presentation of some DW potentials. Some phenomenon and processes of interest, namely the jump phenomenon, the kink-scattering and the low-temperature statistical mechanics, related to the presence of several stable states in the system are briefly discussed in Section **??**. Section **??** gives the motivation as well as the problematic of this thesis which will be addressed in the next chapters. The chapter ends with a conclusion.

I.2 Concept of bistability in some real systems

I.2.1 Bistability

Bistability is a fundamental phenomenon in nature. Something that is bistable can be resting in either of two states. These rest states need not be symmetric with respect to stored energy. The defining characteristic of bistability is simply that two stable states are separated by a peak. In physics, for an ensemble of particles, the bistability comes from the fact that its free energy has three critical points. Two of them are minima and the last is a maximum. By mathematical arguments, the maximum must lie between the two minima. By default, the system state will be in either of the minima states, because that corresponds to the state of lowest energy. The maximum can be visualised as a barrier. A transition from one state of minimal free energy requires some form of activation energy to penetrate the barrier. After the barrier has been

reached, the system will relax into the next state of lowest energy again. The time it takes is usually attributed the relaxation time. There might be uncertainty as to which state will be the new one, but it is often well defined in the situation.

I.2.2 Bistability in chemical and biological systems

Bistability is key for understanding basic phenomena of cellular functioning, such as decision-making processes in cell cycle progression, cellular differentiation [**?**], and apoptosis [**?**]. It is also involved in loss of cellular homeostasis associated with early events in cancer onset and in prion diseases as well as in the origin of new species (speciation) [**?**].

Bistability can be generated by a positive feedback loop with an ultrasensitive regulatory step. Positive feedback loops, such as the simple X activates Y and Y activates X motif, essentially links output signals to their input signals and have been noted to be an important regulatory motif in cellular signal transduction because positive feedback loops can create switches with an all-or-nothing decision [**?**]. Some studies have shown that numerous biological systems, such as Xenopus oocyte maturation, mammalian calcium signal transduction, and polarity in budding yeast, incorporate temporal (slow and fast) positive feedback loops, or more than one feedback loop that occurs at different times [**?**, **?**]. Having two different temporal positive feedback loops or "dual-time switches" allows for (a) increased regulation: two switches that have independent changeable activation and deactivation times; and (b) linked feedback loops on multiple timescales that can filter noise [**?**].

Bistability can also arise in a biochemical system only for a particular range of parameter values, where the parameter can often be interpreted as the strength of the feedback. In several typical examples, the system has only one stable fixed point at low values of the parameter. Yet saddle-node bifurcation gives rise to a pair of new fixed points emerging, one stable and the other unstable, at a critical value of the parameter. The unstable solution can then form another saddle-node bifurcation with the initial stable solution at a higher value of the parameter, leaving only the higher fixed solution. Thus, at values of the parameter between the two critical values, the system has two stable solutions.

A prime example of bistability in biological systems is that of Sonic hedgehog (SHH), a secreted signaling molecule, which plays a critical role in tissue development. SHH functions in diverse processes in tissue development, including patterning limb bud tissue differentiation. The SHH

signaling network behaves as a bistable switch, allowing the cell to abruptly switch states at precise SHH concentrations. *gli1* and *gli2* transcription is activated by SHH, and their gene products act as transcriptional activators for their own expression and for targets downstream of SHH signaling [**?**]. Simultaneously, the SHH signaling network is controlled by a negative feedback loop wherein the *Gli* transcription factors activate the enhanced transcription of a repressor. This signaling network illustrates the simultaneous positive and negative feedback loops whose exquisite sensitivity helps create a bistable switch [**?**].

Bistability is often accompanied by hysteresis. On a population level, if many realisations of a bistable system are considered (e.g. many bistable cells (speciation) [**?**]), one typically observes bimodal distributions. In an ensemble average over the population, the result may simply look like a smooth transition, thus showing the value of single-cell resolution [**?**, **?**]. Bistability can be modified to be more robust and to tolerate significant changes in concentrations of reactants, while still maintaining its "switch-like" character. Feedback on both the activator of a system and inhibitor make the system able to tolerate a wide range of concentrations. An example of this in cell biology is that an activated Cyclin Dependent Kinase 1 will activate its activator *Cdc25* while at the same time inactivating its inactivator, *Wee1*, thus allowing for progression of a cell into mitosis. Without this double feedback, the system would still be bistable, but would not be able to tolerate such a wide range of concentrations [**?**].

I.2.3 Bistability in mechanical systems

Bistability as applied in the design of mechanical systems is more commonly said to be "over centered", that is, work is done on the system to move it just past the peak, at which point the mechanism goes "over center" to its secondary stable position. The result is a toggle-type action- work applied to the system below a threshold sufficient to send it 'over center' results in no change to the mechanism's state.

Springs are a common method of achieving an "over centre" action. A spring attached to a simple two position ratchet-type mechanism can create a button or plunger that is clicked or toggled between two mechanical states. Many ballpoint and rollerball retractable pens employ this type of bistable mechanism.

An even more common example of an over-center device is an ordinary electric wall switch. These switches are often designed to snap firmly into the "on" or "off" position once the toggle

handle has been moved a certain distance past the center-point.

Several categories of bistable mechanisms coexist. For example, we can cite the multi-piece bistable mechanisms whose bistability comes from the use of an assembly of elements such that there are two stable domains (each domain being generally obtained by the use of a spring) separated by a configuration jump. A tool using this type of mechanism is the pen with retractable mine. Another category uses a plate mechanism with a prestressing. This category covers extremely common mechanisms, for example, there is the hair clip, still qualified as a "clic-clac" bar, so the Deformation illustrates the existence of two stable positions separated by a fail-over. A third category uses anisotropic plates, or preformed plates , which make it possible to overcome the pre-constraint of the previous mechanisms. We can then create 3D bistable plates. The best known example is certainly the trouser clamp. This type of structures can be used to modify structures [**?**]. It is also planning to use them for rollable and unfoldable structures, ranging from light aircraft wings to laptop screens [**?**].

I.2.4 Bistability in optical systems

In optics, optical bistability [**?**, **?**] is an attribute of certain optical devices where two resonant transmissions states are possible and stable, dependent on the input. Optical devices with a feedback mechanism, e.g. a laser, provide two methods of achieving bistability. In the first method *Absorptive bistability* utilizes an absorber to block light inversely dependent on the intensity of the source light. The first bistable state resides at a given intensity where no absorber is used. The second state resides at the point where the light intensity overcomes the absorber's ability to block light. However in the second method, *Refractive bistability* utilizes an optical mechanism that changes its refractive index inversely dependent on the intensity of the source light. The first bistable state resides at a given intensity where no optical mechanism is used. The second state resides at the point where a certain light intensity causes the light to resonate to the corresponding refractive index. The optical bistability effect is caused by nonlinear atom-field interaction and feedback effect of mirror. Important cases that might be regarded are atomic detuning, cooperating factor, and cavity mistuning. Applications of this phenomenon include its use in optical transmitters, memory elements and pulse shapers.

When the feedback mechanism is provided by an internal procedure (not by an external entity like the mirror within the Interferometers), the latter will be known as intrinsic optical bistability

[**?**]. This process can be seen in nonlinear media containing the nanoparticles through which the effect of surface plasmon resonance can potentially occur [**?**].

I.2.5 Bistability in electronics

A Bistable is a digital device that has two inputs and a digital output. The SET input makes the output Logic 1 (HIGH) and the output will stay in this state until forced to change. The RESET input makes the output Logic 0 (LOW) and the output will also stay in this state until forced to change. The output of a Bistable circuit is stable in both states - it can remain as either Logic 1 or Logic 0 indefinitely until either the SET or RESET initiate a change of state. The name means that the circuit has two stable states.

The terms Bistable, Latch and Flip-Flop are all used interchangeably to describe Bistable circuits. However, each of these terms does have a specific meaning and care must be taken to understand what circuits are actually being described by each of the different terms [**?**, **?**].

I.3 Potential-well description of bistability

Bistability can be viewed from the point of view of a potential well. For example, consider a circular rubber diaphragm supported around its circumference. Its own weight will cause the center spot to be the lowest. Place a marble in that potential minimum. Now place a hook in the diaphragm some distance from the minimum. By adding weights to that hook, one pulls the diaphragm down further and further until the marble rolls from the center to the new absolute minimum. Clearly a hysteresis occurs, i.e., removing an infinitesimal part of the weight does not cause the marble to return. One must remove weights until it is all "down hill" from the new minimum to the original one. If noise is introduced by shaking the diaphragm or using a jumpy marble, state switching back and forth can occur. This fluctuation switching works best if the two minima have the same depth and the barrier between them is low relative to the noise.

Lugiato and Bonifacio [**?**] have given a nice potential-well description of bistability. Let x be a quantity observed as parameter y is externally varied, resulting in the hysteresis cycle shown in Fig. **??**a For any given value of y there is a suitable stationary probability distribution function $P_{st}(x)$, typically the solution of a master or Fokker-Planck equation. The quantity

$$V(x) \equiv -ln[P_{st}(x)/P_{st}(0)] \tag{1}$$

plays the role of a generalized free energy. Fig. **??**b shows qualitatively the shape of $P_{st}(x)$ and $V(x)$ for some values of y . For $y = y_1$, $P_{st}(x)$ has only one peak centered at $x = x_1$; correspondingly, $V(x)$ has a single minimum at $x = x_1$ In the bistable regime ($y = y_2, y_c$, or y_3), $P_{st}(x)$ has two peaks and $V(x)$ two minima. A minimum in $V(x)$ above the absolute minimum can be thought of as a metastable state. In Fig. **??**a the upper branch between $y_\downarrow$ and y_c and the lower branch between y_c and $y_\uparrow$ are metastable states. A large fluctuation can make the "particle" tunnel from a metastable state to the ground state (and vice versa).

In the case of studies of proton transfer processes in hydrogen-bonded systems, for example in ice,water or proteins, it is usual to consider one-dimensional chains, so-called BernalFowler filaments [**?**, **?**]. In the normal state of a chain each proton is linked to a heavy ion (or oxygen atom in ice) by a covalent bond in one case, or a hydrogen bond in the other. Therefore, there are two kinds of arrangements of hydrogen bonded states in these systems, namely the type $XH\cdots XH\cdots XH\cdots XH\cdots XH$ and the type $HX\cdots HX\cdots HX\cdots HX\cdots HX$. Obviously the two states should have the same energy. In such a case it is accepted that the potential energy of the proton should have the form of a double well with two minima corresponding to the two equilibrium positions of a proton between two neighbouring heavy ions (or oxygen atoms) as shown in Fig. **??**. The barrier which separates them has a height which is in general of the order of the oscillation energy in a covalent bond XH and is approximately 20 times larger than that in a hydrogen bond. In the usual case, the protons in the hydrogen bonds are subject to harmonic vibration with small amplitudes about their equilibrium positions.

Brauman advocated the idea of a DW potential to describe the various stages during a gas phase S_N2 reaction, Fig. **?? [?]**. Passage over the central barrier is essential, but the reaction kinetics is strongly dependent on the detailed balance of the rates of the formation and dissociation of the reactant complex ($[Y\cdots RX]^-$), the rate of passing the central barrier ($[Y\cdots R\cdots X]^-$) thereby forming the product complex ($[Y\cdots R\cdots X]^-$) and the rate of dissociation of the product complex into the final products also taking the possibility of recrossing the barrier back to the reactant complex into account. Thus, the overall reaction rate will depend on the topographic features of the potential energy surface, as well as the relative orientation and internal and translational energy of the reactants.

In the spintronics of a molecule made up of magnetic atoms, its spin results from interactions between the different spins of the atoms. At low temperature, the spins of the different atoms

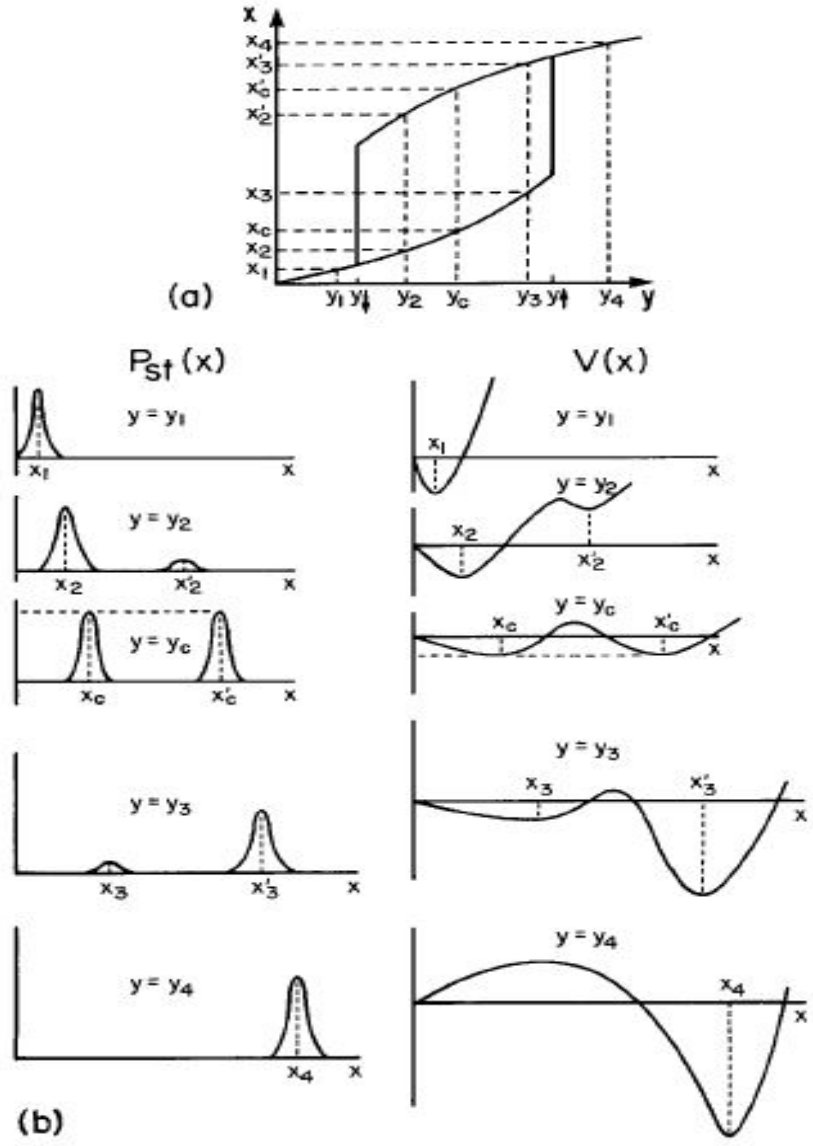

Figure 1: (a) Hysteresis cycle of the observed quantity x versus the external parameter y. (b) Qualitative shape of the stationary probability distribution $P_{st}(x)$ and of the generalized free energy $V(x)$ for the values of y indicated in (a). Figure taken from Lugiato and Bonifacio (1978) [**?**].

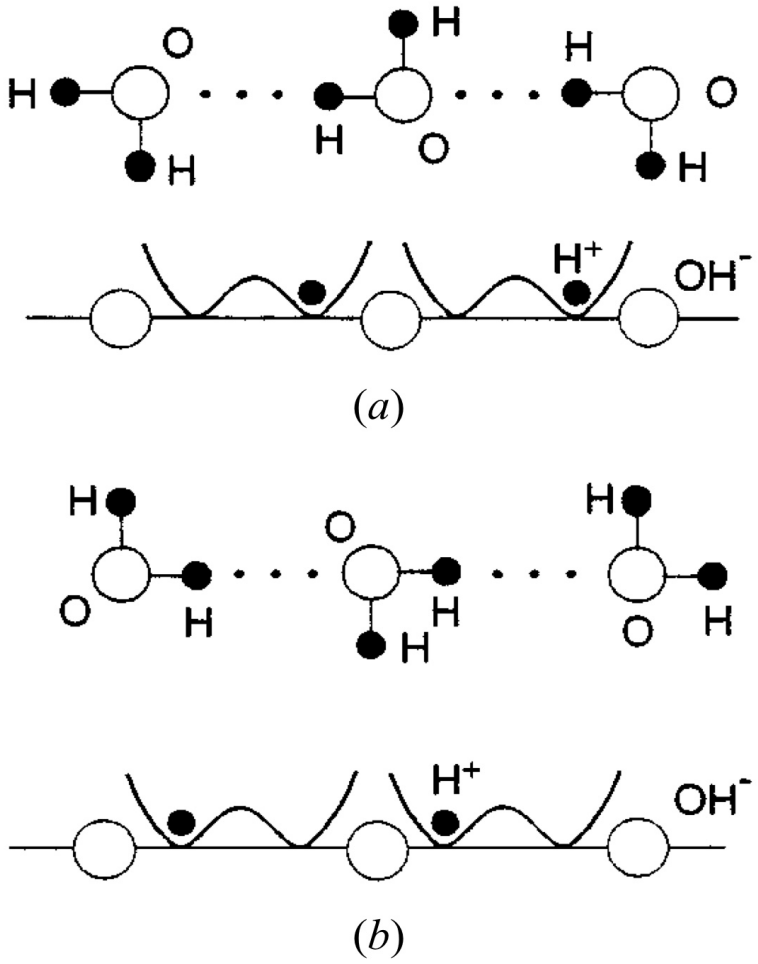

Figure 2: The double-well potential in the hydrogen-bounded system with H^+ in one well (a) or the other (b) of the potential.

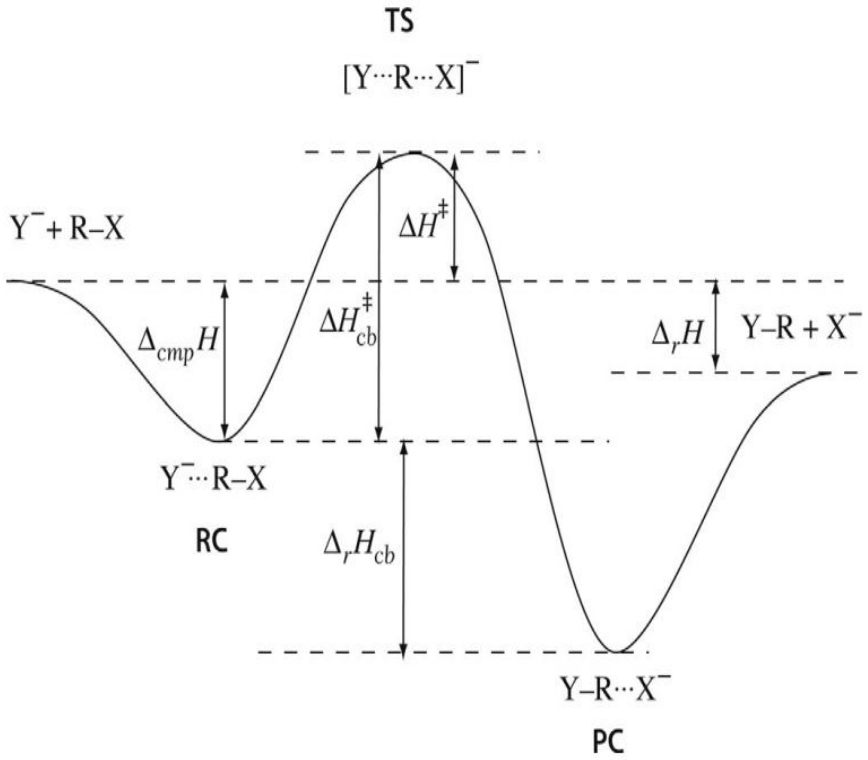

Figure 3: Characteristic double-well potential for a general nucleophilic substitution reaction in the gas phase. The local maximum corresponding to the transition state (TS), while the two minima (wells) are the reactant complex (RC) and product complex (PC). The abbreviation cb stands for central barrier. The diagram describes the energetics in terms of the enthalpy (H) but equivalent descriptions in terms of the Gibbs energy (G) and the energy (E) apply. Figure extracted from Ref. [**?**]

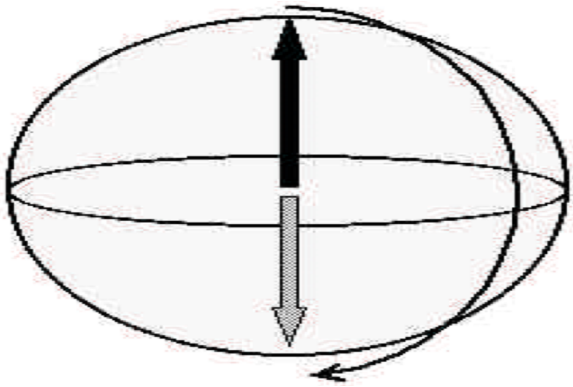

Figure 4: Reversal of a spin. This can be seen as a rotation of the vector between an angle $\theta = 0$ (spin up) and $\theta = \pi$ (spin down), the outside of the vector moving on sphere.

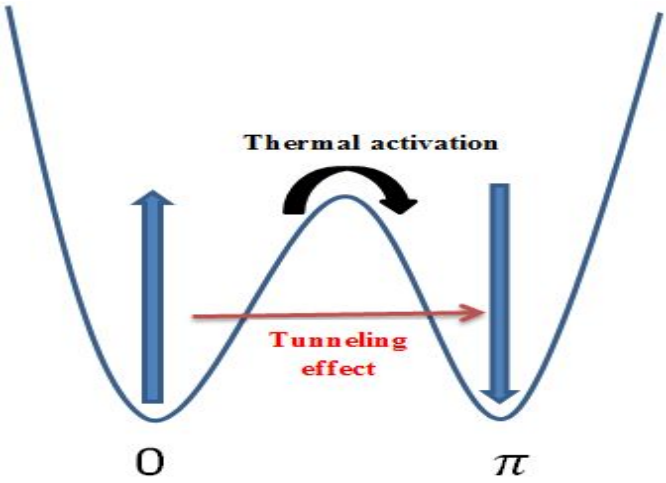

Figure 5: Reversal of a spin with passage of a particle through a potential barrier. The spin can pass over the barrier by thermal activation or through the barrier by tunneling.

are blocked by these interactions and the molecule appears to have a well-defined spin. This disappearance of the internal degrees of freedom constitutes the concept of giant spin to which we will come back in the next chapter. This giant spin is linked to an anisotropy. This can come from internal interactions but also from the specific anisotropy of the magnetic atoms constituting the molecule. In the case of a uniaxial anisotropy, the spin therefore has a privileged direction which minimizes its energy, the direction of easy magnetization. The reversal of this spin can be seen as a rotation of the vector between an angle $\theta = 0$ (spin up) and $\theta = \pi$ (spin down), the exterior of the vector moving on a sphere (see Fig. **??**). In this case, the spin must have enough energy to come out of the easy direction of magnetization. By identifying this problem with that of a particle, we can consider that the spin must cross a potential barrier, to go from the upward spin position to the downward spin position, as shown in Fig. **??**. The spin then has two solutions

to turn around: either pass over the potential barrier by thermal activation, for it this amounts to having an energy greater than the height of the barrier; or pass through this barrier by tunnel effect, as shown in Fig. **??**.

I.4 Solitons in bistable sytems

The history of solitary waves or solitons is unique. The first scientific observation of the solitary wave was made by Russell [**?**] in 1834 on the water surface. One of the first mathematical equations describing solitary waves was formulated in 1895. And only in 1965 were solitary waves fully understood! Moreover, many phenomena which were well known before 1965 turned out to be solitons. Only after 1965 was it realized that solitary waves on the water surface, nerve pulse, vortices, tornados and many others belong to the same category: they are all solitons. That is not all, the most striking property of solitons is that they behave like particles.

Solitary waves or solitons cannot be described by using linear equations. Unlike ordinary waves which represent a spatial periodical repetition of elevations and hollows on a water surface, or condensations and rarefactions of a density, or deviations from a mean value of various physical quantities, solitons are single elevations, such as thickenings etc., which propagate as a unique entity with a given velocity and preserve their properties throughout their propagation. The existence of solitons is a consequence of the balance between nonlinearity and dispersion. Thus, their transformation and motion are described by nonlinear equations of mathematical physics.

Mathematically, there is a difference between ”solitons” and ”solitary waves”. Solitons are localized solutions of integrable equations, while solitary waves are localized solutions of non-integrable equations. Moreover, solitary waves are generally composed of a large global maximun and several subsidiary local maxima. Another characteristic feature of solitons is that they are solitary waves that are not deformed after collision with other solitons. Thus the variety of solitary waves is much wider than the variety of the ”true” solitons. In fluid mechanical systems, solitary waves differentiate form solitons, for the former are interactive and dissipative [**?**]. Some solitary waves, for example, vortices and tornados are hard to consider as waves. For this reason, they are sometimes called soliton-like excitations. To avoid this bulky expression the term soliton is often used in all cases. This is not dangerous when talking about general properties of soliton-like excitations.

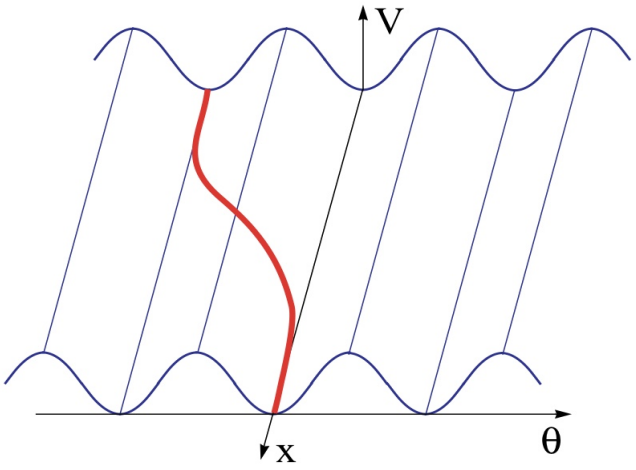

Figure 6: Sketch of a potential with infinite number of equilibrium states such as the sinusoidal potential. The solid curve shows the trajectory of the kink soliton which can be considered as a domain wall between two degenerate energy minima. Figure extracted from Ref. [**?**]

A classification of solitons divides them into two distinct groups: topological and nontopological solitons [**?**]. The main difference between these groups is the fact that the topological solitons have their amplitude independent of their velocity. Also, topological solitons have antisolitons which are analogous to antiparticles. In contrast for nontopological solitons, there are no antisolitons. A nonlinear equation can admit as solution solitons of only one type, never both. The most elementary topological soliton is the kink soliton [**?**, **?**]. The existence of kinks depends on there being multiple equilibrium states (potential minima). So, systems modeled by bistable potentials provide a favorable ground for the generation of kinks. A kink joints two successive potential vacua. It can be considered as a domain wall between two degenerate minima as shown in Fig. **??**, and also be looked up as an excitation which interpolates between these minima. The kink is mathematically obtained in bistable potentials by applying finite energy boundary conditions, and is constructed as a solution with a $tanh$-like shape (see Fig. **??**a). Most of its energy, having the $sech^2$ shape (see Fig. **??**a), is located in its core (in the middle of the kink). Consequently, the soliton is a localized packet of energy.

On the contrary of the case of a potential with more that two equilibrium states, in the DW potential a kink cannot be followed by another kink. Kink-kink configurations are not compatible with finite energy boundary conditions [**?**]. However a kink can be followed by an antikink, which connects the two potential wells, as shown in Fig. **??**. The kink-antikink pair is then considered as a bound state, often called *breather* or *bion* (meaning a "living particle").

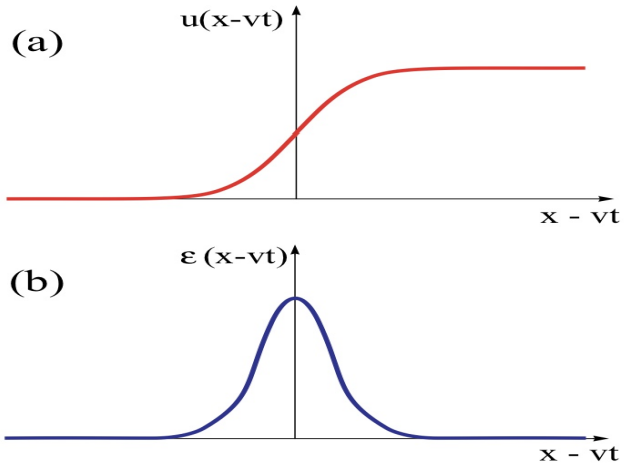

Figure 7: Schematic plots of (a) a kink soliton solution, and (b) the energy density of the kink soliton. Figure extracted from Ref. [**?**]

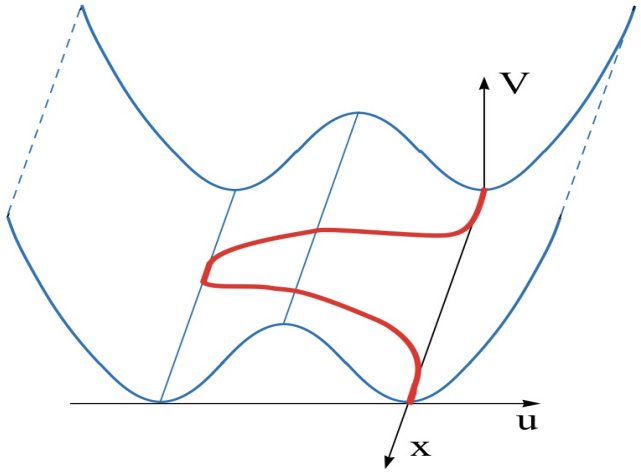

Figure 8: Sketch of a DW potential. The solid curve shows the trajectory of the kink-antikink solution. Figure extracted from Ref. [**?**]

I.5 Examples of some bistable potentials

To remain in the scope of this thesis, our focus is on the case where the DW configuration of the system is symmetric.

From a theoretical viewpoint, every one-dimensional (1D) nonlinear system can be modelled by a chain of particles (atoms, molecules, ions, electric cells, etc.) interacting via springs (site-to-site couplings) and lying on the background of a substrate (on-site coupling). Simple as it sounds, such a view, however, has several advantages among which is the fact that both the dispersion and the nonlinearity are accounted for (through site-to-site and on-site couplings, respectively). Furthermore, it provides a relatively easily tractable dynamical problem which would certainly be unsolved if taken as a whole. While the spring is often assumed linear, the substrate potential is rather always nonlinear and mostly of multiple-well type. Due to the variety of physical systems, several on-site potential have been proposed to enhance the knowledge of the complexity behind nonlinear processes. It should be known that one basic bistable potential model is at the root of all others, namely the Ginzburg-Landau phenomenological ϕ^4 potentials [**?**, **?**] .

Taking the variable x to be capturing the displacement of a particle in the chain from its equilibrium position, the general mathematical formulation for the the so-called ϕ^4 potentials was given as

$$V_4(x) = -\frac{A}{2}x^2 + \frac{B}{4}x^4, \quad A > 0, \text{and } B > 0. \tag{2}$$

The Landau phenomenology was found to be a powerful method with which to test the validity of the model for ferroelectric transitions. The model was constructed around the idea of a 1D lattice made of interacting dipoles which originally occupy the same side, each in one of the wells of a double-minimum substrate. Thus the transition will take place when all dipoles are in the opposite side into the next potential well, over a potential barrier. Some decades ago, the solutions of the Schödinger equation with bistable potentials built around the idea of the Landau phenomenology have applications in the classical theory of diffusion in a bistable field [**?**], and also in the quantum theory of diffusion [**?**]. However, only a few of the models discussed in literature were found to be exactly soluble. The examples most often cited are the double square-well [**?**], the double oscillator [**?**], the two square-wells separated by a delta function [**?**], and the Manning potential [**?**]. For these potentials the Schödinger equation is soluble for all eigenvalues. But in most of the problems the complete solvability is not important, since the

distinctive features of the motion in a DW potential are reflected in the properties of the low-lying quantum states of the system.

An interesting example of a bistable potential for which the wave equation is partially soluble (i.e., few of the lowest eigenfunctions are known analytically) was found as the sum of two hyperbolic cosine functions, and the past decades have witnessed the rise of several new types of quasi-exactly solvable one-dimensional DW potentials have been proposed [**?**, **?**, **?**, **?**, **?**, **?**, **?**]. Their most important property is that the Schrödinger equation for a particle moving in these potentials can be solved exactly for certain values of the potential parameters. It is well-known that the ϕ^4 potential does not have this property.

At first, Razavy [**?**] proposed a model for diffusion in a bistable potential field with a DW formulation as:

$$V_R(x) = \left[\frac{1}{8}\xi^2 cosh4\beta x - (n+1)\xi cosh2\beta x - \frac{1}{8}\xi^2\right] \tag{3}$$

The potential depends on two parameters, n and ξ, which determine the mono- or bi-stability of the model and also the escape frequency of the Brownian particle across the barrier. And, for any integer n, the wave function for the $(n+1)$ lowest states can be found analytically.

Matsushita and Matsubara [**?**] and Lawrence and Robertson [**?**, **?**] proposed a description of a proton in a hydrogen bond with the potential

$$V_L(x) = V_0\left[\frac{1}{2}A^2 cosh2ax - 2Acoshax\right], \tag{4}$$

V_0, A and a are parameters defined by the system. This potential has resulted from the idea of a sum of two Morse potentials [**?**], oriented in opposite (back-to-back) and centered at different points. Various estimations (see e.g. [**?**, **?**]) show that this potential is suitable for the description of the motion of a proton in a hydrogen bond.

A similar potential

$$V_Z(x) = \frac{\hbar^2 a^2}{2m}\left[\frac{1}{4}B^2 sinh^2 ax - B(S+\frac{1}{2})coshax\right] \tag{5}$$

was derived by Zaslavsky and Ulyanov [**?**] and used, in the latter work, for the investigations on the quantum mechanics of spin systems (uniaxial ferromagnets). The most comprehensive discussion of the properties of this potential potential was a decade later given by these authors,

using coherent states representation [**?**]. Special attention was paid to the question of quantum tunneling considered in terms of the WentzelKramersBrillouin approximation.

It is evident that the potentials proposed by Razavy, Matsushita and Matsubara, and Zaslavsky and Ulyanov inspired what was later called the symmetric double-Morse potential proposed in literature by Konwent [**?**],

$$V_{dM}(x) = V_0(Acoshax - 1)^2, \tag{6}$$

V_0, A,a being parameters depending on the system.

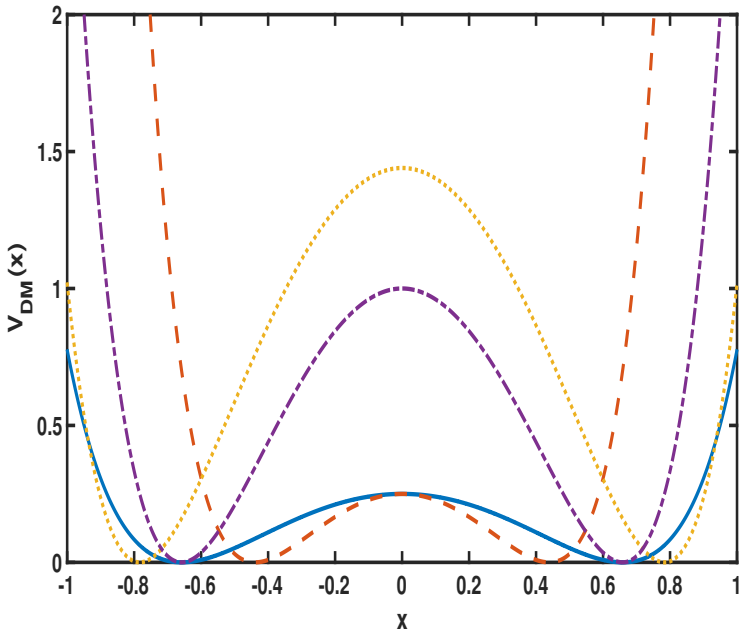

Figure 9: Sketch of for the double-Morse potential for some values of its parameters: $V_0 = 1.0$, $A = 0.5$, $a = 2.0$ (Solid line), $V_0 = 1.0$, $A = 0.5$, $a = 3.0$ (Dashed line), $V_0 = 4.0$, $A = 0.4$, $a = 2.0$ (Dash-dotted line), and $V_0 = 4.0$, $A = 0.5$, $a = 2.0$ (Dotted line)

This general form for the double-Morse potential presents the advantage of accounting for the variation its shape while varying one or several of its parameter which can in that case be considered as control parameters. Indeed the potential possesses several shape depending of the values of its parameters (see Fig. **??**). Potential with this feature as denoted in litterature as "deformable potential", as they can be used as models to analyze a specific variation in the system configuration. In the early $90^{'s}$, Dikandé and Kofané focuses their interest on the dynamics of deformable systems and proposed a class of parametrized DW potentials to model systems whose dynamics cannot be studied efficiently within the standard approach of rigid lattices with

the Landau phenomenology. They proposed the general expression for this class of potentials to be:

$$V(x,\mu) = \frac{a}{8}\left[\left(\frac{sinh(\alpha x)}{\mu}\right)^2 - 1\right]^2, \quad \mu \neq 0, \quad a = a_0 q^2 / \left(sinh^{-1}\mu\right)^2, \tag{7}$$

where a_0 is a positive constant, μ the parameter tuning the deformability of the system, and α and q being two functions of μ whose the mathematical formulation depends on the deformability feature to be addressed.

Three cases for the Dikandé and Kofané (DK) class of potentials have been proposed in :

- The first member is assumed to be a DW potential whose degenerate minima vary, leaving unchanged the barrier height. α and q are defined as [**?**]:

$$q = sinh^{-1}\mu, \quad \alpha = \mu. \tag{8}$$

  The potential was proposed to conveniently describe the dipolar character and bistability of the hydrogen bond when discussing high protonic mobility in filamentary crystals, or nonlinear collective phenomena in biological macromolecules, in ice, or transport of energy across biological cellular membrane. For example it has been found experimentally that in KH_2PO_4(KDP), and the isomorphic substances for instance, the proton replacement by deuterium (the deuteration) causes a drastic shift in the equilibrium positions of the two surrounding PO_4^{2-} groups on the $H-$bonds. These shifts are attributed to changes in the geometric configuration of ionic bonds upon isotopic substitutions [**?**]. Thus, the potential is a good candidate to investigate the dielectric behavior of many ferroelectrics and antiferroelectrics when the phase transition in these substances is caused by order-disorder arrangements of protons.

- For the second case of the class of potentials, only the height of the potential barrier is varied, but not the position of degenerate minima [**?**]:

$$q = \mu/(1+\mu^2)^{1/2}, \quad \alpha = sinh^{-1}\mu. \tag{9}$$

  This potential was proposed in the context of the influence of the shape deformability on the phonon response to nonlinear excitations, and was also found to be a good attempt to describe changes in the hydrogen bonds. Furthermore, the effect of the potential parameter

in this case is similar to that of the applied field in the spin systems [**?**]. It has recently been found that this potential could appear as a good controller of chaos, notably for energy harvesting, as with the control of the barrier height the deformable DW potential may make an originally non-chaotic system chaotic, or suppress irregular behavior and vice-versa [**?**]. In condensed matter physics, the phenomenon of spin tunneling has attracted considerable attention not only in view of the possible experimental test of the macroscopic quantum tunneling, but also because the spin system with an applied field provides various double-well-like potential shapes and the potential barrier height varies with the applied field [**?**]. The present potential case is of interest itself in condensed matter physics. The effect of the potential parameter is similar to that of the applied field in spin systems.

- The third member varies more general manners, i.e. the height of its barrier and positions of its degenerate minima simultaneously change. Here, α and q are defined as [**?**]:

$$q = 1, \quad \alpha = (1+\mu^2)^{-1/2} sinh^{-1}\mu. \tag{10}$$

This third member of the DK class of potentials was proposed as an attempt to combine the features of the previous two cases. This behavior has a similarity with the double-Morse potential previously presented in this section, and intends to address the same applications with the advantage of the possibility to tune the deformability of the system with a single parameter .

Very recently, we have introduced a new case of the DK hierarchy in literature. the functions α and q have been defined as [**?**, **?**]:

$$q = sinh^{-1}\mu, \quad \alpha = sinh^{-1}\mu. \tag{11}$$

In this last case, the potential barrier and the positions of the degenerate minima are kept fixed. However a variation of μ changes the steepness of the barrier walls, and consequently the curvature shape and flatness of the barrier. Quite instructively, this variation of the barrier shape observed is consistent with the experimentally observed rates and experimentally observed kinetic isotope effects, when studying vibrationally assisted hydrogen tunneling in enzyme-catalyzed

reactions [**?**]. Indeed in these biophysical processes, the effect of the enzyme-catalyzed reaction becoming less efficient results in a progressive broadening of the narrowest part of the barrier by steepening its walls, with the shoulder shape of the barrier peak becoming increasingly less pronounced. Such a deformable behavior from the potential has been the justification of the high assisted hydrogen tunneling rates and high kinetic isotope effects in enzyme-catalyzed reactions with trypamine as substrate. Also, for significant values of μ the DWP displays features similar to the double-Morse potential, used to describe proton motion in the hydrogen bond $O-H\cdots O$ in KDP ferroelectrics [**?**]. In these specific materials [**?**], the one-body proton potential rises steeply in the vicinity of the oxygen atoms, with a gentler slope at the sides of the potential barrier. This new parametric DWP can thus reproduce some of the double-Morse potential peculiar features, namely by taking the proton displacement u from the center of the hydrogen bond and using μ to mimic the rate of variation of the $O-O$ bond distance. At last, the deformation addressed by this model is consistent with the theory of hilltop inflation which has proven to be a very successful paradigm in early universe cosmology [**?**, **?**].

Unlike many existing parametrized DW models [**?**, **?**, **?**], the DK hierarchy of potentials forms a complete set covering covering a broad range of physical contexts, as it can model relevant deformation of the system by tuning a single parameter, herein referred as a shape parameter. All the cases of this hierachy possess one particular trend in common, in the limit $\mu \to 0$ they reduce to the so-calledϕ^4 potential ($V(u) = a_0 \left(u^2 - 1\right)^2$) [**?**, **?**] from the Landau phenomenology, and can thus be considered as a generalization of the latter.

I.6 Dynamics of nonlinear excitations in DW potentials

I.6.1 Kink-antikink scattering processes

The generation and interactions of solitary waves and solitons have attracted a great deal of interest over the past years, due to the fact that they can control many features related to the dynamics of natural systems ranging from biology and organic polymers, to classical and quantized fields in condensed-matter and high-energy physics [**?**, **?**, **?**, **?**, **?**, **?**, **?**, **?**, **?**]. Spatially localized topological configurations in nonlinear field theories are solutions with localized energy density that attain topological profile and propagate freely in time without loosing form. Solitons, for instance, maintain their form even after scattering, but there are other localized structures that

present different but still interesting features when they collide with one another. The subject of solitary wave (soliton) phenomena in condensed matter [**?**] is now enjoying a remarkable bloom period. A great deal is know about the properties of solitary waves in a variety of physical situations, and the ease with which these properties can be studied is surely one of the primary ingredients of the soliton success theory. In a seemingly endless string of investigations, workers in the area have been able to carry their studies quite far analytically. Moreover, the principal themes [**?**] regarding solitons can be stated simply and understood quite easily by the novice.

On general grounds, the simplest localized solutions in field theories that present topological profile are kinks and antikinks in (1, 1) space-time dimensions and can be constructed in theories with one or more scalar fields. Kink scattering in integrable systems is surprisingly simple, with the solitons gaining at most a phase shift. Some examples of integrable models are: i) KdV equation, connected to the Fermi-Pasta-Ulan problem [**?**, **?**] in the continuum limit; ii) nonlinear Schrödinger equation, important for describing nonlinear effects in fiber optics [**?**, **?**]; iii) the ubiquitous sine-Gordon equation [**?**], studied among other things in theories describing DNA [**?**] and Josephson junctions [**?**, **?**, **?**].

In non-integrable models, kink scattering has a complex behavior. For ultrarelativistic velocities and arbitrary potentials, there is an analytical expression for the phase shift [**?**]. The simplest nonintegrable and largely studied bistable model is the ϕ^4 model [**?**, **?**, **?**, **?**, **?**, **?**, **?**, **?**, **?**, **?**]. In that model, for larger initial velocities v we have inelastic scattering, with the pair of solitons colliding once and separating thereafter. For smaller velocities than a critical one, $v < v_c$, the kink-antikink forms a composed state named bion that radiates continuously until the complete annihilation of the pair, as shown in Fig. **??**a. There are velocities for which the pair collide and the kink an the antikink bounce once and indefinitely reflect far from each other (see Fig. **??**b) For smaller velocities with $v \lesssim v_c$ there are regions in velocity, named two-bounce windows, where the scalar field at the center of mass bounces twice before the final separation of the pair (see an illustration in Fig. **??**c). There also exist particular regions in velocity (n-bounce windows), where the scalar field at the center of mass can bounce several times (n times) before the final separation of the pair, as sketched in Fig. **??**d. Stability analysis of the ϕ^4 kink leads to a Schrödinger-like equation with two discrete eigenstates: a zero or translational mode, related to the translational invariance of the model and a vibrational mode. An argument for the occurrence of the later n-bounce windows have been explained as the consequence of a resonance mechanism for the

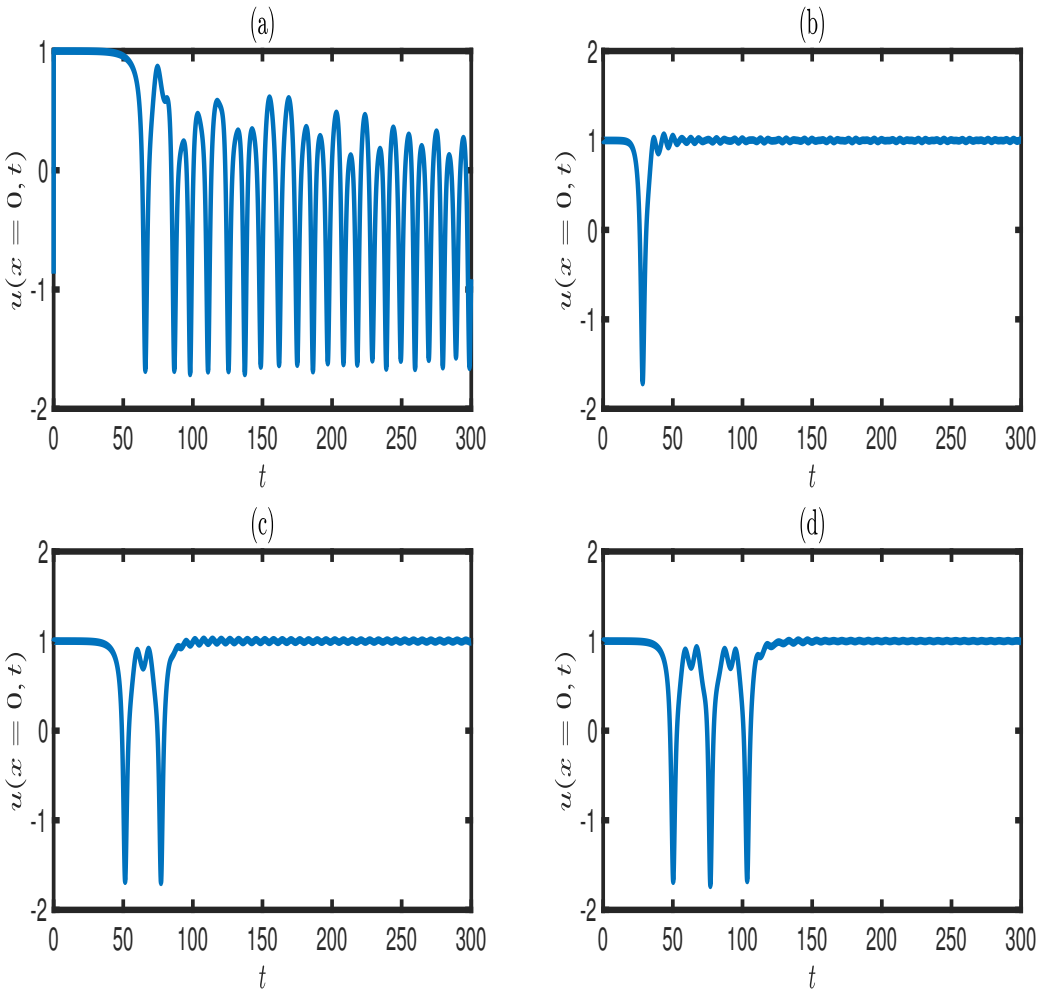

Figure 10: Sketch of the evolution of the center of mass of a kink-antikink pair upon collision in a ϕ^4 potential: $V(u) = (1/8)(u^2-1)^2$. The initial velocities of the soliton pair taken as: (a) $v = 0.15$, (b) $v = 0.40$, (c) $v = 0.20$, (d) $v = 0.205$. Figure extracted from Ref. [**?**]

exchange of energy between the vibrational and the translational modes, resulting from discrete eigenstates of the Schrödinger-like equation [**?**, **?**].

I.6.2 Low temperature statistical mechanics

Leaving aside philosophical arguments concerning the esthetic requirement that "correct" physics should be "simple", one nevertheless can be quite amazed by the beauty and simplicity of the basic and elementary bistable system which bear solitary-wave excitations, namely, those governed by the so-called "ϕ^4" nonlinear wave equation [**?**]. Many discussions of its solitary-wave or "kink" solution can be, and have been [**?**, **?**, **?**, **?**, **?**] on fundamental features the equation has. For example, analytic solutions are known for the kink and its antikink; perturbation theo-

ries for the kink have a structure relying heavily on the existence of a kink "translational mode" [**?**], the kink solution can be quantize [**?**].

One of the fascinating features of DW potential kinks, for instance the ϕ^4 kink, is their transparency to linear extended-wave solutions. The presence of a kink in the system provides a localized "potential" seen by the linear solution ("phonons") in the sense that small deviations from the kink waveform must satisfy a Schrödinger-like equation [**?**, **?**, **?**] in which the potential well is due to the presence of the kink. Remarkably, the ϕ^4 kink potential appearing in this one-dimensional Schrödinger problem is completely reflectionless [**?**, **?**, **?**, **?**] since the reflection coefficient [**?**] for the scattering (or "continuum") states vanishes for all k values.

The fact that the ϕ^4 kink is reflectionless or transparent to small oscillations has enable Currie *et al.* [**?**] to carry out an analytic investigation of the statistical mechanics of the system at low temperature. By comparing with exact results obtained via the transfer-operator formalism, these workers were able to justify the use of a phenomenological approach which treats the system as an "ideal gas" of kinks and "phonons" at low temperature, based on the work of Krumhansl and Schrieffer [**?**]. The transfer-operator formalism has been generalized to kink-bearing systems for which kink-phonon interactions lead to reflectionless scattering potentials [**?**]. One of the key points in the work of Currie *et al.* [**?**] is that care must be exercised in treating the effect of kinks on the phonon density of states, since phonon degrees of freedom are taken up by the kinks and this provides the mechanism for free-energy sharing among the modes of kink-bearing systems. The reflectionless property of the kinks allows one to easily examine the effect of kinks on the phonon density of states in an analytic fashion and obtain closed-form expressions for various thermodynamics functions via the phenomenological approach.

I.6.3 Phase transition in quantum tunneling

In chemistry, thermodynamics, and many other related fields, phase transitions (or phase changes) are the physical processes of transition between the basic states of matter: solid, liquid, and gas, as well as plasma in rare cases.

A phase of a thermodynamic system and the states of matter have uniform physical properties. During a phase transition of a given medium, certain properties of the medium change, often discontinuously, as a result of the change of external conditions, such as temperature, pressure, or others. For example, a liquid may become gas upon heating to the boiling point, result-

ing in an abrupt change in volume. The measurement of the external conditions at which the transformation occurs is termed the *phase transition*. Phase transitions commonly occur in nature and are used today in many technologies.

Phase transitions occur when the thermodynamic free energy of a system is non-analytic for some choice of thermodynamic variables. This condition generally stems from the interactions of a large number of particles in a system, and does not appear in systems that are too small. It is important to note that phase transitions can occur and are defined for non-thermodynamic systems, where temperature is not a parameter. Examples include: quantum phase transitions, dynamic phase transitions, and topological (structural) phase transitions. In these types of systems other parameters take the place of temperature. For instance, connection probability replaces temperature for percolating networks.

At the phase transition point (for instance, boiling point) the two phases of a substance, liquid and vapor, have identical free energies and therefore are equally likely to exist. Below the boiling point, the liquid is the more stable state of the two, whereas above the gaseous form is preferred.

It is sometimes possible to change the state of a system diabatically (as opposed to adiabatically) in such a way that it can be brought past a phase transition point without undergoing a phase transition. The resulting state is metastable, i.e., less stable than the phase to which the transition would have occurred, but not unstable either. This occurs in superheating, supercooling, and supersaturation, for example.

Paul Ehrenfest classified phase transitions based on the behavior of the thermodynamic free energy as a function of other thermodynamic variables [**?**]. Under this scheme, phase transitions were labeled by the lowest derivative of the free energy that is discontinuous at the transition. First-order phase transitions exhibit a discontinuity in the first derivative of the free energy with respect to some thermodynamic variables [**?**]. The various solid/liquid/gas transitions are classified as first-order transitions because they involve a discontinuous change in density, which is the (inverse of the) first derivative of the free energy with respect to pressure. Second-order phase transitions are continuous in the first derivative (the order parameter, which is the first derivative of the free energy with respect to the external field, is continuous across the transition) but exhibit discontinuity in a second derivative of the free energy . These include the ferromagnetic phase transition in materials such as iron, where the magnetization, which is the first derivative of the free energy with respect to the applied magnetic field strength, increases con-

tinuously from zero as the temperature is lowered below the Curie temperature. The magnetic susceptibility, the second derivative of the free energy with the field, changes discontinuously. Under the Ehrenfest classification scheme, there could in principle be third, fourth, and higher-order phase transitions.

The Ehrenfest classification implicitly allows for continuous phase transformations, where the bonding character of a material changes, but there is no discontinuity in any free energy derivative. An example of this occurs at the supercritical liquid-gas boundaries.

In the case of the escape at finite temperature of a particle trapped in a potential well, the original idea is to superpose the escape rates from the tunneling effects and thermal activation

$$\Gamma = \Gamma_{quatum} + \Gamma_{thermal}. \tag{12}$$

Following the definition of these rates,

$$\Gamma_{thermal} = \Gamma_0 \exp\left(-\Delta U/T\right) \quad and \quad \Gamma_{thermal} = B \exp\left(-B\right), \tag{13}$$

where B is the WBK constant, T the temperature, ΔU the barrier height, and A and Γ_0 constant prefactors, the transition form the classical regime to the quantum regime (considering tunneling at ground state) occurs at a critical temperature

$$T_0^{(0)} = \Delta U/T. \tag{14}$$

The classical escape greatly contributes to the global escape rate for temperatures greater than the critical temperature: $\Gamma \approx \Gamma_{thermal}$ when $T > T_0^{(0)}$, while for temperatures lower than the critical one, only the contribution from the quantum escape matters: $\Gamma \approx \Gamma_q$ when $T < T_0^{(0)}$. The transition between the two regimes occurs in a temperature interval comparable to the ratio of the critical temperature and the WBK constant, i.e., $\Delta T \sim T_0^{(0)}/B$, so, in a very small interval.

This scenario is a prototype of the so-called "first-order phase" quantum-classical transition [**?**], as at the critical temperature the variation of the escape rate with respect to temperature presents a discontinuity. However another scenario arises for common metastable and bistable potentials such as the cubic and quartic potentials. Below the temperature T_0 activating the classical escape, the particle crosses the barrier at a favorable energy $E(T)$ that can vary from

the barrier top to the bottom of the well fro a decreasing temperature. This regime is defined by a thermally-assisted quantum tunneling. The transition from the classical regime to this regime occurs smoothly at a temperature $T_0^{(2)} = \omega_0/2\pi$ (ω_0 being the frequency of the instanton [**?**, **?**] expected to dominate the thermal rate [**?**, **?**]), and without in the variation of the global escape rate with respect to the temperature at T_0. Here, we are instead in the case of a "second-order " quantum-classical transition [**?**], as it has been found that the case presents a discontinuity at $T > T_0^{(2)}$ of the second-order derivative of the escape rate with respect to temperature.

The terms "first-order" and "second-order" for the the quantum-classical transitions take their denotation from the work of Larkin and Ovchinikov on the topic. But later on, Chudnovsky put the emphasis on the analogy of these transitions and the phase transitions classified by Ehrenfest and analysed the general conditions that could yield the two types of transitions which are now known as phase transitions in quantum tunneling. These phenomena have recently attracted a great deal of interest; in particular, it was demonstrated that some physical systems can exhibit not only a smooth second-order transition at a critical temperature T_0 but also a first-order transition [**?**, **?**, **?**, **?**, **?**, **?**, **?**] at some other temperatures.

I.7 Motivations

I.7.1 Deformable potential

The last decades has witnessed a regain of interest in kink scatterings in non-integrable models, marked by intensive studies for instance of multi-kink collision [**?**, **?**, **?**, **?**, **?**, **?**], the interactions of a kink or an anti-kink with a boundary or a defect [**?**, **?**], the scattering processes in models with generalized dynamics [**?**], non-polynomial models [**?**, **?**, **?**, **?**], polynomial models with one [**?**, **?**, **?**, **?**, **?**, **?**, **?**, **?**, **?**, **?**, **?**] and two [**?**, **?**, **?**, **?**, **?**] scalar fields and so on. However, all these studies involve mostly two universal models which are the sine-Gordon model [**?**, **?**, **?**], assumed to describe systems with periodic on-site potentials, and the ϕ^4 model intended for physical systems with DW potentials. Also, most of the studies on the phase transitions in quantum tunelling, and the low-temperature statistical mechanics of multi-state systems rested mainly on the assumption of these two universal models and concentrated on the behaviour and the selective control of the emerging phenomena as a function of parameters of the system such as temperature, energy barrier, or some other intrinsic variables. The sine-Gordon and ϕ^4 models are still quite

interesting. For example, the ϕ^4 kink has very recently been linked with topological excitations observed in buckled graphene nanoribbon [**?**]. Yet real physical systems to which these models and studies address are actually far more complex, sometimes also displaying a rich diversity with unique structural features. For instance, the sine-Gordon and ϕ^4 potentials both have fixed extrema, in addition to their shape profiles that are rigid and hence restrict their applications to only very few physical contexts.

To obtain a physically more realistic bistable model for several complex systems (atomic chains, catalyst's action in chemical reaction), the effects of physical parameters such as temperature and pressure should be considered. Under such constraints, some physical systems may undergo changes such as shape distortion, variation of crystalline structures, or conformational changes. Hence, it appears necessary to take into account the deformable character of the bistable system. Indeed, deformable models have been considered both from mathematical and physical point of view. From a mathematical point of view, the foundations of deformable models represent a confluence of geometry, physics, and approximation theory. Geometry serves to represent object shape, physics imposes constraints on how the shape may vary over space and/or time, and optimal approximation theory provides the formal underpinnings of mechanisms for fitting the models to measured data. From a physical point of view, deformable models are viewed as elastic bodies that respond naturally to applied forces and constraints [**?**, **?**]. In fact, the term deformable model stems primarily from the use of elasticity theory at the physical level, generally with a Lagrangian dynamics setting.

To lift the shortcomings related to the rigidity of shape profiles, it has been shown that these weaknesses can be overcome by envisaging a parameterization of these two universal models. Indeed, the sine-Gordon model was generalized by Remoissenet and Peyrard [**?**, **?**, **?**] into a parameterized periodic potential (the so-called RemoissenetPeyrard potential) [**?**, **?**, **?**], and the ϕ^4 potential was parameterized [**?**, **?**, **?**, **?**] into a DW potential model with a tunable shape profile. It is worthwhile to stress that although some other parametric DW potentials exist in the literature [**?**, **?**, **?**] (some are mentioned in Sec. **??**), the class of DW potentials proposed in other studies [**?**, **?**, **?**, **?**] is peculiar in that it groups three different classes with distinct shape deformability features. Also, the three classes admit the ϕ^4 potential as a specific limit.

I.7.2 New phenomena and more physical insight with deformable potentials

The importance of shape deformability in the context of bistable systems lies in three issues related to their structural properties.

The first issue is linked with the problem of symmetry breaking, for which the ϕ^4 model predicts the transition in quantum tunneling to be strictly of second order [**?**, **?**, **?**, **?**]. This issue was recently addressed by Zhou *et al* [**?**] who formulated the problem of transitions in quantum tunneling for one [**?**] among the three existing classes of parametrized DW potentials [**?**, **?**, **?**, **?**]. Thus, Zhou et al [**?**] obtained that due to the extra degree of freedom accounting for shape deformability, bistable systems which can be described by the parametrized DW potential could exhibit a first-order transition occurring at a finite critical value of the shape deformability parameter, besides the second-order transition predicted by the ϕ^4 model.

Speaking of interest, the possibility of tailoring their functionalities at the molecular scale makes molecular nanomagnets interesting for applications in information technologies where the race for extreme miniaturization will soon lead at requiring components of few nanometers in size. Properties like the magnetic bistability or the switchability by external stimuli actually allow one to mimic, at the molecular scale, basic operations commonly used in computers while embedding magnetic molecules in suitable electronic circuits allows the fabrication of novel spintronic devices [**?**, **?**]. Even more challenging is the control and the exploitation of quantum properties in molecular spin clusters that may allow the encoding of quantum information with molecules. Thus, gaining insight on the possibility to control the nature of the quantum-classical tunneling during the spin reversal of the molecular magnets is a knowledgeable perspective for information technologies.

The second issue is related to observations [**?**, **?**] that the transfer-integral formalism always reduces the classical statistical mechanics of a one-dimensional (1D) ϕ^4-field theory, to a time-dependent quantum mechanical problem for which no exact solution exists. Given that the classical statistical mechanics of a field theoretical system can be fully analyzed with just the knowledge of its low-lying eigenstates, parametrized DW models are quite likely to introduce the possibility for quasi-exactly solvable (QES) systems in field theory [**?**, **?**, **?**, **?**, **?**].

The third issue rises from the fact that the deformability gives room for the appearance of new phenomena as a consequence of kink scattering processes, while such phenomena have never been observed in the conventional ϕ^4 potential. Indeed in two recent studies [**?**, **?**], Bazeia *et al.*

addressed the issue of the influence of shape deformability of DW potentials, on kinks-antikink scatterings with production of oscillon bound states [**?**, **?**, **?**]. They first applied the shape deformability procedure to the standard ϕ^4 by introducing a bistable model with non-polynomial potential, which they called sinh-deformed ϕ^4 potential [**?**]. Despite this new model showing similar feature with the ϕ^4 model a new phenomenon was observed. Indeed, under certain conditions the kink-antikink pair in the new model was found to convert, after collision, into long-lived low amplitude and almost harmonic oscillations of the scalar field around one vacuum. They interpreted these almost harmonic oscillations as a bound state of individual oscillons [**?**]. Later on the authors investigated [**?**, **?**] kink-antikink collisions with production of oscillons, considering two cases of the class of DK DW potentials [**?**, **?**, **?**, **?**]. One case was a DW potential with variable separation between the two degenerate minima but with fixed barrier height [**?**] and the other case was the DW potential with variable barrier height but fixed positions of the two degenerate minima. The oscillons production in these two cases of the class of DK DW potentials were also established. In the context of the inflation theory within the framework of early universe cosmology, oscillons are suspected to be the source of gravitational waves [**?**]. The topics questioning oscillons properties and lifetime are quite actual [**?**, **?**].

I.7.3 Limitations of usual approaches of deformability

Systems with deformable features abound in nature, ranging from biology to soft matters such as lipid membranes [**?**], linear polymer chains, molecular crystals, and hydrogen-bonded ferroelectrics and antiferroelectrics. In these systems, chemical processes such as the effects of catalyst or solvants, isotopic substitutions, or simply the intrinsic structure of molecular chains (e.g., flexible chain backbones and soft interactions) can favor changes in bond lengths and characteristic parameters of the DW energy landscape as for instance the height of the potential barrier, positions of the potential wells, and the steepness of the potential walls. As for example of the influence of these shape characteristic parameters on the dynamics of a bistable system we can cite the work of Zhou *et al.* [**?**], in which the parameterized DW potential was one for which the height of the potential barrier could be varied continuously by varying a shape deformability parameter, leaving unchanged the positions of the two degenerate minima [**?**]. They found the system to be able to display a first-order transition in quantum tunneling while lowering the potential barrier height. The possibility of such transition was justified by the fact that while

lowering the barrier, it becomes very flat and resembles a rectangular barrier, thus inducing the thermally assisted tunneling to be suppressed and the thermal activation to compete directly with the ground-state tunneling.

Another example is the work of Bazeia *et al.*, reporting the appearance of oscillons in hyperbolic models [**?**] for two deformable DW potentials, they showed that the production of oscillons is boosted by applying the conformational changes from those potentials deformability such as reducing the distance between the minima keeping the barrier height fixed, or decreasing the barrier height while keeping the minima fixed. They pointed out that the factor unifying the two contexts is the lowering of the kink energy by the deformability in the two models.

Finally, as the search for analytically tractable model for investigations on the statistical mechanic of the system is in progress, several DW potentials were proposed (some are listed in Sec. **??**). These potential were found to be adequate in their context, but also found to be modified versions of the double-Morse potential [**?**] possessing several parameter controlling independently the barrier height and the barrier width. The Schrödinger equation resulting from transfert-operator formalism being exactly solvable at some discrete temperature with the double-Morse potential [**?**], it is expected that its modified versions display the same features.

Despite the already known number of systems showing first-order transition in quantum tunneling, and the numerous potentials holding the QES feature, in the former circumstance these system are mostly of several degree of freedom and in the later context the potentials yield eigenvalues and eigenfunctions which are not always elementary functions. Thus the inquiry for physical systems analogous to a particle in a potential and candidate for a first-order transition, together with the seek for analytical tractable DW potential for the Schrödinger equation still remain actual fronts of concern.

In litterature, the problems of deformability in symmetric bistable systems is usually approached by a mathematical formulation of a symmetric DW potential comprising a shape parameter that can be used to tune the position of the degenerate minima [**?**], the height of the potential barrier [**?**], both the position of the minima and the barrier height simultaneously [**?**, **?**, **?**, **?**, **?**, **?**, **?**, **?**, **?**, **?**], or even the confinement strength of the potential well [**?**, **?**]. However any modification in the potential characteristics will automatically lead to changes in the potential shape, such as a variation of the steepness of the potential's barrier wall, the mid-height of the barrier and also the curvature of the barrier top. Consequently, this latter variation may instead

be the factor having the major contribution in the phenomena observed. For instance, Chudnosky [**?**] suggested the class of potentials has the trend of changing slowly near the top and the bottom, but rather being steep in the middle as a good candidate for a first-order transition. This thus agrees with the observation of Zhou *et al.* [**?**]. Curiously the trend stated by Chudnosky [**?**] appear to be common to all the potentials considered by Bazeia *et al.* [**?**, **?**, **?**].

As part of the present study, one-dimensional bistable systems characterized by the DK class of deformable DW energy landscape will be considered in order to investigate the effect of shape deformability on the order of phase transition in quantum tunneling, kink scattering, and on the quasi-exact integrability of the classical statistical mechanics of these systems. In this regards, the deformability parameter will trigger respectively a variation of the potential degenerate minima, the barrier height, and both the barrier height and the position of the minima. In addition to the DK class cases we also propose a parametric DWP in which only the curvature shape of the barrier varies as the system is deformed. That is, the deformation in the latter model is manifested through an increase of the steepness of the potential walls, with the barrier top becoming flattened hence imposing an anharmonic shape to the potential barrier. Such variation of the barrier curvature being only observed as an implicit result of deformability in the existing models, its direct impact on the dynamics of the system can thus be fully investigated with our proposed model.

The study presented in the present thesis is, to our knowledge, the first of the kind addressing this approach of deformability in the context of symmetric bistable deformable systems. We shall develop the procedures and results of our investigations on the basis of a simple model of itinerant particles subjected to an "on-site" bistable deformable potential.

I.8 Conclusion

In this chapter, we have presented the concept of bistability in numerous real systems. These systems displaying a bistable energy landscape are generally modeled by a bistable potential of which the potential wells represents the stable states of the system. We have discussed some of the observed dynamics of systems modeled by DW potentials, i.e., the generation of kink (antikink) solitons allowing investigations on kink-antikink scattering processes, the low temperature statistical mechanics of the system, and also the possible transitions from the quantum tunneling to the classical crossover occurring during a particle escape from one state to another.

Under some particular constraints, some physical systems and nonlinear lattices may undergo changes which are usually represented by the deformable feature of the potential modeling these systems. The investigations of the consequences of these changes on quantum-classical phase transitions, Hamiltonian solvability and the production of oscillons, these being our main motivations, are developed in the next chapters.

CHAPTER II

MODELING AND MATHEMATICAL METHODS

II.1 Introduction

In the previous chapter, we presented some problems related to systems admitting bistable states in their energy landscape, and the conditions of their studies using a bistable potential, which is the purpose of our work. In this chapter on the other hand, we are interested in the phenomena appearing in real systems that can be modeled by a chain of interacting particles of mass m, spaced by a lattice constant l and subjected to an "on-site" bistable potential V (as depicted in Fig. **??**). The Hamiltonian of this chain of interacting particles is of the form

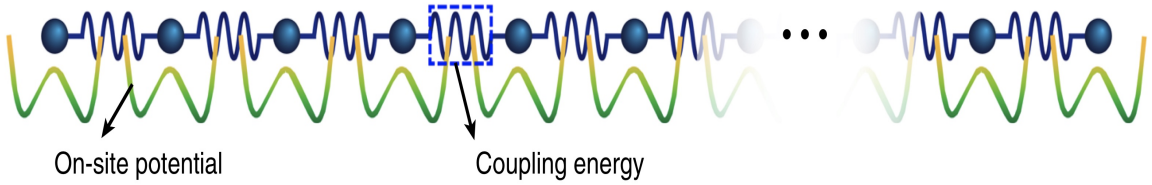

Figure 11: A 1D chain of identical massive particles interacting with a DWP.

$$\mathcal{H} = \sum_i \left[\frac{1}{2} m \dot{\varphi}^2 + \frac{k}{2} \left(\varphi_{i+1} - \varphi_i \right)^2 + V_0 V(\varphi_i) \right], \tag{15}$$

where φ_i is the longitudinal displacement of the ith particle from its equilibrium position along the x axis, and the over dot $(\cdot)$ is the time derivative. The interatomic attractions are taken into account in the second term of (**??**), where k is a harmonic coupling constant between nearest particles of the chain. The parameter V_0 is the amplitude of the substrate potential. For convenience, the dimensionless displacement $u_i = \varphi_i / \ell$ is considered and the Hamiltonian (**??**) is then

reduced to a class of Hamiltonians of the form

$$\mathcal{H} = \sum_{\ell}^{N} \ell A \left[\frac{1}{2}\dot{u}^2 + \frac{1}{2}C_0^2 \left(u_{i+1} - u_i\right)^2 + \omega_0^2 V(u_i) \right], \tag{16}$$

with

$$A = m\ell, \quad C_0^2 = \frac{k}{m}, \quad \omega_0^2 = \frac{V_0}{m}, \tag{17}$$

where C_0 is the sound velocity in the lattice and ω_0 the characteristic frequency of the system. The constant A may be considered as the energy scale.

In this chapter we aim to analyze the physical systems modeled by the general class of nonlinear Hamiltonians of the form (**??**), as regards to the integrability of their classical statistical mechanics, together with the appearance of kink-antikink induced phenomena, and also the nature of phase transitions from quantum tunneling regime to thermal hopping regime. We specifically consider two scenarios: In the first scenario, detailed in Sec.**??**, the strength of the coupling between the particles are considered to be competing with the influence of the potential, allowing the creations of kinks solitons in the system. On the other hand, In the second scenario the coupling between the particles is considered very weak such that compared to the the coupling constraints are no more relevant. Taking the impact on a particle of its surrounding to have the nature of a thermal bath, the situation can then be regarded as the problem of the dynamics of a particle residing in a potential well and subjected to thermal fluctuations, then raising the possibility of an escape from one well to another at fixed temperature. Sec.**??** is devoted to the analytical approaches used in our analysis, while Sec.**??** and Sec.**??** present the different numerical approaches.

II.2 Case 1: Particle residing in a bistable potential well and subjected to thermal fluctuations

In this section, we consider the situation in which the inter-atomic coupling in the model is nonexistent. Each particle can then be considered as a system with the influence of its surrounding being considered as stochastic thermal fluctuations. In this case the problem can be safely reduced to the study of the dynamics of a Newtonian particle of constant mass ($m = 1$ for simplicity), subjected to a bistable potential energy field. The total energy of such particle is given

by

$$E_c = T_c + V = \frac{1}{2}\left(\frac{du}{dt}\right)^2 + V(u), \tag{18}$$

where V_0 has be merged in the analytical expression of V. We restrict ourselves to the case where the local dimensionless potential $V(u)$ possesses two degenerate minima as shown in Fig. **??**. Classically, the particle is not allowed to enter the space where the potential energy is greater

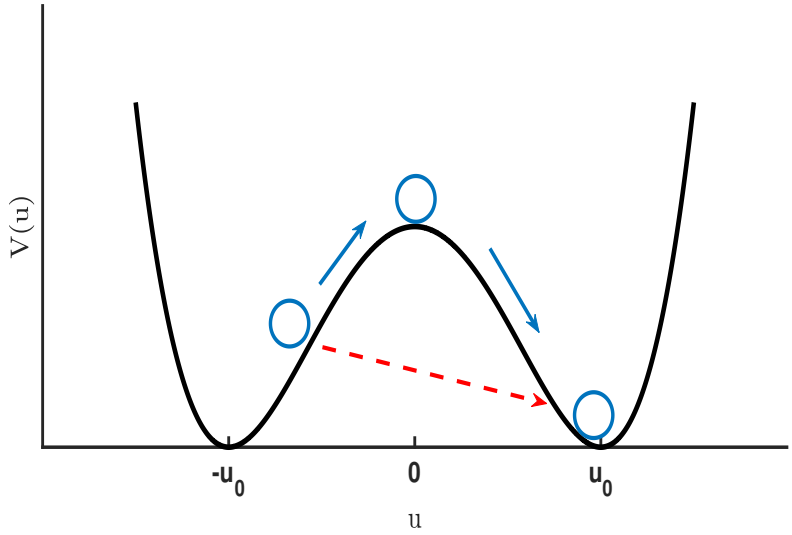

Figure 12: Illustration of the possible escapes from one well to another of a massive particle residing a well of a potential $V(u)$ having stable positions $u = \pm u_0$. The blue arrows indicate the thermally activated jump over the barrier, and the red arrow indication the barrier traversing via tunneling effects.

than the total energy of the particle. Then, for classically fixed energy, regions where $E_c < V(u)$ requires that $T_c = (1/2)\dot{u}^2 < 0$, which means that the kinetic energy T_c has to be negative, and such regions are classically forbidden. Heuristically, such a forbidden region is attainable if the time t becomes imaginary. Indeed, if $t \to i\tau$, then

$$\left(\frac{du}{dt}\right)^2 \to \left(i\frac{du}{d\tau}\right)^2 = -\left(\frac{du}{d\tau}\right)^2. \tag{19}$$

T_c thus becomes negative In the Euclidean time τ and the initially forbidden regions can now be considered accessible. In this consideration, two scenarios are possible. The first one is the case in which the particle at rest at a potential minimum can have sufficient energy to classically hump over the barrier and move to the other minimum. The second scenario is that quantum mechanically the particle can tunnel through the hump from one well to another.

The classical action of the over a time period of the trajectory is $S = \int dt\mathcal{L}$, where $\mathcal{L}$ denote the Lagrangian, obtained as

$$\mathcal{L} = \left(\frac{du}{dt}\right)^2 - V(u). \tag{20}$$

In Euclidean time, the corresponding Euclidean action is obtained as

$$S_E = -iS = \int d\tau \left[\frac{1}{2}\left(\frac{du}{dt}\right)^2 + V(u)\right]. \tag{21}$$

In the path integral formalism [**?**], the most favorable trajectory u_c of the particle is that minimizing the action. With (**??**), the equation of motion of the particle then yields

$$\left(\frac{du_c}{dt}\right)^2 = 2(V(u_c) - E). \tag{22}$$

Taking into consideration the definition (**??**), E in (**??**) is a constant having the nature of energy. In fact, it can be consider as the initial energy of the particle following the trajectory u_c. Also, the solution $u_c(\tau)$ can be looked at as describing the motion of a Newtonian particle of $m = 1$ in potential $-V(u)$.

II.2.1 Analysis of the semi-classical solutions of the problem

We are interested in solutions of (**??**) which start at and return to either $\pm u_0$, or those that interpolate between $\pm u_0$, each during a time $\tau_p = \beta$ ($\hbar = 1$ for simplicity). The trivial solution $u_c(\tau) = \pm u_0$ satisfy the first condition while the second condition can be obtained by integrating (**??**). Choosing the solution that interpolates from $-u_0$ to $+u_0$, we straightforwardly get

$$\int_{-u_0}^{u_c(\tau)} \frac{du}{\sqrt{2(V(u_c) - E)}} = \int_{-\tau_p/2}^{\tau} d\tau = \tau + \frac{\beta}{2}, \tag{23}$$

and E is determined by

$$\int_{-u_0}^{u_0} \frac{du}{\sqrt{2(V(u_c) - E)}} = \beta. \tag{24}$$

Note that (**??**) does not depend on the details of the solution, but only on the fact that it must interpolate from $-u_0$ to $+u_0$. The initial energy E is not arbitrary, the trajectory must interpolate from $-u_0$ to $+u_0$, and (**??**) gives implicitly E as a function of β. There is no trajectory that starts with vanishing energy but interpolates between $\pm u_0$; zero initial energy requires infinite β.

The action for the trivial trajectories $u_c(\tau) = \pm u_0$ is evidently zero. For the interpolating trajectory implicitly determined by (**??**), it is

$$S_E = \int_{-\beta/2}^{\beta/2} d\tau \left[\frac{1}{2}\left(\frac{du(\tau)}{dt}\right)^2 + V(u)\right] = \int_{-\beta/2}^{\beta/2} d\tau \left[\frac{1}{2}\left(\frac{du(\tau)}{dt}\right)^2 + E\right] \quad (25)$$

$$= \left[\int_{-\beta/2}^{\beta/2} \sqrt{2(V(u)-E)}\frac{du}{d\tau}\right] + E\tau_p = \left[\int_{-u_0}^{u_0} du\sqrt{2(V(u)-E)}\right] + E\tau_p. \quad (26)$$

II.2.2 Sphaleron, instanton and periodon solutions

As $\beta \to \infty$, the only way for the integrand in (**??**) to diverge and give an infinite or large β is for the denominator to vanish. This occurs for $V(u) \to 0$ and for $E \to 0$. $V(u) \to 0$ occurs as $u \to \pm u_0$,which is near the start and end of the trajectory. Heuristically, for small E, the particle spends most of its time near $u = \pm u_0$ and classically interpolates from one to the other quickly. The trajectory in this case is called "instanton". Then the major contribution to the integral in (**??**) comes from the region around $u = \pm u_0$. Since the integral diverge logarithmically when $E = 0$, for a typical potential V (which must vanish quadratically at $u = \pm u_0$ as V has a bouble zero at $\pm u_0$), the integral must behave as $-lnc$, i.e., $\beta \sim lnE$. Thus for sufficiently large β, we may neglect E altogether. In this case , we may choose the time arbitrarily at which the trajectory crosses over from $-u_0$ to u_0. Then the instanton which crosses over around $\tau = \tau_0$ is obtained as solution of

$$\int_0^{u_c(\tau)} \frac{du}{\sqrt{2V(u_c)}} = \tau - \tau_0, \quad (27)$$

with its action given by

$$S_0 = \int_{-u_0}^{u_0} du_c\sqrt{2V(u_c)}. \quad (28)$$

For finite β, a trivial solution $u_c(\tau) = 0$ is obtained in the case $E = V_0$, V_0 being the height of the potential barrier. This trajectory is a sphaleron and its action is the thermodynamic action [**?**]. Finally, we are interested in the behavior of the particle in the the limit $\beta_s < \beta < \infty$, β_s being the time at which the sphaleron occurs. The limit implicitly defines the possible values of E to lie in the range $]0, V_0[$. In this case, the particle may interpolate several times from one potential well to another via tunneling processes. We then consider the case in which the particle starts from the turning point $-u_0$ at imaginary time $-\tau_p$ and reaches the other turning point u_0 at τ_p. After the same time interval, at time $2\tau_p$, the particles returns to its original position, i.e., it tunnels through

the barrier twice in the whole period. The tunneling behavior can be understood by construction from (**??**) of a periodic trajectory called "periodon", satisfying the periodic boundary conditions

$$u_c|_{\tau=-2\beta} = u_c|_{\tau=2\beta} = 0. \tag{29}$$

As E grows near the barrier height, the interpolation from one well to another transit from a quantum tunneling regime to a hoping across the barrier hump.

The variation with respect to E of the periodon characteristic quantities such as its period or its action, together to the behavior of the sphaleron around the barrier peak the hold great importance as they determine the nature of the phase transition from quantum tunneling to thermal hopping. In Sec.**??** we shall present the criteria that permit us to define the nature of the phase transition in the system.

II.3 Case 2: Chain of interacting particles subjected to an on-site DW potential

We consider the general class of nonlinear Hamiltonians restricted to one-component fields defined (initially) on one-dimensional lattices, having the following form (**??**). We recall that in a number of physical systems, the interatomic interaction (accounted for in the second term of (**??**)) is repulsive or has at least a repulsive branch. This interaction can be due to couloumb repulsion between ion in supersonicconductors [**?**], between proton in hydrogen bonded molecules [**?**], Coulomb or dipole-dipole repulsion of atoms adsorbed on semiconductors or metal surfaces [**?**].

It is important to distinguish between two different regimes according to whether the length $d \equiv c_0/\omega_0$ is on the order of the lattice constant ℓ or large compared to ℓ. The first results when the interaction energy between neighbors is small compared to the on-site potential $(d \ll \ell)$ and is termed "order-disorder" limit, since field values on neighboring sites can fluctuate (thermally) almost independent of one another. In the opposite limit $(d \gg \ell)$, the coupling between sites is strong enough to ensure that variations of u from site to site are quite small, at least at low temperatures. In this "displacive" limit we may replace the site index i by a continuous position variable x so that u becomes a continuous function of x and t, i.e., $u_i = u(x = \ell i, t)$. Although the order-disorder limit is a physically interesting case (e.g Ising), we shall restrict ourselves to

the displacive limit where nonlinear kinks become well-defined [**?**] elementary excitations with long lifetimes and as such behave [**?**] very much like particles.

II.3.1 Equation of motion in the displacive limit

In the continuum (displacive) limit the Hamiltonian (**??**) is transformed approximately to

$$\mathcal{H} = A \int dx \left\{ \frac{1}{2}[\dot{u}(x,t)]^2(x,t) + \frac{1}{2}c_0^2[u_x(x,t)]^2 + \omega_0^2 V(u) \right\}, \tag{30}$$

where $u_x(x,t) = (\partial/\partial x)u(x,t)$ replaces the finite difference $(u_{i+1} - u_i)/l$. Solitary-wave (kink) and linear (phonon) excitations of the system arise as solutions of the Euler-Lagrange equation of motion [**?**] following from (**??**):

$$\ddot{u} - c_0^2 u_{xx} + \omega_0^2 \frac{dV}{du} = 0. \tag{31}$$

The only restriction on the local dimensionless potential $V(u)$ is that it has at least two degenerate minima ($V = 0$) at, for example, $u_1 = -u_0$ and $u_2 = +u_0$. This is sufficient to elementary solitary-wave (kink) solutions $u_K^{(v)}$ to (**??**).

II.3.2 The solitary-wave (kink) solution and its associated energy

We look for a kink moving with velocity v and impose appropriate boundary conditions, that is,

$$\frac{du_K^{(v)}(s)}{ds}|_{s=\pm\infty} = 0, \quad V(u_K^{(v)}(s=\pm\infty)) = 0, \quad u_K^{(v)}(s=\pm\infty) = u_{1,2}, \tag{32}$$

with $s \equiv x - vt$. The solution obtained from the first integral of (**??**),

$$\frac{du_K^{(v)}(s)}{ds} = \pm \left[\frac{2\omega_0^2}{c_0^2} \left(1 - \frac{v^2}{c_0^2}\right)^{-1} V(u_K^{(v)}) \right]^{1/2}, \tag{33}$$

by integrating a second time:

$$x - vt = \pm \left(1 - \frac{v^2}{c_0^2}\right)^{1/2} \frac{d}{\sqrt{2}} \int_{u_K^{(v)}(0)}^{u_K^{(v)}(x-vt)} du[V(u)]^{-1/2}, \qquad d = c_0/\omega_0. \tag{34}$$

(**??**) provides an implicit solution for $u_K^{(v)}$ as a function of $x - vt$. The "relativistic" dependence on v follows from the covariant form of (**??**) and appears again in the energy, E_k, associated with

a single kink:

$$E_k^{(\upsilon)} = E_k^{(0)} \left(1 - \frac{\upsilon^2}{c_0^2}\right)^{-1/2} = \sqrt{(E_k^{(0)})^2 + (pc_0)^2}, \tag{35}$$

where $p = M_k \upsilon \left(1 - \upsilon^2/c_0^2\right)^{-1/2}$ is the relativistic momentum and $E_k^{(0)}$ is the rest energy of the kink, $E_k^{(0)} = M_k c_0^2$. The kink rest mass M_k is given by

$$M_k = \frac{2A}{d^2} \int_{-\infty}^{+\infty} dx V[u_k^{(0)}(x)] = \frac{\sqrt{2}A}{d} \int_{u_2}^{u_1} du |V(u)|^{1/2}. \tag{36}$$

It is worth nothing that if $V(u)$ has sufficient structure, more that one type of kink may be possible [**?**].

We shall have the occasion to employ both forms [(**??**) and (**??**)] of the Hamiltonian for the system. The discrete form (**??**) is used in obtaining the exact statistical mechanical results via the transfer-operator formalism, where-upon the explicit process of taking the continuum limit follows. The continuum form (**??**) is used to study the scattering and nature of the solitary-wave (kink) and linear (phonon) excitations of the system.

II.4 Analytical methods

II.4.1 Perturbation scheme for localized excitations spectrum around the kink

After obtaining the formulation of the kink solution for (**??**), Rich information can be obtained by analysing its interactions with small amplitude excitations of the lattice. First of all, we suppose that phonons manifest themselves *a priori* about a static kink so that the kink waveform undergoes a slight harmonically-varying shape change localized about its center. Thus writing solutions of (**??**) in a new form

$$u(x,t) = u_k(x) + m(x,t), \tag{37}$$

where $u_k(x)$ is the static kink and $m(x,t)$ a phonon. Linearisation in u_k leads to the following equation

$$m_{tt} - c_0^2 m_{xx} + \omega_0^2 \left(\frac{d^2}{du^2} V(u_k)\right) m = 0. \tag{38}$$

Taking for (**??**) solutions in the form of plane waves, i.e.,

$$m(x,t) = \eta(x) \exp(-i\omega t), \tag{39}$$

we obtain the eigenvalue equation

$$-c_0^2\eta_{xx} + \omega_0^2 U(x)\eta = \omega^2\eta. \tag{40}$$

$U(x) = (d^2/du^2)V(u_k)$ is then scattering potential. A numerical treatment of (**??**) with the Numerov method can now help obtain the different modes with their corresponding frequencies ω.

II.4.2 Transfer Integral method

The classical partition function of the NKG system can be obtained exactly by the transfer-integral method. Although this method does not tell explicitly anything about solitons, the result obtained by this method works as a rigid reference (since it is exact) for any theories based on the picture to be compared with.

Starting at the discrete Hamiltonian (**??**), the classical partition function Z of the system is defined by

$$Z = \int \prod_{i=1}^{N} \left(\frac{dp_i du_i}{2\pi\hbar}\right) e^{-\beta H}, \tag{41}$$

where N is the degree of freedom (number of lattice sites) of the system and $\beta = (\kappa_B T)^{-1}$. The momentum integrations can be carried out readily to yield

$$Z = (\ell/\beta\hbar c)^2 \int du_i \cdots du_N K(u_0, u_1) \cdots K(u_{N-1}, u_N), \tag{42}$$

where the "transfer matrix" K is defined by

$$K(u, u') = \left(\frac{\beta\kappa}{2\pi}\right)^{1/2} \exp\left\{-\beta\left[\frac{\kappa}{2}(u-u')^2 + \frac{V_0}{2}V(u) + \frac{V_0}{2}V(u')\right]\right\}, \tag{43}$$

and $c = \ell(\kappa/I)^2$ with a being the lattice distance. (**??**) is derived assuming the periodic boundary condition ($u_0 = u_N$). Since K is real and symmetric $K(u, u') = K(u', u)$, it can be expressed in terms of the eigenfunctions $\psi_n(u)$ and the eigenvalues λ_n of the integral equation with kernel K:

$$K(u, u') = \sum_n \lambda_n \psi_n^*(u)\psi_n(u), \quad \int du' K(u, u')\psi_n(u) = \lambda_n\psi_n(u). \tag{44}$$

The eigenvalue equation (**??**) is called the transfer-integral equation [**?**]. By using (**??**), the integrations in (**??**) can be carried out to obtain

$$Z = (\ell/\beta\hbar c)^N \sum_n \lambda_n^N \int du_N \psi_n^*(u_N)\psi_n(u_N). \tag{45}$$

For periodic V, the set of eigenvalues forms a band structure. However, If the potential V is of DW the situation becomes simpler. In this case, the set of eigenvalues λ_n is discrete [**?**]. Therefore, in the thermodynamic limit $(N \to \infty)$ only the largest λ_0 contributes to Z. In both situations, the free energy F is obtained from the largest eigenvalue λ_0 as

$$-\beta F = \ln Z = N \ln(\lambda_0 \ell/\beta\hbar c) + \mathcal{O}(\ln N), \tag{46}$$

where the last term is absent in the DW case.

The equal-time correlation function for any function $f(u)$ of u is defined by

$$\langle f(u_j) f(u_{j+1})\rangle = Z^{-1} \int \prod_i \left(\frac{dp_i du_i}{2\pi\hbar}\right) f(u_j) f(u_{j+1}) e^{-\beta H}. \tag{47}$$

In the thermodynamic limit this quantity can be expressed as

$$\langle f(u_j) f(u_{j+1})\rangle = \sum_n (\lambda_n/\lambda_0)^{|l|} |\langle n|f|0\rangle|^2, \tag{48}$$

where

$$\langle n|f|0\rangle|^2 = \int du \psi_n^*(u) f(u) \psi_0(u), \tag{49}$$

The derivation of the formula (**??**) is straightforward for DWPs, because the eigenvalues are discrete [**?**]. The derivation for periodic potentials is not, since, in addition to the continuous nature of the eigenvalues, one need to keep the term of order $\ln N$ in (**??**) when evaluating the right-hand side of (**??**).

Since the derivations of (**??**) and (**??**) are exact in the thermodynamic limit, the exact values of the free energy and various correlation functions can be obtained if the transfer-integral equation (**??**) is solvable. In the continuum limit ($\kappa \gg V_0$, or $d = c\sqrt{I/V_0} \gg a$), the transfer-integral equation is reduced to a more familiar and tractable eigenvalue equation of the Schrödinger

type:

$$\left[-\frac{T^{*2}}{2}\frac{d^2}{du^2}+V_0V(u)\right]\psi_n(u)=\varepsilon_n\psi_n(u), \tag{50}$$

where

$$T^*=\kappa_BT\sqrt{\ell/V_0A^2c^2},\quad\text{and}\quad\lambda_n=\exp(-\beta V_0\varepsilon_n). \tag{51}$$

In the latter equation the dimensionless temperature T^* plays the role of the Planck's constant. The free energy of the system is now obtained from the ground-state eigenvalue ε_0 by

$$-\beta F/L=a^{-1}\ln(\beta\hbar c/a)+d^{-1}(\varepsilon_0/T^*). \tag{52}$$

The solution of the pseudo-Schrödinger equation (**??**) can be found analytically in the form of asymptotic expansion.

II.4.3 The Sommerfeld polynomial method

In this subsection, (**??**) is considered with $V(u)$ taken to be the harmonic potential for the sake of example, that is, $V(u)=u^2/2$ In order to make the equations easier to work with, a dimensionless operator $\widehat{Q}$ is defined as

$$\widehat{Q}=\left(\frac{V_0}{T^{*2}}\right)^{1/4}\widehat{u}, \tag{53}$$

together with the change of variable $E_n=\varepsilon_n/(T^*V_0^{1/2})$. In these new variables, the pseudo-Schrödinger equation (**??**) can be rearranged to the following second-order ordinary differential equation,

$$\frac{d^2\psi_n(Q)}{dQ^2}+(2E_n-Q^2)\psi_n(Q)=0. \tag{54}$$

a general technique called the Sommerfeld polynomial method [**?**] can be applied to solve (**??**). This method consists of four steps:

- An asymptotic solution is obtained.
- A differential equation for the remainder is determined.
- The remainder is expressed as a power series, and a recursion formula is developed for the coefficients.

- Finally, the power series is truncated to obtain quantized eigenvalues.

Step 1: Asymptotic solution

Since the range of coordinate of the harmonic oscillator is $-\infty \leq u \leq \infty$, the range of the Q coordinate is the same. Thus, we seek an asymptotic solution to the equation as $Q \to \pm\infty$. The equation

$$\frac{d^2\psi_n(Q)}{dQ^2} + (2E_n - Q^2)\psi_n(Q) = 0 \tag{55}$$

takes the form

$$\frac{d^2\psi_n(Q)}{dQ^2} - Q^2\psi_n(Q) = 0 \tag{56}$$

in the limit as $Q \to \pm\infty$ since $Q^2 \gg E_n$ in the factor $2E_n - Q^2$. Rearranging the equation yields

$$\frac{d^2\psi_n(Q)}{dQ^2} = Q^2\psi_n(Q), \tag{57}$$

and admits solution of the form

$$\psi_n(Q) \approx e^{\pm Q^2/2}, \tag{58}$$

in the limit as the absolute value of Q becomes large. Since the wavefunction must remain finite as $Q \to \pm\infty$, we have to throw out the solution with the positive exponent since it blows up in the limit. Therefore, the asymptotic solution has the form $\psi_n(Q) \approx e^{-Q^2/2}$ as $Q \to \pm\infty$.

Step 2: Equation for remainder

Having the asymptotic form of the solution, an equation for the remainder is sought. In this scope, the full solution is written in the form

$$\psi_n(Q) \approx S_n(Q)e^{\pm Q^2/2}, \tag{59}$$

where the asymptotic form has been explicitly included, and $S_n(Q)$ is the remainder function. To obtain a differential equation governing the remainder function, the full solution is substituted back into the original equation (**??**) . Before substitution, the second derivative should be evaluated. Obtaining the second derivative of $\psi_n(Q)$ and substituting into (**??**) yields

$$e^{\pm Q^2/2}\left[S_n''(Q) - 2QS_n'(Q) - S_n(Q) + 2E_nS_n(Q)\right] = 0. \tag{60}$$

The terms involving Q^2 cancel to give

$$e^{\pm Q^2/2}\left[S_n''(Q) - 2QS_n'(Q) - S_n(Q) + Q^2 S_n(Q)\right] + (2E_n - Q^2)S_n(Q)e^{\pm Q^2/2} = 0. \tag{61}$$

Dividing both side of the later equation by the factor $e^{\pm Q^2/2}$ leads to the differential equation for the remainder,

$$\frac{d^2 S_n(Q)}{dQ^2} - 2Q\frac{dS_n(Q)}{dQ} + (2E_n - 1)S_n(Q) = 0. \tag{62}$$

Step 3: Polynomial solution for remainder

The solution of (**??**) is assumed to be in the form of a power series,

$$S_n(Q) = \sum_{n=0}^{\infty} a_n Q^n, \tag{63}$$

where a_n are coefficients to be found. The aim is to find the coefficients a_n such that the function $S_n(Q)$ satisfies (**??**). To obtain the coefficients a_n, we must first compute the derivatives of $S_n(Q)$ and substitute them into the differential equation.

Substituting the expressions for $S_n(Q)$ and its first and second derivatives into (**??**) yields

$$\sum_{n=2}^{\infty} n(n-1)a_n Q^{n-2} - 2Q\sum_{n=1}^{\infty} n a_n Q^{n-1} + (2E_n - 1)\sum_{n=0}^{\infty} a_n Q^n = 0. \tag{64}$$

In order to combine the power series in (**??**) the limits must match.This can be achieved by rewriting the first power series for the second derivative in the form

$$S_n''(Q) = \sum_{n=0}^{\infty}(n+1)(n+2)a_{n+2}Q^n. \tag{65}$$

One can verify that this form is identical to the original form for the second derivative by expanding the series. The second power series in (**??**), the one for the first derivative, can be rewritten by adding in a term that is zero,

$$S_n'(Q) = \sum_{n=0}^{\infty} n a_n Q^{n-1}. \tag{66}$$

Using (**??**) and (**??**) in (**??**), we get

$$\sum_{n=0}^{\infty}(n+1)(n+2)a_{n+2}Q^n - 2\sum_{n=0}^{\infty} n a_n Q^n + (2E_n - 1)\sum_{n=0}^{\infty} a_n Q^n = 0. \tag{67}$$

Notice that now all the power series have the same range and also the same power of Q, so we can collect terms and add the power series,

$$\sum_{n=0}^{\infty} \left[(n+1)(n+2)a_{n+2} - 2na_n + (2E_n - 1)a_n\right] Q^n = 0. \tag{68}$$

or

$$\sum_{n=0}^{\infty} \left[(n+1)(n+2)a_{n+2} - (2n+1-2E_n)a_n\right] Q^n = 0. \tag{69}$$

The functions Q^0, Q^1, Q^2, ..., Q^n in the summation form a complete, linearly independent set. The only way for the equation to be satisfied is if each factor multiplying the powers is independently set equal to zero. Thus we must have

$$(n+1)(n+2)a_{n+2} - (2n+1-2E_n)a_n = 0. \tag{70}$$

Solving (**??**) for the coefficient a_{n+2} yields,

$$a_{n+2} = \frac{2n+1-2E_n}{(n+1)(n+2)} a_n. \tag{71}$$

(**??**) is called a recursion formula or recursion relation. Given the value of one coefficient, such as a_0, it allows us to determine the values of all others. This particular formula is called a two-term recursion relation because the coefficients are spaced two units apart (n and $n+2$). An interesting feature of the two-term recursion formula is that the coefficients generated are either all even or all odd. If we start with a_0, then the coefficients generated from the recursion formula are a_2, a_4, a_6, a_8, etc. On the other hand, if we start with a_1, then the coefficients generated from the recursion formula are a_3, a_5, a_7, a_9, etc. This means that there are two types of solutions, even and odd, such that

$$\psi_n(Q) = e^{-Q^2/2} \sum_{\ell=0}^{\infty} a_{2\ell} Q^{2\ell}, \tag{72}$$

for even solutions, and

$$\psi_n(Q) = e^{-Q^2/2} \sum_{\ell=0}^{\infty} a_{2\ell+1} Q^{2\ell+1}, \tag{73}$$

for odd solutions. Note that the fact that we got solutions that are either even or odd is a reflection of the symmetry of the potential. In general, for arbitrary differential equation, this will not be the case.

Step 4: Truncation of the series

The solutions (**??**) and (**??**) involve infinite power series. They are valid solutions for the differential equation (**??**). However, they do not satisfy all the criteria of a wavefunction. One of the requirements for a wavefunction is that it remains finite so that its square is integrable (in order to represent a probability). Because the solutions contain infinite power series, they grow infinitely as $Q \to \pm\infty$. The only way to address this issue is by truncating the infinite power series so that the wavefunction remains finite.

Suppose the truncation of the power series occurs after v terms in the power series. All the higher coefficients then become zero, i.e., $a_{v+2} = a_{v+4} = a_{v+6} = ... = 0$. Using the recursion relation (**??**), this means

$$a_{v+2} = \frac{2v + 1 - 2E_v}{(v+1)(v+2)} a_v. \tag{74}$$

Since we truncated the series at v terms, we know that the coefficient a_v is not zero. Therefore, we can divide both sides of (**??**) by a_v,

$$\frac{2v + 1 - 2E_v}{(v+1)(v+2)} = 0. \tag{75}$$

Multiplying by the factor in the denominator in (**??**) and solving for the dimensionless energy E gives

$$E_v = v + \frac{1}{2}, \qquad v = 0, 1, 2, 3, ... \tag{76}$$

This is the quantization condition for the energy. Note that the quantum number v can be any integer since truncation of the power series can occur at any term less than an infinite value. To get the quantization for the original energy, recall the definition of the dimensionless energy E_v form our change of variables and obtain

$$\varepsilon_v = T^* V_0^{1/2} \left(v + \frac{1}{2} \right), \qquad v = 0, 1, 2, 3, ... \tag{77}$$

II.4.4 Criteria for first-order phase transitions in quantum-mechanical tunneling

The characteristic ways in which phase transitions appear in quantum-mechanical tunneling processes have been worked out in literature. Three criteria for first-order phase transitions are presented in the following:

- A first-order transition occurs when a sharp change is observed in the plot of the action S versus temperature T. In Ref. [**?**], this change was found to be very analogous to that of the free enthalpy versus pressure of a van der Waals gas, whose equation of state plotted as pressure versus volume corresponds to the plot of the period $P(E)$ (of the periodic bounce or instanton) versus energy in the consideration of quantum-mechanical systems.

- In the case of a periodic problem in Euclidean time, the derivative of the action with respect to the energy E is the negative of the oscillation time $\tau(E)$ or period $P(E)$ at that energy that has to be identified with $-\hbar/T$ [**?**]. If $\tau(E)$ is a monotonically decreasing function with increasing E, one has a second-order transition; if $\tau(E)$ has a minimum and then rises again within the domain $0 < E <$ barrier height, one has a first-order transition, i.e., in this case there is an energy E_c within this range with $T_c = \hbar/\tau(E_c)$ at which the first-order transition takes place.

- A criterion for a first transition is also obtained by studying the Euclidean time period in the neighborhood of the sphaleron configuration at the peak of the potential barrier, i.e., at the bottom of the well of the inverse potential [**?**]. If the frequency of oscillation about the sphaleron point is ω_s and oscillations different form ω_s about it are possible, a first-order transition requires $\omega^2 > \omega_s^2$ or $\tau - \tau_s < 0$. The mathematical analog of this criterion is obtained from the following analytical development.
  Consider a Euclidean action integral of the form

$$S = \int d\tau \left[\frac{1}{2}M(q)\dot{q}^2 + V(q)\right] \tag{78}$$

  with Euler-Lagrange equation

$$M(q)\ddot{q} + \frac{1}{2}\frac{\partial M(q)}{\partial q}\dot{q}^2 = \frac{\partial V(q)}{\partial q} \tag{79}$$

  and $q(\tau + P) = q(\tau)$, where $P = 1/T$ is the period, T the temperature, and V a bistable potential field. Since the solutions near the sphaleron solution at the top of the potential barrier have information on the order of the "phase" transition between quantum and thermal activity regimes, the present analysis is confined to this region in solution space. We

define (as for a maximum of $V(q)$ at q_s)

$$\omega_s^2 \equiv \frac{V''(q_s)}{M(q_s)} \tag{80}$$

and, in (**??**), we set q as $q = q_s + \eta(\tau)$, where q_s is the sphaleron position with $V'(q_s) = 0$ and $\eta(\tau)$ representing some fluctuations around the sphaleron. Expanding $M\left[q_s + \eta(\tau)\right]$ and $V\left[q_s + \eta(\tau)\right]$ and their derivatives in powers of $\eta(\tau)$, we obtain the fluctuation equation

$$\begin{aligned} &\left[M(q_s) + M'(q_s)\eta(\tau) + \frac{1}{2}M''(q_s)\eta^2(\tau)\cdots\right]\ddot{\eta}(\tau) \\ +\frac{1}{2}&\left[M'(q_s) + M''(q_s)\eta(\tau) + \frac{1}{2}M'''(q_s)\eta^2(\tau)\cdots\right]\ddot{\eta}^2(\tau) \\ &= V''(q_s)\eta(\tau) + \frac{1}{2}V'''(q_s)\eta^2(\tau) + \frac{1}{6}V''''(q_s)\eta^3(\tau)\cdots. \end{aligned} \tag{81}$$

We are interested in small fluctuations $\eta^3(\tau)$. The first-order equation

$$M(q_s)\ddot{\eta}(\tau) - V''(q_s)\eta(\tau) = 0 \tag{82}$$

has the even solution

$$\eta(\tau) = a\cos(\omega_0\tau), \quad \text{where} \quad \omega_0^2 = \omega_s^2. \tag{83}$$

This is the solution we choose for the following reason, which we explain for simplicity for the case $M(q) = 1$. The classical equation $\ddot{q} = \partial V/\partial q$ is invariant under time translations $\tau \to \tau + const$. The operator of the fluctuation equation or second variational derivative of the action S at the classical configuration q_c must therefore possess a zero eigenvalue with eigenfunction $dq_c/d\tau$. This operator is also obtained by differentiating the classical equation and implies the fluctuation equation

$$\left(\frac{d^2}{d\tau^2} - V''(q_c)\right)\psi_i = \omega_i\psi_i. \tag{84}$$

If q_c is the constant q_s, and if this is a saddle point, we must have (at and around q_s) $\omega_1^2 = 0$, ψ_i odd (the first excited state), and $\omega_0^2 < 0$, and ψ_0 even (the ground state). Thus in this case, ψ_0 is proportional to $\cos(\omega_0\tau)$. This explains the ansatz (**??**), which is the component of a general fluctuation in the direction of the negative eigenmode of the fluctuation equation.

For the solution in the next order of perturbation theory we set

$$\eta(\tau) = a\cos(\omega\tau) + a^2\eta_1(\tau), \quad \omega^2 = \omega_0^2 + a\Delta_1\omega^2. \tag{85}$$

(**??**) is inserted (**??**) while retaining only terms up to and including those of $O(a^2)$. Also powers of $\cos(\omega\tau)$ are re-expressed in terms of $\cos(n\omega\tau)$, where n is an integer. Using (**??**) yields

$$\begin{aligned} a^2\left[M(q_s)\frac{d^2}{d\tau^2} - V''(q_s)\right]\eta_1(\tau) = a^2\Delta_1\omega^2 M(q_s)\cos(\omega_0\tau) \\ +a^2\left[\left(\frac{\omega^2 M'(q_s) + V'''(q_s)}{4}\right) + \left(3\frac{\omega^3 M'(q_s) + V'''(q_s)}{4}\right)\cos(2\omega_0\tau)\right]. \end{aligned} \tag{86}$$

The fluctuation $\eta_1(\tau)$ is now expanded in terms of lowest-order functions, i.e., setting

$$\eta_1(\tau) = \sum_{n=0,1,2,\ldots} c_n\cos(n\omega_0\tau) \tag{87}$$

and using the orthogonality of the latter, i.e.,

$$\int_{-P/2}^{P/2}\cos(m\omega_0\tau)\cos(n\omega_0\tau)d\tau = \frac{P}{2}\delta_{mn}, \quad P = \frac{2\pi}{\omega_0}. \tag{88}$$

The remaining steps are standard in perturbation theory. Thus, multiplying (**??**) by $\cos(\omega_0\tau)$ and integrating one obtains immediately that

$$\Delta_1\omega^2 = 0 \tag{89}$$

and the fluctuation $\eta_1(\tau)$ is obtained to be

$$\eta_1(\tau)g_1 + g_2\cos(2\omega_0\tau), \tag{90}$$

with

$$g_1(\omega) = -\frac{\omega^2 M'(q_s) + V'''(q_s)}{4V''(q_s)}, \quad \text{and} \quad g_2(\omega) = -\frac{3\omega^2 M'(q_s) + V'''(q_s)}{4\left[4\omega_0^2 M(q_s) + V''(q_s)\right]}, \tag{91}$$

where in these first-order expressions $\omega^2 = \omega_0^2$. Thus, in order to obtain a non-vanishing deviation from the sphaleron value, we have to proceed to the next order of perturbation

theory. Hence we set

$$\eta(\tau) = a\cos(\omega\tau) + a^2\eta_1(\tau) + a^3\eta_2(\tau), \quad \omega^2 = \omega_0^2 + a\Delta_1\omega^2 + a^2\Delta_2\omega^2, \tag{92}$$

and insert this into (**??**) and expand up to and including terms of $O(a^3)$. The procedure is the same as before but the calculations are now much more involved, so that we can only cite a main intermediate result. The equation corresponding to (**??**) above and multiplied by $\cos(\omega_0\tau)$ and integrated over yields the equation

$$\begin{aligned} -aM(q_s)a^2\Delta_2\omega^2\frac{P}{2} = a^3V'''(q_s)\left(\frac{2g_1+g2}{4}\right)P + a^3\frac{1}{6}V''''(q_s)\frac{3}{8}P \\ +a^3 4M'(q_s)\omega^2 g_2\frac{P}{4} + a^3M'(q_s)\omega^2\left(\frac{2g_1+g2}{4}\right)P \\ +a^3\frac{1}{2}M''(q_s)\omega^2\frac{3}{8}P - 2a^3M'(q_s)\omega^2 g_2\frac{P}{4} - a^3\frac{1}{2}M''(q_s)\omega^2\frac{P}{8}. \end{aligned} \tag{93}$$

From this the condition of a first-order phase transition, i.e., $\Delta_2\omega^2 > 0$, becomes

$$\left[V'''(q_s)\left(\frac{2g_1+g2}{2}\right) + \frac{V''''(q_s)}{8} + M'(q_s)\omega^2 g_2 + M'(q_s)\omega^2\left(\frac{2g_1+g2}{2}\right) + \frac{M'(q_s)\omega^2}{4}\right]_{\omega_0} < 0. \tag{94}$$

II.5 Numerical treatment of deterministic differential equations

Mathematical modeling of physical systems may lead to partial differential equations. The derivation of these equations often neglects fluctuations inherent to the system as well as the influence of the surrounding. We can cite two typical examples of such equations.

we first cite the wave equation governing the propagation of waves in a media subjected to an external force field. In general this equation is obtain in a general (dimensionless) form similarly to (**??**), that is

$$\frac{\partial^2 u}{\partial t^2} - \frac{\partial^2 u}{\partial x^2} + f(u) = 0. \tag{95}$$

An example of physical model form which (**??**) can be derived was discussed in Sec. **??**.

Secondly, we cite the Schrödinger equation that governs the evolution of an element $\psi(t)$ describing the state of a quantum system at a particular time t. The square of the modulus of $\psi(t)$ represents the outcome probability densities of all possible measures of a system. Choos-

ing a base x corresponding to the representation of position in one dimension, the Schrödinger equation can be written on the form

$$i\hbar\frac{\partial\psi(x,t)}{\partial t} = -\frac{\hbar^2}{2m}\frac{\partial^2\psi(x,t)}{\partial x^2} + U_0(x,t)\psi(x,t), \tag{96}$$

where $\hbar$ is the Dirac constant, m the mass of element composing the system and $U_0(x,t)$ a potential field.

The Schrödinger equation involves linear operators , thus every linear combination of solution is a solution of the equation. This leads to favor the search of solutions with great practical and theoretical interest: The eigenstates of the Hamiltonian operator. This states are solution to the eigenvalue problem described by the equation

$$\left(\frac{\hbar^2}{2m}\frac{\partial^2}{\partial x^2} - V_0(x)\right)\psi_n(x) = E_n\psi_n(x), \tag{97}$$

often called time-independent Schrödinger equation. The eigenstate ψ_n are associated to the eigenvalue E_n, that is the energy of the quantum element of which ψ_n is the state.

While (**??**) can be numerically solved using a semi-discrete approach by combining a fourth-order central differential scheme for the spatial derivatives with a fourth-order Runge-Kutta method for the temporal evolution of the solution, (**??**) can be numerically treated using the Numerov method.

II.5.1 Fourth order central-difference scheme for derivatives

In conventional calculus the operation of differentiation of a function is a well-defined formal procedure with the operations highly dependent on the form of the function involved. Many different types of rules are needed for different functions . In numerical methods a digital computer is unemployed which can only perform the standard arithmetic operations of addition, subtraction, multiplication, and division, and certain logical operations. Thus we need a technique for differentiating functions by employing only arithmetic operations. The finite difference calculus satisfies this need.

Consider a function $f(x)$ which is analytic in the neighborhood of a point x. The forward

and backward Taylor series expansions about x are respectively

$$f(x+h) = f(x) + hf'(x) + \frac{h^2}{2}f''(x) + \frac{h^3}{6}f'''(x) + \frac{h^4}{24}f''''(x) + ..., \tag{98}$$

$$f(x-h) = f(x) - hf'(x) + \frac{h^2}{2}f''(x) - \frac{h^3}{6}f'''(x) + \frac{h^4}{24}f''''(x) - .... \tag{99}$$

Subtracting the backward expansion (**??**) from the forward expansion (**??**), we note that the terms involving even powers of h cancel, yielding

$$f(x+h) - f(x-h) = 2hf'(x) + \frac{h^3}{3}f'''(x) + ... \tag{100}$$

or, solving for $f'(x)$,

$$f'(x) = \frac{f(x+h) - f(x-h)}{2h} + \frac{h^2}{6}f'''(x) + ... \tag{101}$$

Employing subscript notation,

$$f'(x) = \frac{f_{j+1} - f_{j-1}}{2h} + O(h^2). \tag{102}$$

This differential representation, called a central differential difference representation, is accurate to $O(h^2)$. Note that the point x itself is not involved, and that from the error in term in (**??**), this expression is exact for polynomials of degree 2 and lower. An expression of $O(h^2)$ for $f''(x)$ is readily obtainable from (**??**) and (**??**) by adding these equations and solving for $f''(x)$ to yield

$$f'(x) = \frac{f_{j+1} - 2f_j + f_{j-1}}{h^2} + O(h^2). \tag{103}$$

To obtain $f'''(x)$ and $f^{iv}(x)$ requires one additional Taylor series expansion in each direction and some manipulations similar to those carried out to obtain $f'(x)$ and $f''(x)$. A convenient memory aid for these central difference expressions of $O(h^2)$ in terms of ordinary forward and backward differences is given by

$$\frac{d^n f}{dx^n} = \frac{\nabla^n f_{j+n/2} + \Delta^n f_{j-n/2}}{2h^2} + O(h^2), \quad n \text{ even} \tag{104}$$

$$\frac{d^n f}{dx^n} = \frac{\nabla^n f_{j+(n-1)/2} + \Delta^n f_{j-(n-1)/2}}{2h^2} + O(h^2), \quad n \text{ odd}. \tag{105}$$

Central difference expressions of $O(h^4)$ may be obtained by employing many tedious operations

with the Taylor series expansions which will not be repeated here. These expressions for derivatives up to order four are tabulated in For illustration, from the table the approximation of $f''(x)$ up to the fourth-order ($O(h^4)$) gives

$$f''(x) = \frac{1}{12h^2}(-f_{j-2} + 16f_{j-1} - 30f_j + 16f_{j+1} - f_{j+2}) + O(h^4). \tag{106}$$

II.5.2 Fourth order Runge-Kutta method for initial value problems

In this section, we wish to approximate the solution to a first order differential equation given by

$$\frac{y(t)}{dt} = y'(t) = f(y(t), t), \quad y(t_0) = y_0. \tag{107}$$

Runge-Kutta (RK) methods, order 2 or 4, are very commonly used for solving ordinary differential equations (ODE) [**?**, **?**, **?**]. These are single step methods, directly derived from Euler's method [**?**, **?**], which is an RK1 method. They have the advantage of being simple to program and fairly stable for common physics functions. In terms of numerical analysis, they have above all the immense advantage of not requiring anything other than knowledge of the initial values. They start up on their own.

Nevertheless, they have a drawback, especially the method RK of order 4 (RK4): they are quite consuming in computing time. They can therefore be used when the computation time is not too great. Otherwise, it is better to turn to a predictor / corrector method (Adams for example) [**?**, **?**, **?**]. If the required precision is very important, you will have to choose the adaptive RK4 method [**?**] or better still towards the Bulirsch-Stoer method [**?**].

Here is a quick description of the RK4 method. Only the results will be presented, for more details on the derivation of the methods see Ref. [**?**].

Let's denote the time at the nth time-step by t_n and the computed solution at the nth time-step by y_n, i.e., $y_n \equiv y(t = t_n)$. The step size h (assumed to be constant for the sake of simplicity) is then given by $h = t_n - t_{n-1}$. We start from Euler's formula [**?**], which gives

$$y_{n+1} = y_n + h * f(x_n, y_n), \quad \text{and} \quad x_{n+1} = x_n + h \tag{108}$$

The second order RK method produces two coefficients k_1 and k_2, which make it possible to

write:

$$k_1 = h * f(x_n, y_n), \quad k_2 = h * f(x_n + h/2, y_n + k_1/2), \quad \text{and} \quad y_{n+1} = y_n + k_2 + O(h^3). \tag{109}$$

This method therefore requires two evaluations of f. The consistency error is in $O(h^3)$ and the global convergence error is of order $O(h^2)$. To obtain more precision, but by doubling the computation time since we carry out 4 evaluations of f, here is the RK4 method:

$$\begin{aligned} k_1 = h * f(x_n, y_n), \quad k_2 = h * f(x_n + h/2, y_n + k_1/2) \\ k_3 = h * f(x_n + h/2, y_n + k_2/2), \quad k_4 = h * f(x_n + h, y_n + k_3), \\ \text{and} \quad y_{n+1} = y_n + \frac{1}{6}(k_1 + 2k_2 + 2k_3 + k_4) + O(h^5). \end{aligned} \tag{110}$$

The RK4 method therefore requires 4 evaluations of f, which can be troublesome if f is complicated. The consistency error is in $O(h^5)$ and the global convergence error is of order $O(h^4)$.

II.5.3 Numerov method for eigenvalue problems

The Numerov method is a general numerical method to solve second order differential equations of the form

$$\frac{d^2y}{dx^2} + g(x)y(x) + s(x) = 0, \tag{111}$$

where $g(x)$ and $s(x)$ are continuous functions on the domain $[a, b]$. (**??**) becomes (**??**) by considering the change of variables $y(x) = \eta(x)$, $g(x) = (\omega^2 - \omega_0^2 U(x))/C_0^2$, and $s(x) = 0$. To solve (**??**), we will need to solve the problem as a boundary value problem : $y(a)$ and $y(b)$ are known.

Numerov Algorithm

At this point, the first thing to be done is to discretize the interval $[a, b]$ using n equally spaced point. That is, the points are equally distributed such that $x_1 = a$, $x_b = b$, and the intermediate points are obtained as $x_i = i * a$. Then the solution $y(x)$ is also obtained as a discrete set of point for each x_i. This means that we now have $y(x) = y(x_i) = y_i$, and (**??**) becomes

$$\frac{d^2y_i}{dx^2} + g_i(x)y_i(x) + s_i(x) = 0. \tag{112}$$

To obtain the wanted relation we start by writing the Taylor expansion of the function $y(x)$ around a point x_0. If we denote the space between x and x_0 by $h = x - x_0$, we can use the development than in Sec.**??** to write

$$y(x+h) + y(x-h) = 2y(x) + h^2 y''(x) + \frac{h^4}{12} y''''(x) + O(h^6), \tag{113}$$

which is equivalent, by using the discrete notation, to

$$y_{i+1} = -y_{i-1} + 2y_i + h^2 y_i'' + \frac{h^4}{12} y_i'''' + O(h^6). \tag{114}$$

Now, to solve (**??**) for y_1 we first obtain the expression for y_i'' from (**??**), and expression for $y_i^{(4)}$ by differentiating (**??**) twice and approximate it the same way we did above:

$$y_i^{(4)} = \frac{d^2}{dx^2}(-g_i(x)y_i(x) + s_i) = 0, \tag{115}$$

$$h^2 y_i^{(4)} = -g_{i+1}y_{i+1} + s_{i+1} + 2g_i y_i - 2s_i - g_{i-1}y_{i-1} + s_{i-1} + O(h^4). \tag{116}$$

If we now substitute (**??**) and (**??**) in (**??**), we obtain

$$y_{i+1}+y_{i-1} = 2y_i + h^2(-g_i(x)y_i(x)+s_i) + \frac{h^2}{12}(-g_{i+1}y_{i+1}+s_{i+1}+2g_i y_i - 2s_i - g_{i-1}y_{i-1}+s_{i-1}) + O(h^6). \tag{117}$$

If we neglect the terms of order h^6 (**??**) yields the Numerov algorithm:

$$y_{i+1} = \frac{2y_i\left(1 - \frac{5h^2}{12}g_i\right) - y_{i-1}\left(1 + \frac{h^2}{12}g_{i-1}\right) + \frac{h^2}{12}\left(s_{i+1} + 10s_i + s_{i+1}\right)}{1 + \frac{h^2}{12}g_{i+1}}. \tag{118}$$

So with (**??**), we can now find the value of the solution of the differential equation (**??**) at different discrete points y_{i+1} if we have its value at two points (y_{i-1}, y_i). Because we have a discrete interval, all we have to do to find an approximate solution is to find the value for the two first points (x_1 and x_2) then we use (**??**) to find all the values for the next points in the interval $[a, b]$

Numerov method for time-independent Schrödinger equation

In this subsection the Numerov method is used to solve the one-dimensional time-independent Schrödinger equation (**??**). The dimensionless version of this equation can be written as

$$\frac{d^2\psi(x)}{dx^2} + 2(E - U_0(x))\psi(x) = 0. \tag{119}$$

Again, (**??**) agrees with (**??**) with $E = (1/2)\omega^2/C_0^2$ and $U_0(x) = (1/2)\omega_0^2 U(x)$. So, with the analogy $g(x) = 2(E - U_0(x))$ and $s(x) = 0$, we can then use the Numerov method with this differential equation, and (**??**) becomes

$$\psi_{i+1} = \frac{2\psi_i\left(1 - \frac{5h^2}{12}g_i\right) - \psi_{i-1}\left(1 + \frac{h^2}{12}g_{i-1}\right)}{1 + \frac{h^2}{12}g_{i+1}}. \tag{120}$$

We recall that the two first points of a discrete interval where we know the boundary conditions are required to implement the method. So we should first define an interval where we will find the approximate wave function.

The problem is that the wave function has a domain that goes from $-\infty$ to ∞. Thus for most case, the wave function isn't only defined in a small definite interval. But to address this issue we can use the fact that the wavefunction must also respect the following conditions:

- $\psi(x) \to 0$ as $x \to \pm\infty$
- $\int_{-\infty}^{\infty} \psi(x)dx = 1$
- $\psi(x)$ and $\psi'(x)$ are continuous

To define our interval we can use the first condition: we find two points where the wavefunction converges uniformly to zero and is very close to zero, let's call them x_a and x_b. At these points we set the wave function at zero ($\psi(x_a) = 0$ and $\psi(x_b) = 0$). We then have an interval ($[x_a, x_b]$) where we know the limit conditions.

The next is to find these two points where the wavefunction will be set to zero. To do that we restrict our method to bound states (in quantum physics, a bound state is a special quantum state of a particle subject to a potential such that the particle has a tendency to remain localized in one or more regions of space). In such a state, the energy levels are always lower than the maximum value of the potential in the region where the particle is localized. In fact, for a certain

energy level, we can define a classically forbidden region corresponding to a potential energy greater than the energy of the particle.

Furthermore, according to the Born interpretation, the square of the module of the wavefunction represents the probability density to find a particle at a certain point. Such a probability will fastly decrease in the classical forbidden region (because the particle doesn't have a great probability to be bound in such a region). Thus, all we have to do to define an interval with known borders value is to go deep into the classically forbidden region and fix the wavefunction at zero at this point. We then have an interval that goes from x_{min} and x_{max} and where the wavefunction is zero.

We now have to discretize our interval with points equally spaced (of distance h) and approximate the wavefunction. To do so, all we have to do is start from x_{min}, then we define an initial augmentation that corresponds to the value of the wavefunction at the point x_{min+1} (this value is arbitrary, it doesn't change the general look of the wavefunction, it only multiply the latter by an arbitrary numerical value). Knowing these two points, (**??**) can be used to find the value of the wavefunction for all the other points in the interval. However (**??**) requires to make an energy guess. This is the crucial point : the wavefunction will only respect the second boundary condition ($\psi(x_max) = 0$) if the energy guess corresponds to an allowed energy level. We then need to recursively make energy guess and calculate to wavefunction until we find one that respects the conditions at x_{min} and x_{max}.

To synthesize, to find the energy levels, all we have to do is follow this procedure

- Make a guess for an energy level.
- Find the smallest and the greatest meeting points of the potential with this energy (x_a and x_b).
- With these points, go deep into the classically forbidden area and fix the wavefunction at zero for two points ($\psi(x_max) = \psi(x_min) = 0$) that define the interval.
- Discretize the interval $[x_{min}, x_{max}]$ with the desired number of point.
- Define an arbitrary initial augmentation for the value of the wavefunction at x_{min+1}.
- With (**??**) find the value for the wavefunction at all the other points in the interval.

- To verify that E_{guess} corresponds to an energy levels, verify if the value of the wavefunction at the point x_{max} is approximately zero ($\psi(x_max) \approx 0$).
- If it doesn't respect this condition, make a new energy guess.

One question is still left to be answered: having an energy guess that respects the conditions, how to know if this energy level corresponds to the ground state or an excited state? The answer lies in the following theorem.

Theorem For the one-dimensional time-independent Schrödinger equation, the energy level for a given wavefunction corresponds to the number of nodes (the number of time $\psi(x) = 0$) rejecting those when $x \to \pm\infty$.

II.6 Numerical treatment of the stochastic wave equation

In this section, we consider (**??**) in a more general form

$$\frac{\partial^2 u}{\partial t^2}(x,t) = \sum_{i=1}^{n} c_i \frac{\partial^i u}{\partial x^i}(x,t) - \gamma \frac{\partial u}{\partial t}(x,t) + f(u(x,t)), \tag{121}$$

where the second term in the right hand side of the equation is the inertia term accounting for the viscosity of the system, with γ the viscosity parameter. Evidently, in this case the contribution of the force f is only a mean value: Thus, considering an ensemble of identical systems, the change in each system differs from the calculated value by a small amount. These deviations are caused by statistical fluctuations. The stochastic term $\zeta(x,t)$ is defined by its mean value and covariance [**?**, **?**]

$$\langle \zeta(x,t) \rangle = 0, \quad \langle \zeta(x,t)\zeta(x',t') \rangle = \delta(x-x')\delta(t-t'). \tag{122}$$

The stochastic partial differential equation obtained from (**??**) then reads

$$\frac{\partial^2 u}{\partial t^2}(x,t) = \sum_{i=1}^{n} c_i \frac{\partial^i u}{\partial x^i}(x,t) - \gamma \frac{\partial u}{\partial t}(x,t) + f(u(x,t)) + \sigma(u(x,t))\zeta(x,t) \tag{123}$$

In (**??**), the function $\sigma(u)$ is a weighting factor which controls the influence of fluctuation on the system. In the special case $\sigma(u) =$ constant one speaks of additive noise, otherwise the noise is called multiplicative. With (**??**), it is possible to numerically obtain characteristic properties of the kink in our model, but also quantities such as correlation functions, probability density

function, and so on.

Applying the change of variables $v = \partial u/\partial t$, (**??**) splits to the system of two equation:

$$\frac{\partial u}{\partial t} = v(x,t) \tag{124}$$

and

$$\frac{\partial v}{\partial t}(x,t) = \sum_{i=1}^{n} c_i \frac{\partial^i u}{\partial x^i}(x,t) - \gamma v(x,t) + f(u(x,t)) + \sigma(u(x,t))\zeta(x,t) \tag{125}$$

We can now proceed with the numerical treatement of the problem. While an Euler algorithm (**??**) or Runge-kutta algorithm as in (**??**) can be used to solve (**??**), the stochastic nature the PDE (**??**) requires of a more complicated approach.

II.6.1 An algorithm for the solution of SPDEs

The aim of this section is to approximate the nth order equation (**??**) by a system of stochastic ordinary differential equations. Apart from handling the stochastic term $\zeta(x,t)$ this procedure is similar to the case of deterministic partial differential equations. The stochastic term requires a special treatment which leads to the concept of a stochastic Ito-integral [**?**].

First, we introduce a one-dimensional lattice in space. It is advantageous to choose the lattice points as

$$x_k = \begin{cases} k\Delta x, & \text{if } c_i = 0 \text{ for odd integer } i \\ k\frac{\Delta x}{2}, & \text{otherwise.} \end{cases} \qquad \Delta x \ll 1, \quad k \quad \text{integral number,} \tag{126}$$

where c_i denotes the constant of (**??**). To approximate this equation by a system of stochastic ordinary differential equation we integrate the partial equation n times according to its order over the space variable x. For the sake of simplicity we introduce the integration operator

$$\Im_n = \int_{-\frac{\Delta x}{2}}^{\frac{\Delta x}{2}} dy_1 \int_{-\frac{\Delta x}{2}}^{\frac{\Delta x}{2}} dy_2 \cdots \int_{-\frac{\Delta x}{2}}^{\frac{\Delta x}{2}} dy_n, \tag{127}$$

where Δx is the lattice spacing introduced above. In (**??**) we also replace x by $x_k + \sum_{r=1}^{n} y_r$; the variables y_r serve as integration variables which disappear when the integration is carried out.

Applying the integration operator $\Im_n$ on (**??**) we get

$$\Im_n\left\{\frac{\partial v}{\partial t}\left(x_k+\sum_{r=1}^{n}y_r,t\right)\right\}=\sum_{i=1}^{n}c_i\Im_n\left\{\frac{\partial^i u}{\partial x^i}\left(x_k+\sum_{r=1}^{n}y_r,t\right)\right\}-\gamma\Im_n\left\{v\left(x_k+\sum_{r=1}^{n}y_r,t\right)\right\}$$
$$+\Im_n\left\{f\left(u\left(x_k+\sum_{r=1}^{n}y_r,t\right)\right)\right\}+\Im_n\left\{\sigma\left(u\left(x_k+\sum_{r=1}^{n}y_r,t\right)\right)\zeta\left(x_k+\sum_{r=1}^{n}y_r,t\right)\right\} \quad (128)$$

Except for the last integral all terms can be approximated by a straightforward calculation. The following formulas are obtained by expanding the integrand in a Taylor series around x_k:

$$\Im_n\left\{\frac{\partial v}{\partial t}\left(x_k+\sum_{r=1}^{n}y_r,t\right)\right\} = (\Delta x)^n\frac{\partial v}{\partial t}(x_k,t)+O((\Delta x)^{n+2}), \quad (129)$$

$$\sum_{i=1}^{n}c_i\Im_n\left\{\frac{\partial^i u}{\partial x^i}\left(x_k+\sum_{r=1}^{n}y_r,t\right)\right\} = \sum_{i=1}^{n}(\Delta x)^{n-i}c_i\sum_{j=0}^{i}\binom{i}{j}(-1)^j u\left(x_k+\left(\frac{i}{2}-j\right)\Delta x,t\right)$$
$$+O((\Delta x)^{n+2}), \quad (130)$$

$$\gamma\Im_n\left\{v\left(x_k+\sum_{r=1}^{n}y_r,t\right)\right\} = (\Delta x)^n\gamma v(x_k,t)+O((\Delta x)^{n+2}), \quad (131)$$

$$\Im_n\left\{f\left(u\left(x_k+\sum_{r=1}^{n}y_r,t\right)\right)\right\} = (\Delta x)^n f(u(x_k,t))+O((\Delta x)^{n+2}). \quad (132)$$

The evaluation of the last integral appearing in (**??**) is lengthy. Nevertheless, this calculation is fundamental for our purpose. We obtain

$$\Im_n\left\{\sigma\left(u\left(x_k+\sum_{r=1}^{n}y_r,t\right)\right)\zeta\left(x_k+\sum_{r=1}^{n}y_r,t\right)\right\}=\sigma(u(x_k,t))(\Delta x)^{n-1/2}+O((\Delta x)^{n+1/2}), \quad (133)$$

where $\xi_k(t)$ denotes Gaussian white noise. Its features such as zero mean and covariance

$$\langle\xi_k(t)\rangle=0,\quad \langle\xi_k(t)\xi_{k'}(t')\rangle=\delta(t-t')\delta_{kk'} \quad (134)$$

are analogous to properties (**??**) of the Gaussian random field $\zeta(x,t)$.

Inserting results (**??**)-(**??**) into (**??**) and dividing by $(\Delta x)^n$ leads to

$$\frac{\partial v}{\partial t}(x_k,t) = \sum_{i=1}^{n}(\Delta x)^{n-i}c_i\sum_{j=0}^{i}\binom{i}{j}(-1)^j u\left(x_k+\left(\frac{i}{2}-j\right)\Delta x,t\right)-\gamma v(x_k,t)$$
$$+ f(u(x_k,t))+\frac{\sigma(u(x_k,t))}{\sqrt{\Delta x}}\xi_k(t)+O(\sqrt{\Delta x}). \quad (135)$$

All space coordinates of this equation are lattice points corresponding to (**??**). Defining functions

$$U_k(t) = \begin{cases} u(x_k,t) = u(k\Delta x,t), & \text{if } c_i = 0 \text{ for odd integers } i \\ u(x_k,t) = u\left(k\frac{\Delta x}{2},t\right), & \text{otherwise,} \end{cases} \tag{136}$$

$$I(i,j) = \begin{cases} \frac{1}{2}i - j, & \text{if } c_i = 0 \text{ for odd integers } i \\ i - 2j, & \text{otherwise,} \end{cases} \tag{137}$$

and neglecting the terms $O(\sqrt{\Delta x})$, the result (**??**) can be written as

$$\begin{aligned} \frac{\partial V_k}{\partial t}(t) &= \sum_{i=1}^{n} \frac{c_i}{(\Delta x)^i} \sum_{j=0}^{i} \binom{i}{j} (-1)^j U_{k+I(i,j)}(t) - \gamma V_k(t) \\ &+ f(U_k(t)) + \frac{\sigma(U_k(t))}{\sqrt{\Delta x}} \xi_k(t). \end{aligned} \tag{138}$$

The system of stochastic ordinary differential equations can be solved with the aid of a stochastic Euler-procedure. Next, we briefly review this procedure

II.6.2 Euler-procedure for numerical solution of the system of Stochastic ordinary differential equations

We refer to the Stochastic Euler-procedure which is appropriate for the numerical solution of systems of stochastic differential equations [**?**, **?**]: As starting point we consider the system

$$\frac{\partial W_k}{\partial t}(t) = g_k(W(t)) + \sigma_k(W(t))\xi_k(t), \tag{139}$$

where k labels the equations. $W(t)$ denotes that g_k and σ_k may depend on all components $W_i(t)$. The recursion formula for the approximation of this system is

$$W_k(l+1,h) = W_k(l,h) + hg_k(W_k(l,h)) + \sqrt{h}\sigma_k(W_k(l,h))\gamma_k(l), \tag{140}$$

where $h \ll 1$ is a tiny time step. $\gamma_k(l)$, $k \in \mathbb{N}$ is a series of independent uniformly distributed random number with mean value 0 and variance 1. It can be shown [**?**] that the discretization

error of (**??**) is of order $O(h^{3/2})$. $W_k(l,h)$ is an approximation of the exact value $W_k(t=lh)$.

For the system (**??**) the stochastic Euler-procedure presented above leads to the difference equation

$$\begin{aligned} V_k(l+1,h) &= V_k(l,h) + h\sum_{i=1}^{n}\frac{c_i}{(\Delta x)^i}\sum_{j=0}^{i}\binom{i}{j}(-1)^j U_{k+I(i,j)}(l,h) - \gamma h V_k(l,h) \\ &+ hf(U_k(t)) + \frac{\sigma(U_k(l,h))}{\sqrt{\frac{h}{\Delta x}}}\xi_k(l). \end{aligned} \tag{141}$$

With this formula we have a method at our disposal to solve numerically (**??**). To complete the description, initial conditions are necessary and one defines

$$U_k(0,h) = \begin{cases} u(k\Delta x,0), & \text{if } c_i = 0 \text{ for odd integers } i \\ u(k\Delta x/2,0), & \text{otherwise,} \end{cases} \tag{142}$$

and $V_k(0,h) = v(k\Delta x,0)$. To handle the numerical simulations the stability condition $h < 0.7(\Delta x)^2$ for the lattice spacing Δx and time step h must be taken into account, otherwise the recursion formula (**??**) diverges [**?**]

II.6.3 Generating Gaussian random variables

To realize the simulation described above, we need to generate Gaussian random variables with zero mean. The following method generates two independent zero mean Gaussian variables with variance $\sigma = 1$ [**?**, **?**, **?**]. We first take two random variables, x and y, that are uniformly distributed on the interval $[0,1]$ (All modern programming languages include in-built functions to generate such variables). We then calculate

$$x' = 2x - 1, \text{and} \quad y' = 2y - 1. \tag{143}$$

The new random variables are now uniformly distributed on the interval $[-1,1]$. We now calculate

$$r = x'^2 + y'^2. \tag{144}$$

If $r = 0$, or $r \geq 1$, we return to the first step and find new random variables x and y. However if $r \in]0, 1]$, we then do

$$g_1 = x'\sqrt{-2ln(r)/r}, \text{and} \quad g_2 = y'\sqrt{-2ln(r)/r}. \tag{145}$$

The variables g_1 and g_2 are Gaussian with zero mean and unit variance, and mutually independent. If instead we want g_1 and g_2 to have a variance a, we simply multiply them by $\sqrt{a}$.

II.6.4 Numerical computation of probability density function

Once we have obtained the ability of computing solution $u(x,t)$ of (**??**) according to different realizations of the $\zeta(x,t)$, quantities of interest can be evaluated as time-dependent ensemble averages as it is done for stochastic ordinary differential equations [**?**, **?**]. In the case one wants to estimate the probability density function $\langle u(x,t)\rangle$. First one generates a set of R realizations $u_r(x,t)$, $r = 1, ..., R$. Then The probability density is obtained as the mean value on the realization of the time average of $u(x,t)$. mathematically, the probability density function is evaluated with the formula

$$pdf(x) = \frac{1}{R}\sum_{r=1}^{R}\left(\frac{1}{Nh}\sum_{i=1}^{N+1} u_r(x, t_i + (i-1)h)\right), \tag{146}$$

where t_i and t_f are respectively the initial and final computation time for a realization, and N is the total number of subdivisions of $[t_i, t_f]$ taking the time step h.

II.7 Conclusion

In this chapter, we have described the mathematical modeling of the dynamics of the model used in this thesis. We have presented some analytical and numerical methods used to investigate the nature of transitions in quantum tunneling, the exact integrability of the classical statistical mechanics, and the kink scattering according to two possible scenario in the system. Having a (1+1) dimensional field theory from a first scenario in dynamics of the model, the transfer integral formalism has been applied to study the low-temperature statistical mechanics. Thanks to the Sommerfeld method, the groundstates allowing the calculation of the partition function have been obtained. These results can be confirmed by the numerical treatment of a stochastic wave equation. It is also possible to examine kink-scattering induced phenomena in the theory using numerical schemes such as the Numerov scheme and also the numerical treatment of a wave equation, taking a kink-antikink pair as the initial configuration of the system. In a (0+1) field

theory arising instead from a second scenario, some criteria to consulted to analyze the nature of transitions from a quantum tunneling regime to a thermal hopping regime have been discussed. The methods developed in this chapter are used to obtain the results presented in chapter **??**.

CHAPTER III

RESULTS AND DISCUSSION

III.1 Introduction

In this chapter, we present and discuss the main results of our work using both analytical and numerical methods presented in chapter **??**. This chapter is organized as follows: In section **??**, We consider systems of which the deformability can be modelled by the DK hierachy of parametric potentials. Moreover, we propose a class of DWPs, standing as a new member of the latter family of potentials. The shape parameter of the new potential addresses a deformability of the system resulting in only the variation of the anharmonicity of the potential barrier. The following analysis are implemented for models accounting for the type of deformability addressed by one or several members of the DK family of potentials, including also our newly proposed class of potentials. In section **??** the system is first investigated in the context of phase transitions in quantum tunneling and the influence of the deformability on the nature of the transitions is discussed. Later on, section **??** the solvability condition for the parametrized DWPs is derived. Also, the lowest eigenstate formulation required for the treatment of the low-temperature statistical mechanics of the system is presented. Finally, in section **??** some kink-antikink scattering-induced phenomena arising in the model are presented. In this case however, several DK family members have already been investigated in litterature. Thus, our results are only presented for the case of the newly introduced member of the DK family of potentials.

III.2 The parametrized DWPs

We are interested in $1D$ systems for which the bistable energy landscape is represented by a DWP of the general form:

$$V(u,\mu) = a(\mu)\left[\frac{\sinh^2(\alpha(\mu)u)}{\mu^2} - 1\right]^2, \quad \mu > 0, \tag{147}$$

where $a(\mu) > 0$ and $\alpha(\mu)$ are two functions of the shape deformability parameter μ. From a general standpoint the variable u is a one-component dimensionless field defined on a one-dimensional lattice points. In the context of phenomenological theory for phase transition, this variable plays the role of order parameter. In physical systems such as one-dimensional atomic and molecular chains (our model in chapter **??**), the variable u can be associated with the coordinate of an atom or a molecule relative to a stable equilibrium position along the chain.
$V(u, \mu)$ given by (**??**) defines to a hierachy (a family) of parametric DWPs [**?**, **?**, **?**, **?**, **?**, **?**] whose shape profiles can be tuned differently with respect to the chosen expression of $a(\mu)$ and $\alpha(\mu)$. As previously mentioned in Sec. **??** four cases belonging to this family of potential have already been introduced in literature:

- Model 1

$$\alpha(\mu) = \mu \quad and \quad a(\mu) = a_0, \quad (a_0 = constant). \tag{148}$$

  The model is a DWP whose degenerate minima vary, leaving unchanged the barrier height. In Fig.**??**a we see that an increase of μ keeps the barrier fixed at a_0 while the degenerate minima continuously come close to each other, consequently reducing the barrier width.

- Model 2

$$\alpha(\mu) = sinh^{-1}\mu \quad and \quad a(\mu) = a_0\mu^2 \left[\alpha(\mu)\sqrt{1+\mu^2}\right]^{-2}, \quad (a_0 = constant). \tag{149}$$

  The model is a DWP with fixed degenerate minima while the barrier height stays fixed. Fig.**??**b shows the degenerate minima appearing at $u = \pm 1$ and As μ increases the barrier height continuously decreases. Moreover with this decrease, the peak of the barrier is flattened gradually.

- Model 3

$$\alpha(\mu) = (1+\mu^2)^{-1/2} sinh^{-1}\mu \quad and \quad a(\mu) = a_0\mu^2 \left[sinh^{-1}\mu\right]^{-2} \quad (a_0 = constant). \tag{150}$$

  The model is a DWP with both the degenerate minima and the barrier height simultaneously varying with the shape deformability parameter. In Fig.**??**c we note an increase of the barrier height together with the barrier width as μ increases.

- Model 4

$$\alpha(\mu) = sinh^{-1}\mu, \quad a(\mu) = a_0 \quad (a_0 = constant) \tag{151}$$

In this fourth model, $V(u,\mu)$ is a DWP with two degenerate minima fixed at $u = \pm 1$, and also a barrier height fixed at a constant value a_0. However a variation of μ changes the steepness of the potential walls, and consequently the sharpness (or confinement) of the potential wells. In Fig. **??**, $V(u,\mu)$ is sketched for some arbitrary values of μ. When μ is varied, the slope of the potential walls gets steeper and the mid-height width of the barrier becomes wider. Hence the narrowest part of the potential barrier broadens while the flatness of the barrier top becomes more pronounced, resulting in an enhancement of the confinement of the potential wells.

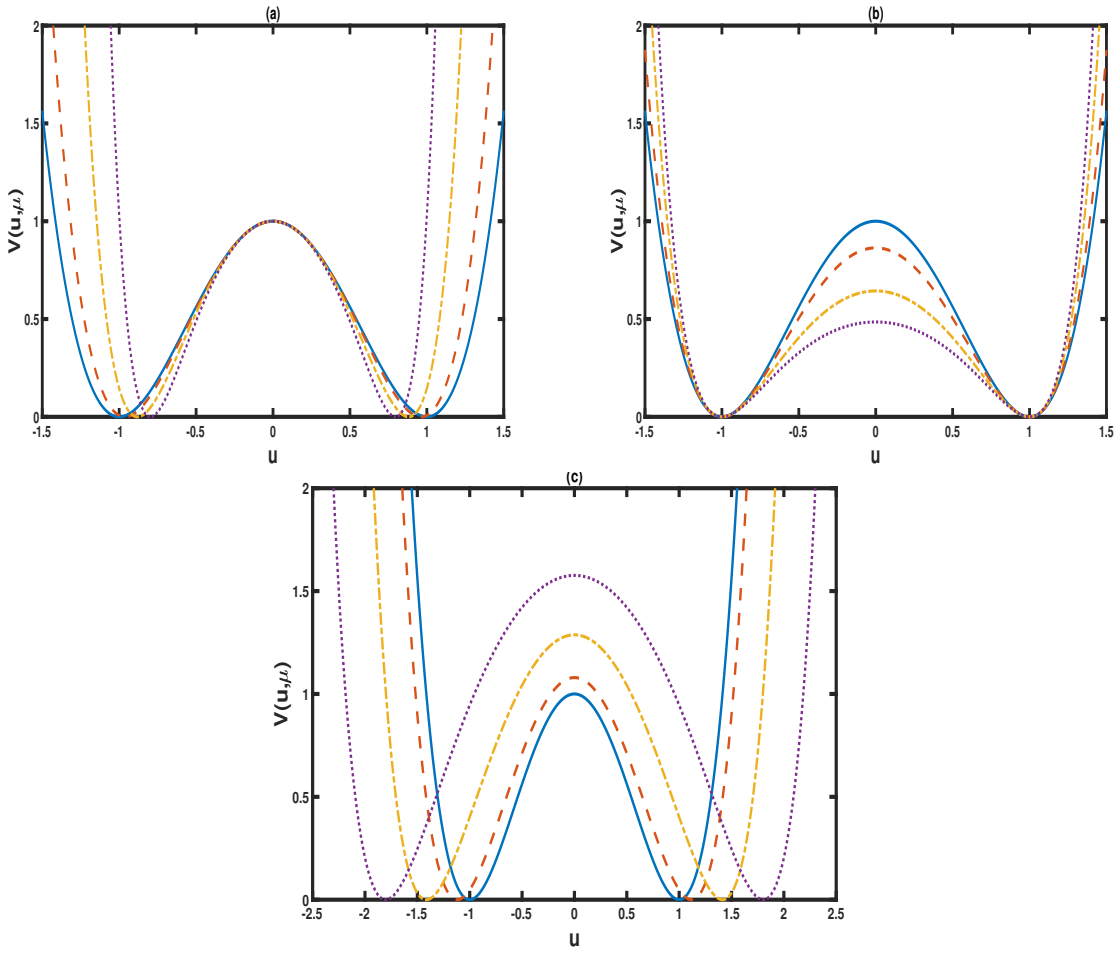

Figure 13: Sketch of the DK family of potentials. (a) First member with variable position of the minima, (b) second member with variable barrier height, (c) third member with variation of both the position of minima and barrier height. For all the graphs, $\mu \to 0$ (Solid line), $\mu = 1$ (Dashed line), $\mu = 2$ (Dashed-dotted line), $\mu = 3$ (Dotted line).

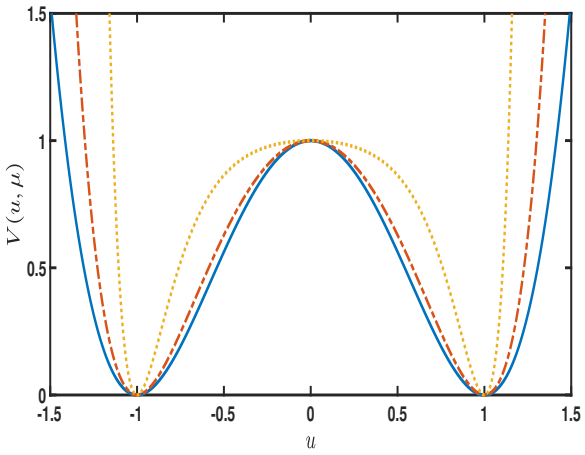

Figure 14: Profiles of the parametrized DWP $V(u,\mu)$, for different values of the shape deformability parameter μ: $\mu \to 0$ (Solid line), $\mu = 1.0$ (Dot-dashed line), $\mu = 4.0$ (Dotted line). $a_0 = 1$.

When μ tends to zero, the four parametrized DW models reduces to the universal bistable potential[**?**, **?**] $V(u) = a_0\left(u^2-1\right)^2$

III.3 First-order transition in quantum tunneling

III.3.1 Determination of action and period of the periodon

Consider a $1D$ quantum system modeled as in Sec. **??**. The Euclidean action (in dimensionless form) of such system reads:

$$S = \int d\tau \left(\frac{1}{2}\left(\frac{du}{d\tau}\right)^2 + V(u,\mu) \right), \tag{152}$$

where u is a scalar field in one time and zero space dimension, $\tau = it$ is the imaginary time and $V(u,\mu)$ is a parametrized DWP energy of the form (**??**). The integral is taken over the period τ_p of the path. In statistical mechanics this period is related to temperature T through the relation $\tau_p = \hbar/(k_B T)$, where k_B is the Boltzmann constant. Without loss of generalities we will take $\hbar \equiv 1$.

The decay rate of the system in the semi-classical limit is of the form:

$$\Gamma \sim \exp\left(-F_{min}/T\right), \tag{153}$$

where F_{min} is the minimum of the effective "free energy" **[?]** $F \equiv E + TS(E) - E_{min}$. E is the energy of a classical pseudo-particle in the system, while $E_{min} = 0$ corresponds to the bottom of the potential. The minimum of the effective Euclidean action i.e. S_{min}, is obtained by minimizing (**??**) along the trajectories $u_c(\tau)$ satisfying the energy-integral equation:

$$\left(\frac{du_c}{d\tau}\right)^2 = 2\left(V(u_c,\mu) - E\right). \tag{154}$$

When $E = 0$, corresponding to $\tau_p = \infty$ and $T = 0$, the particle is at rest at the bottom of one of the two degenerate potential wells. The solution to eq. (**??**) in this case is a regular vacuum instanton (kink soliton) given by:

$$u_c(\tau) \to \frac{1}{\alpha(\mu)} \tanh^{-1}\left[\frac{\mu}{\sqrt{1+\mu^2}} \tanh\frac{\tau}{d(\mu)}\right], \tag{155}$$

where $d(\mu) = 2\mu\sqrt{2a(\mu)}[\alpha(\mu)\sqrt{(1+\mu^2)}]^{-1}$ is the kink width. Imposing periodic boundary conditions, with τ_p the period of motion, leads instead to the following expression for the trajectory $u_c(\tau)$ with energy $E \geq 0$:

$$u_c(\tau) = \frac{1}{\alpha(\mu)} \tanh^{-1}\left[C_1 \cdot sn\left(C_2\tau, \kappa\right)\right], \tag{156}$$

with $sn(\tau,\kappa)$ a Jacobi elliptic function **[?]** the modulus κ of which is given by:

$$\kappa = \sqrt{\frac{\left(1-\sqrt{E/a(\mu)}\right)\left[1+\mu^2\left(1+\sqrt{E/a(\mu)}\right)\right]}{\left(1+\sqrt{E/a(\mu)}\right)\left[1+\mu^2\left(1-\sqrt{E/a(\mu)}\right)\right]}}. \tag{157}$$

The two parameters C_1 and C_2 appearing in formula (**??**) were defined as:

$$C_1 = \sqrt{\frac{\mu^2\left(1-\sqrt{E/a(\mu)}\right)}{1+\mu^2\left(1-\sqrt{E/a(\mu)}\right)}}, \tag{158}$$

$$C_2 = \frac{\alpha(\mu)}{\mu}\sqrt{2a(\mu)\left(1+\sqrt{\frac{E}{a(\mu)}}\right)\left[1+\mu^2\left(1-\sqrt{\frac{E}{a(\mu)}}\right)\right]}. \tag{159}$$

The trajectory (**??**) possesses real periods for values of its argument equal to $4m\mathcal{K}(\kappa)$, where m is an integer and $\mathcal{K}(\kappa)$ is the quarter period determined by the complete elliptic integral of the first

kind [**?**]. Eq. (**??**) therefore describes a periodic trajectory which we can refer to as periodon, the period of which is:

$$\tau_p = \frac{4}{C_2}\mathcal{K}(\kappa). \tag{160}$$

The classical action of the periodon eq. (**??**) is obtained as:

$$S_p(E) = E\,\tau_p + W\left(u_c(\tau_p)/2, E\right), \tag{161}$$

where:

$$W\left(u_c(\tau_p)/2, E\right) = \frac{2C_2}{(\alpha(\mu)C_1)^2}[(C_1^4 - \kappa^2)\Pi(C_1,\kappa) + \kappa^2\mathcal{K}(\kappa) + C_1^2(\mathcal{K}(\kappa) - \mathcal{E}(\kappa))].$$

$\mathcal{E}(\kappa)$ and $\Pi(C_1,\kappa)$ in the last formula are the complete elliptic integrals of the second and third kinds, respectively [**?**].

At $E = a_0$, which corresponds to the top of the potential barrier, the solution to eq. (**??**) is the trivial configuration $u_c(\tau) = 0$. This trajectory is a sphaleron [**?**] and its action is the thermodynamic action namely:

$$S_0(\mu) = a(\mu)\tau. \tag{162}$$

For the sphaleron the escape rate has the Boltzmann signature, characteristic of a pure thermal activation i.e.:

$$\Gamma_c \sim \exp\left(-a(\mu)\tau_p\right) = \exp\left(-a(\mu)/k_BT\right). \tag{163}$$

From the above results we can conclude that a periodon interpolates between the sphaleron $u_c(\tau) = 0$, and the instanton given by eq. (**??**). Hence the escape rate in the periodon sector will be:

$$\Gamma \sim \exp\left(-S_{min}(E)\right), \tag{164}$$

where $S_{min}(E) = min\left\{S_0, S_p(E)\right\}$.

III.3.2 First-order phase transition occurence in the parametrized DW model

To examine the possible occurrence and characteristic features of the transition(s) in quantum tunneling, for the $1D$ quantum system with the action given by formula (**??**), it is useful to start with the remark that for periodic problems in classical statistical mechanics, the derivative of the

action with respect to the energy is equivalent to the oscillation time τ of the system with this energy. Since the oscillation time τ is proportional to the inverse temperature, with the action corresponding to motion in the periodon sector we can readily define the period of motion as:

$$\tau_p(E) = \frac{1}{k_B T} = \frac{dS_p(E)}{dE}, \quad \frac{dS_0}{d\tau_p} = a(\mu). \tag{165}$$

Taking (**??**) together with (**??**) and (**??**), it is possible to analyze the influence of the shape deformability parameter μ on the temperature dependence of S_{min}, based upon the energy dependence of the period of periodon $\tau_p(E)$. In particular these equations will help us obtain the critical value of μ at which a first-order transition from quantum to thermal regime can be expected.
Two well-established criteria are known [**?**, **?**] which determine conditions for occurrence of transitions in quantum tunnelings, in the general problem of decay of a metastable state [**?**, **?**, **?**, **?**, **?**]. The first criterion states that the transition will be of first order if the period $\tau_p(E)$ decreases to a minimum, and next increases again when E increases from the potential bottom to the barrier height. If $\tau_p(E)$ instead decreases monotonically with increasing E, the transition will be of second order. This first criterion is equivalent to solving the equation:

$$\frac{d}{dE}\tau_p(E) = 0, \tag{166}$$

where one seeks for nontrivial solutions with the temperature dependence of $\tau_p(E)$ given by (**??**). We solved the last equation numerically by setting $a_0 = 1/2$, and evaluated the energy E_1 corresponding to the minimum of $\tau_p(E)$ when varying μ from 3 downwards.. Results are shown in tables **??**-**??**, respectively for model 1 - 4.

Table 1: Numerical estimation of critical value of E_1 in model 1 (fixed barrier height, variable minima)

μ^2	Energy E_1 at minimum of $\tau_p(E)$	$E_0 = a_0$ (barrier height)
9	0.150	0.5
4	0.228	0.5
2	0.382	0.5
1.6	0.469	0.5
1.501	0.499	0.5

Table 2: Numerical estimation of critical value of E_1 in model 2 (fixed minima and variable barrier height)

μ^2	Energy E_1 at minimum of $\tau_p(E)$	$E_0 = a_0\mu^2\left[\alpha(\mu)\sqrt{1+\mu^2}\right]^{-2}$ (barrier height)
9	0.041	0.136
4	0.087	0.192
2	0.194	0.254
1.6	0.258	0.275
1.501	0.281	0.282

Table 3: Numerical estimation of critical value of E_1 in model 3 (variable barrier height and minima)

μ^2	Energy E_1 at minimum of $\tau_p(E)$	$E_0 = a_0\mu^2\left[sinh^{-1}\mu\right]^{-2}$ (barrier height)
9	0.409	1.361
4	0.437	0.960
2	0.581	0.761
1.6	0.672	0.716
1.501	0.704	0.705

Table 4: Numerical estimation of critical value of E_1 in model 4 (fixed minima and barrier height, but variable curvature shape of the barrier).

μ^2	Energy E_1 at minimun of $\tau_p(E)$	$E_0 = a_0$ (barrier height)
9	0.1503	0.5
4	0.2278	0.5
2	0.3817	0.5
1.6	0.4691	0.5
1.501	0.4994	0.5

Curiously, the tables indicates that in the four models the quantity E_1 approaches the maximum energy E_0, when μ tends to $\sqrt{3/2}$. Therefore the critical value of μ for a transition in quantum tunneling would be $\mu_c = \sqrt{3/2}$, and smaller values of μ should correspond to unphysical values of the energy E. Clearly, a first-order quantum-classical transition will occur in the parametrized DW models when the deformability parameter lies in the range $\mu > \sqrt{3/2}$. For values of μ far above the critical threshold μ_c, we should have $E_1 \approx 0$ and $E_1 \to E_0$ as μ decreases to μ_c. So to say, increasing the deformability parameter above the critical value μ_c should result in a sharper first-order transition in quantum tunneling [**?**].

Fig. **??-??** illustrate respectively in model 1-4 the energy dependence of the period τ_p of the periodon, taking two values of the shape deformability parameter μ respectively below and above

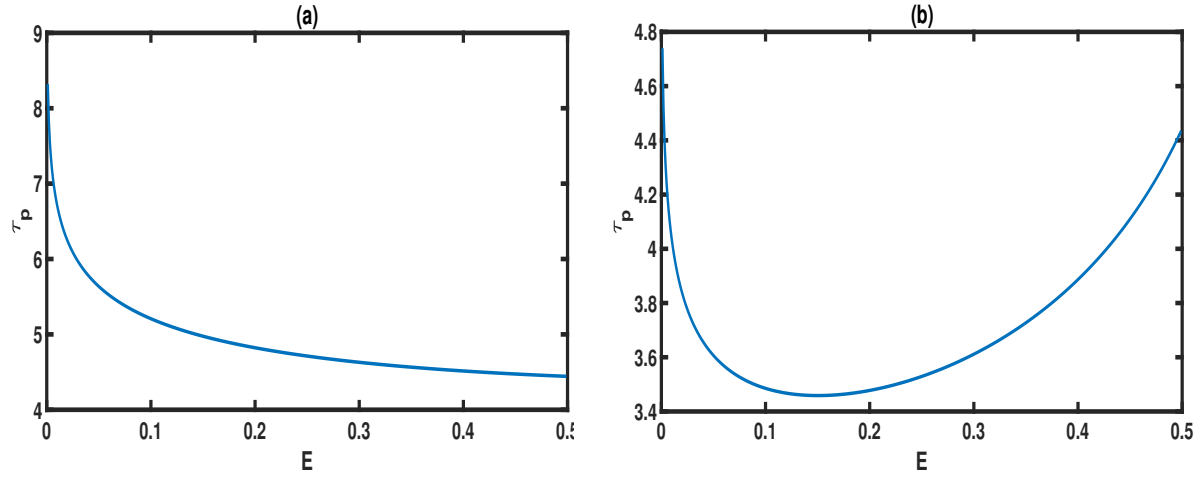

Figure 15: Variation of the instanton period with the energy period E in model 1. (a) $\mu = 1$, and (b) $\mu = 3$. Here $a_0 = 0.5$.

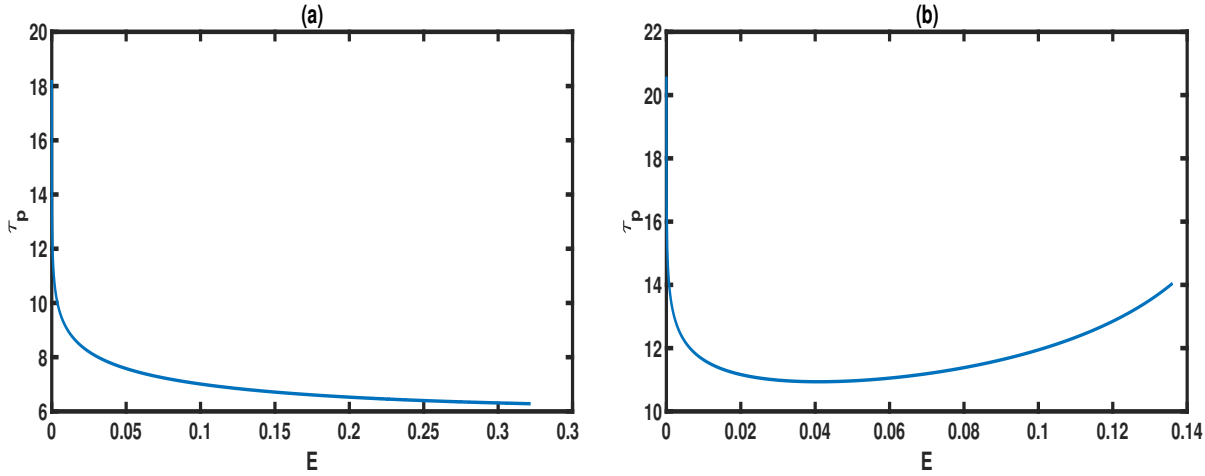

Figure 16: Variation of the instanton period with the energy period E in model 2. (a) $\mu = 1$, and (b) $\mu = 3$. Here $a_0 = 0.5$.

the critical value μ_c. In the four models, the figures show a monotonically decrease of the period with increasing energy for $\mu = 1$, lower than μ_c. However for $\mu = 3$, which is a value greater than μ_c, the period has a re-entrant behavior after decreasing until a critical value of the energy. This re-entrant behavior of the period actually reflects favorable conditions in order to generate a first-order transition.

The second criterion states that if at some critical temperature the first derivative of $S_{min}(T)$ is discontinuous, and an abrupt change is observed in the temperature dependence of the action, then the transition from quantum to thermal regime is a first-order transition in temperature. The temperature dependence of the periodon and thermodynamic actions is depicted in Fig. **??-??**, respectively for model 1-4, here also for $\mu = 1$ and $\mu = 3$. The physical behaviours

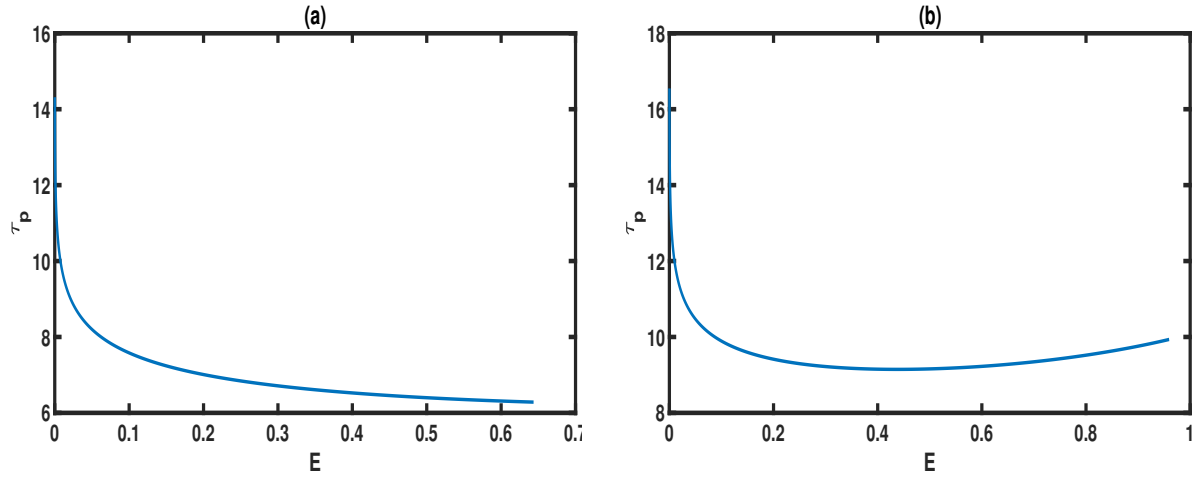

Figure 17: Variation of the instanton period with the energy period E in model 3. (a) $\mu = 1$, and (b) $\mu = 3$. Here $a_0 = 0.5$.

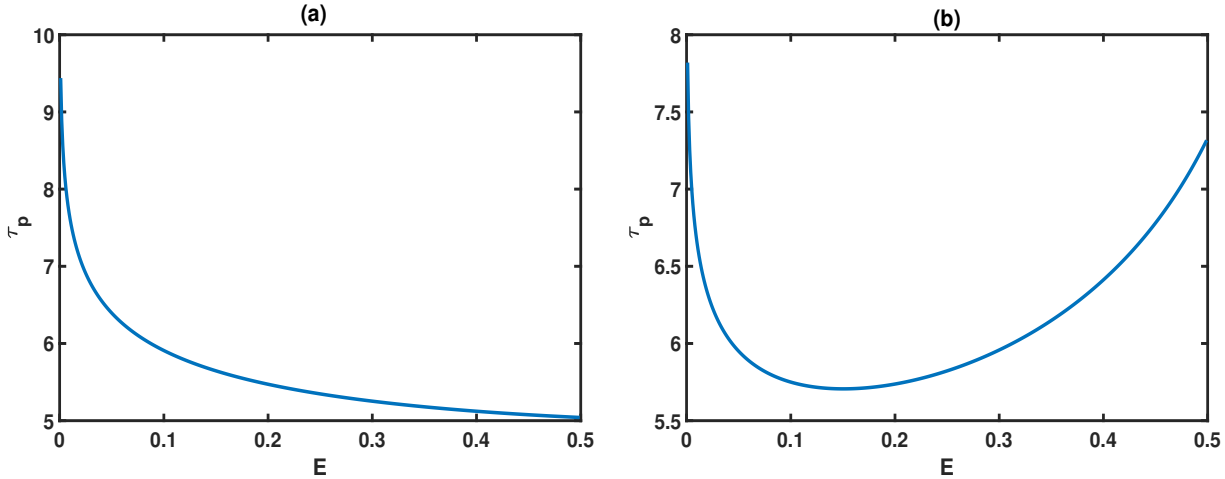

Figure 18: Variation of the instanton period with the energy period E in model 4. (a) $\mu = 1$, and (b) $\mu = 3$. Here $a_0 = 0.5$.

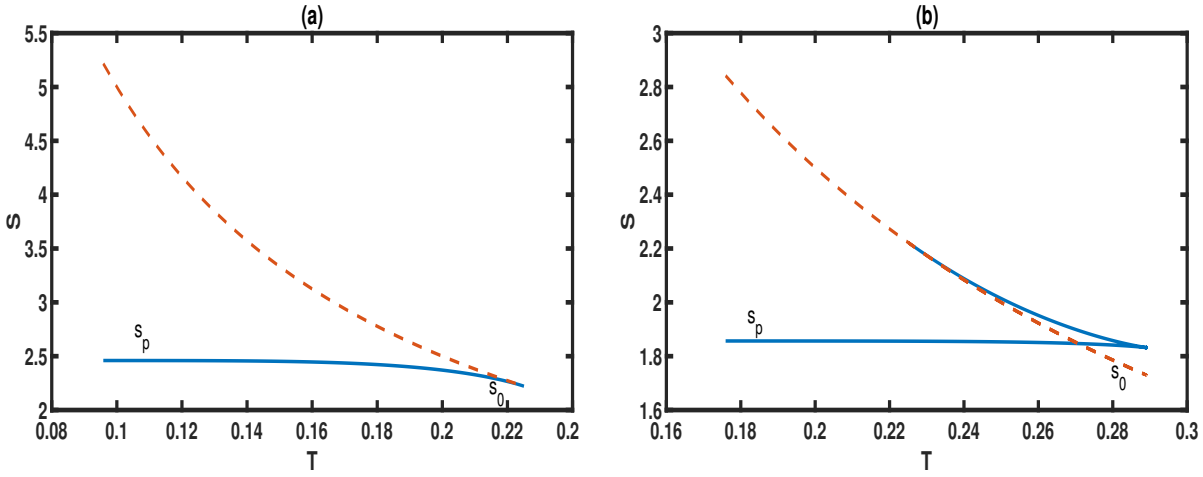

Figure 19: Plots of the action versus temperature in model 1, the dashed line corresponds to the thermodynamic action and the solid line to the periodon action: (a) $\mu = 1$, second-order transition from quantum to thermal regimes, (b) $\mu = 3$, First-order transition from quantum to thermal regimes. Here $a_0 = 0.5$.

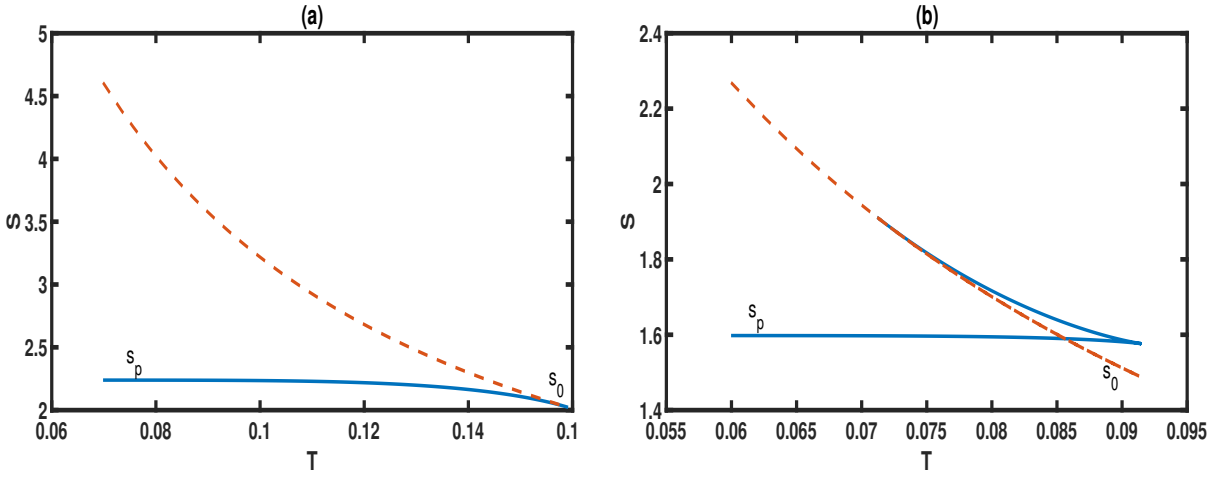

Figure 20: Plots of the action versus temperature in model 2, the dashed line corresponds to the thermodynamic action and the solid line to the periodon action: (a) $\mu = 1$, second-order transition from quantum to thermal regimes, (b) $\mu = 3$, First-order transition from quantum to thermal regimes. Here $a_0 = 0.5$.

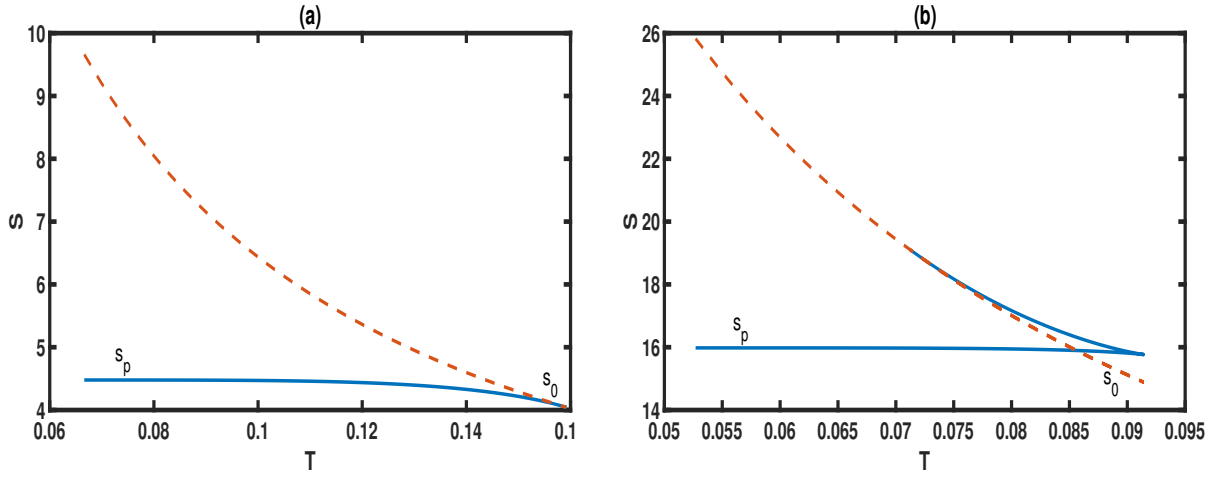

Figure 21: Plots of the action versus temperature in model 3, the dashed line corresponds to the thermodynamic action and the solid line to the periodon action: (a) $\mu = 1$, second-order transition from quantum to thermal regimes, (b) $\mu = 3$, First-order transition from quantum to thermal regimes. Here $a_0 = 0.5$.

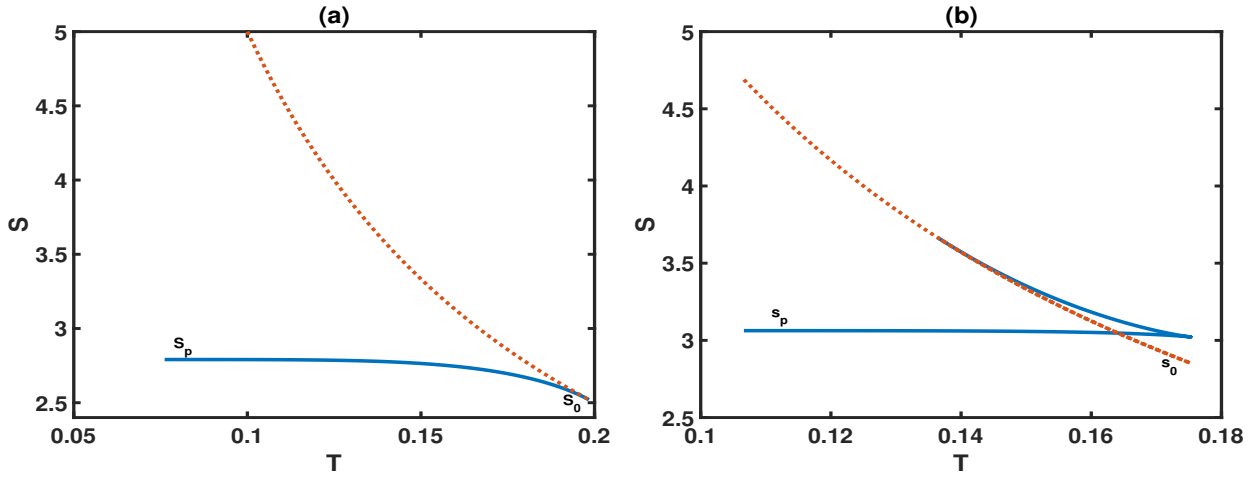

Figure 22: Plots of the action versus temperature in model 4, the dashed line corresponds to the thermodynamic action and the solid line to the periodon action: (a) $\mu = 1$, second-order transition from quantum to thermal regimes, (b) $\mu = 3$, First-order transition from quantum to thermal regimes. Here $a_0 = 0.5$.

just discussed and emerging from Figs. **??-??**, can also be observed in the corresponding plots of the periodon and thermodynamic actions shown in Fig. **??-??**. The four models again show similar behavior. Indeed, a smooth change from S_p to S_0 is observed when the temperature increases at $\mu = 1$, as shown in Figs. **??**a, **??**a, **??**a, and **??**a. Such change is the signature of a second-order transition. Though Figs. **??**b, **??**b, **??**b, and **??**b show an abrupt change in the temperature dependence of the minimum action, satisfying the Chudnovsky [**?**] second criterion for a first-order phase transition from quantum to thermal regimes.

III.3.3 Determination of the critical value of the deformability parameter for the occurence of a first-order phase transition

It can be useful to be able to determine analytically the critical value μ_c of μ for a first-order transition. In this respect we exploit the proposal of ref. [**?**], who extended the criteria for determining the order of transition in quantum tunneling, to the dependence of the Euclidean action with the instanton period. Indeed the authors proposed that when the period $\tau_p(E \to V_0)$ of the periodon close to the barrier peak is accessible, the condition $\tau_p(E \to V_0) - \tau_s < 0$ or $\omega^2 - \omega_s^2 > 0$ will be sufficient for a first-order transition. Here V_0 and τ_s denote, respectively, the barrier height and period of small oscillations around the sphaleron, ω and ω_s are the corresponding frequencies. In our context the last criteria translates to:

$$V''''(u_{sph}, \mu) - \frac{5\left[V'''(u_{sph}, \mu)\right]^2}{3V''(u_{sph}, \mu)} < 0, \tag{167}$$

where $u_{sph} = 0$ corresponds to position of the sphaleron solution. Since the potential is symmetric we must have $V'''(0, \mu) = 0$, such that the criteria reduces to $V''''(0, \mu) < 0$. Using the general expression of the potential given by formula (**??**), the criteria can be expressed more generally as:

$$4\left(\frac{3}{\mu^2} - 2\right)\frac{\alpha(\mu)^4 a(\mu)}{\mu^2} < 0, \tag{168}$$

which suggests a critical value of $\mu_c^2 = 3/2$ irrespective of the specific forms of $\alpha(\mu)$ and $a(\mu)$. This is in agreement with the results of ref. [**?**], where the phase transition in quantum tunneling was investigated with different forms of $a(\mu)$ and $\alpha(\mu)$ corresponding to the complete hierarchy of Dikandé-Kofané DWPs.

As to end this section, we wish to recall that the four members of the DK potentials family we

considered in these investigations exhibit distinct shape deformation as the shape deformability parameter varies: the first model has only its degenerate minima varying, the second model has only its barrier height varying, the third model has both its barrier height and position of degenerate minima varying, while the fourth model has only the curvature shape of the barrier varying leaving unchanged the position of the minima and the barrier height. The four models allowing first-order transitions for shape parameter values above the same critical value μ_c has as explanation for the moment only the crucial role that plays the curvature shape of the potential barrier. Indeed the four models considered in this study belong to a class of potentials with a barrier changing slowly near the bottom and the top, which were recently found to stand as good candidate for a first-order transitions in quantum regime [**?**]. In the limit $\mu \to 0$, all the models turn to the ϕ^4 model that only accounts for second-order transitions. But when μ rises, the degenerate minima in model 1 come closed to each other, rising the abruptness of the barrier walls. In model 2 the barrier continuously decreases with its flatness becoming more and more pronounced. In model 3 the minima go far from each other with a simultaneous rise of the barrier, leading to a noticeable increase of the barrier width. In model 4 the barrier continuously becomes anharmonic, together of a rise of the abruptness of the walls and the mid-height width. So as μ approaches the critical value μ_c the probability of thermally assisted tunneling just below the barrier gradually decreases due to the increase of the tunneling distance, as the barrier top becomes similar to that of a rectangular barrier. Thus in the region $\mu > \mu_c$ this tunneling becomes unfavorable and a direct competition between ground state tunneling and thermal activation leads to the occurrence of a first-order transition.

III.4 Statistical mechanics and quasi-exact solvability for the DW models

III.4.1 Derivation of the solvability criterion

We now turn to the low-temperature statistical mechanics of the the family of parametrized DWP models given in (**??**), paying attention to the canonical partition function using the transfer-integral formalism [**?**, **?**, **?**, **?**, **?**]. For the low-temperature statistical mechanics, we apply the transfer-integral formalism and with the Hamiltonian given in eq. (**??**). We find a Schrödinger-

like equation for eigenstates of the transfer-integral operator:

$$-\frac{1}{2\beta^2}\frac{\partial^2}{\partial u^2}\psi_j + a(\mu)\left(\frac{\sinh^2(\alpha(\mu)u)}{\mu^2} - 1\right)^2 \psi_j = \epsilon_j \psi_j. \tag{169}$$

In the thermodynamic limit, the lowest eigenstate with energy ϵ_0 brings the most relevant contribution to the partition function. In this context Z can readily reduce to the classical partition function;

$$Z_c = (2\pi/\beta h)^N \exp\left(-\beta N \epsilon_0\right), \tag{170}$$

where $\beta = (k_B T)^{-1}$ and N ($\to \infty$) is the total number of particles in the system.

Most generally, finding exact values of the partition function Z depends on the solvability of the eigenvalue problem (**??**). To transform this eigenvalue problem into a form for which the exact solvability is established [**?**, **?**, **?**], we use the variable change $z = \alpha(\mu)u$ and introduce $\xi = (1 + 2\mu^2)^{-1}$, $E_j = 4\mu^4\xi^2\epsilon_j/a(\mu)$. With these new variables the eigenvalue problem (**??**) becomes:

$$\frac{1}{2\beta^2}\frac{\partial^2}{\partial z^2}\psi_j + \frac{a(\mu)}{4\mu^4(\alpha(\mu)\xi)^2}\left[E_j - (\xi\cosh(2z) - 1)^2\right]\psi_j = 0. \tag{171}$$

Remark that by taking $2\beta = 1$, and rescaling the parameter $E_j \to E_j/\eta^2$ with the relations $\eta = \sqrt{a(\mu)}/[2\mu^2\alpha(\mu)\xi]$ and $\eta = n + 1$, $n = 0, 1, 2, ...$, the eigenvalue problem (**??**) turns exactly to the equation treated in ref. [**?**]. In this last work the author obtained exact expressions of eigenfunctions and energy eigenvalues of the corresponding eigenvalue problem, for some energy levels n. By following a similar idea in our context, this will mean taking one energy level at a fixed temperature which yields the value of μ for which the system is quasi-exactly solvable. However, what we really want is instead to obtain eigenstates at different temperatures for each value of μ. This is possible by considering a distinct picture in which the temperature is related to the shape deformability parameter through:

$$\beta^2 = \frac{2\mu^4(\alpha(\mu)\xi)^2}{a(\mu)}q^2, \tag{172}$$

where q is a positive integer hereafter referred to as "temperature order". The condition for quasi-exact solvability of the system at several temperatures, is defined by relation (**??**). This relation can be exploited to analyze the ratio $a(\mu)/\beta^{-1}$ of the temperature at which the solvability holds and the barrier energy that, in the Boltzmann constant unit, has the sense of the transi-

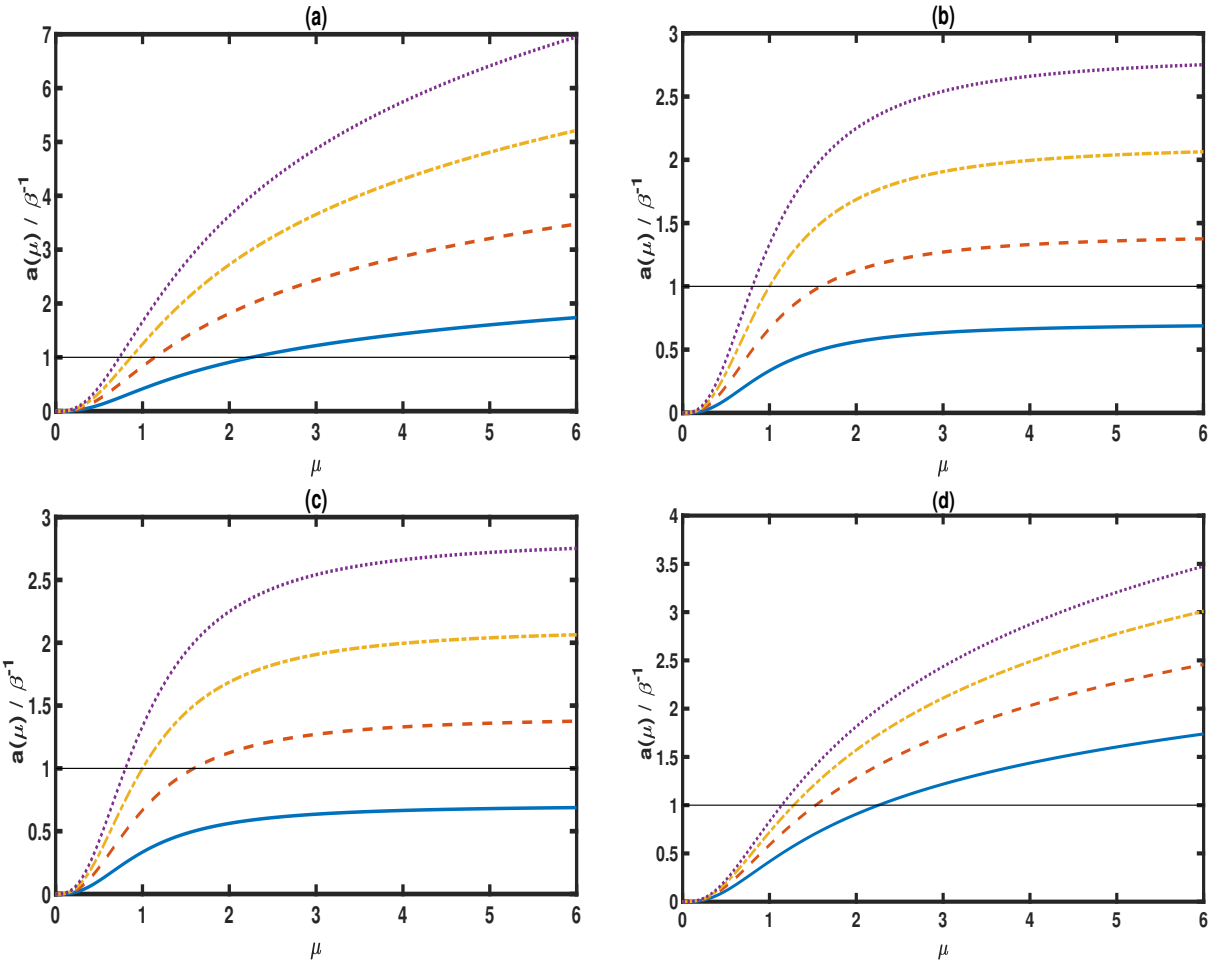

Figure 23: Plot of the ratio of the temperature and barrier energy versus the shape deformability parameter taking $q = 1$ (Solid line), $q = 2$ (Dashed line), $q = 3$ (Dash-dotted line), $q = 4$ (Dotted line) in (a) model 1, (b) model 2, (c) model 3, and (d) model 4. Here $a_0 = 1$ and the horizontal line mark the region where the temperatures coincide the symmetry breaking temperature.

tion temperature. This ration is illustrated in Fig. **??**. One can note from the figure that in the four potential models the solvability requires $\beta^{-1} \to \infty$ in the limit $\mu \to 0$. This agrees with the transfer-operator integrability problem of the ϕ^4 model not having exact solution at finite temperature. For small values of μ, the four models need temperatures far higher than the barrier energy. As μ increases, the temperatures obtained from the lowest to the largest q steadily decrease. But while respectively going far below the energy barrier in model 1 and in model 4 for $q = 1$ as shown respectively in Fig. **??**(a) and Fig. **??**(d), it is seen from Fig. **??**(b) and Fig. **??**(c) that the temperatures in model 2 and model 3 instead tend to a particular limit. It was analytically found that this limit is coincidentally the same for both models, and $a(\mu)/\beta^{-1} \to q/\sqrt{2}$ as $\mu \to \infty$. So, for sufficiently large values of μ the solvability condition will hold at four temperatures below the symmetry breaking temperature in model 1 and model 4, while only three temperatures below the barrier energy will meet the condition in both model 2 and model 3, as the temperature at $q = 1$ in those models will stay greater than the barrier energy despite its decrease with increase μ.

III.4.2 Exact formulation for the ground-states

Substituting (**??**) into (**??**) we obtain:

$$\frac{\partial^2}{\partial z^2}\psi_j + q^2\left[E_j - (\xi\cosh(2z) - 1)^2\right]\psi_j = 0. \tag{173}$$

Equation (**??**) describes a quasi-exactly solvable system similar to the one studied in refs. [**?**, **?**, **?**], for the energy level $n = 1$. We are interested in solutions which vanish in the limit $z \to \pm\infty$. In this respect, we can readily define:

$$\psi(z) = r(z)\exp\left[-z_0\cosh(2z)\right], \tag{174}$$

where the function $r(z)$ is a polynomial expressed as a linear combination of $\cosh m_p z$ or $\sinh m_p z$ and their powers, with z_0 and m_p ($p = 0, 1, 2, ...$) being constant quantities to be determined. Applying the Sommerfeld method (see Sec. **??**), the exact expressions for the (unnormalized) ground-state wavefunctions, and of the associated energy eigenvalues, are found for the first four values of q and are list:

$q = 1$:

$$\begin{aligned} \psi_0(u) &= \exp\left[-\frac{\cosh(2\alpha(\mu)u)}{2(1+2\mu^2)}\right], \\ \epsilon_0 &= \frac{a(\mu)}{4\mu^4}\left[1+(1+2\mu^2)^2\right]. \end{aligned} \tag{175}$$

$q = 2$:

$$\begin{aligned} \psi_0(u) &= \cosh(\alpha(\mu)u)\exp\left[-\frac{\cosh(2\alpha(\mu)u)}{1+2\mu^2}\right], \\ \epsilon_0 &= \frac{a(\mu)}{16\mu^4}\left[3(1+2\mu^2)^2-8\mu^2\right]. \end{aligned} \tag{176}$$

$q = 3$:

$$\begin{aligned} \psi_0(u) &= [\frac{6}{1+2\mu^2}+\left(1+\sqrt{1+\frac{36}{(1+2\mu^2)^2}}\right)\cosh(2\alpha(\mu)u)]\exp\left[-\frac{3\cosh(2\alpha(\mu)u)}{2(1+2\mu^2)}\right], \\ \epsilon_0 &= \frac{a(\mu)}{36\mu^4}[9-2(1+2\mu^2)\sqrt{(1+2\mu^2)^2+36}+7(1+2\mu^2)^2]. \end{aligned} \tag{177}$$

$q = 4$:

$$\begin{aligned} \psi_0(u) &= 2[\frac{6\cosh(\alpha(\mu)u)}{1+2\mu^2}+\left(2\mu^2-1+\sqrt{12-8\mu^2+(1+2\mu^2)^2}\right)\frac{\cosh(3\alpha(\mu)u)}{1+2\mu^2}] \\ &\times \exp\left[-\frac{2\cosh(2\alpha(\mu)u)}{1+2\mu^2}\right], \\ \epsilon_0 &= \frac{a(\mu)}{16\mu^4}[2-4\mu^2-(1+2\mu^2)\sqrt{(1+2\mu^2)^2-8\mu^2+12}+\frac{11}{4}(1+2\mu^2)^2]. \end{aligned} \tag{178}$$

Eigenfunctions and eigenvalues for some higher energy levels are given in the appendix .

The free energy is strongly related to the ground state energy. The influence of the shape parameter μ on the ground state energies is illustrated in Fig.**??**. The four models are expected to allow infinitely high eigen-energies in the limit $\mu \to 0$. Unsurprisingly, this agrees with the non-integrability of the ϕ^4 model in the transfer-operator formalism. As μ rises, the ground state energies in model 1, model 2 and model 4 drastically decrease to a particular limit, as shown respectively in Fig.**??**(a), Fig.**??**(b) and Fig.**??**(d). As for the case of model 3, Fig.**??**(c) plots the energies decreasing to a minimum then steadily rising back to infinitely large values. Greater

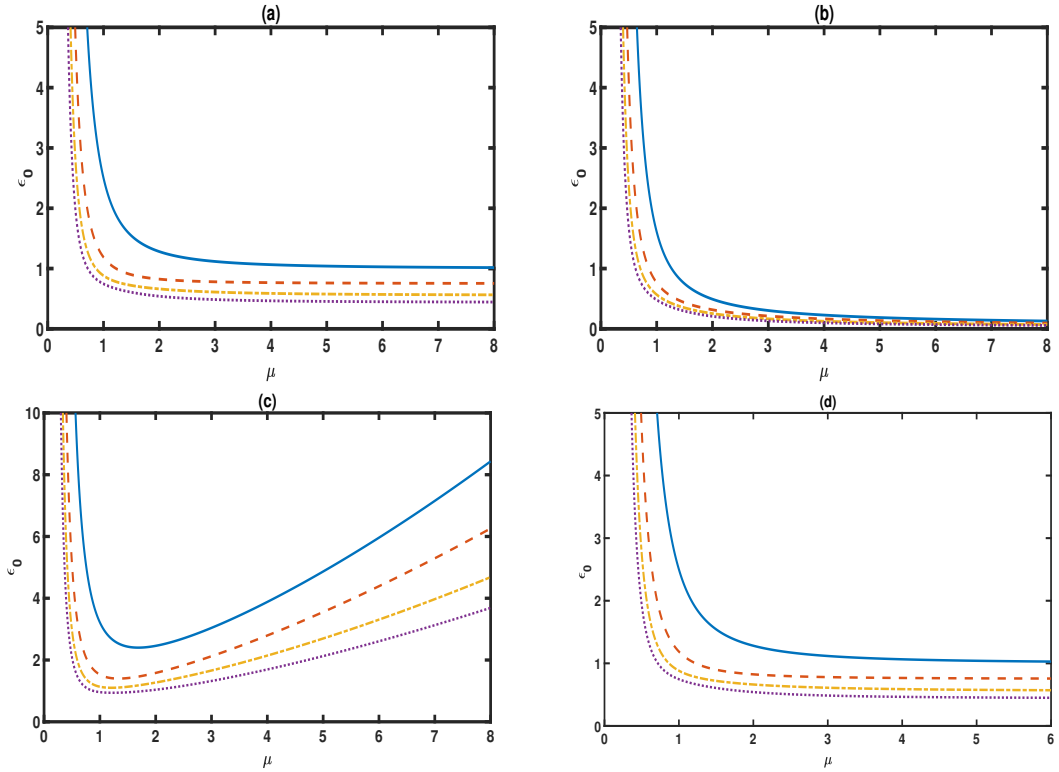

Figure 24: Variation of the ground state energy ϵ_0 with the shape deformability parameter μ, for four different values of q(corresponding to four different temperatures) namely: $q = 1$ (Solid line), $q = 2$ (Dashed line), $q = 3$ (Dash-dotted line), $q = 4$ (Dotted line) in (a) model 1, (b) model 2, (c) model 3, and (d) model 4. Here $a_0 = 1$.

interest on the ground state energy levels lies instead on the dependence of their relative position with respect to the energy barrier on the shape deformability parameter, combined with the impact of the temperature through the choice of q. This relative position can be analyzed from the behavior of the ratio $\epsilon_0/a(\mu)$, sketched in Fig.**??**. One advantage to study such ratio lies in the fact that it does not depend on the choice of $a(\mu)$ and $\alpha(\mu)$, so the observations done on the relative position of the energy levels will, without distinction, be valid in the four models considered in this study. From Fig.**??**, we remark that the ground state energies are infinitely higher than the energy barrier for $\mu \to 0$, and drop with an increase of μ whatever the choice of the temperature. However, combining the influence of μ together with the choice of q affects the position of the energy level with respect to the energy barrier. Taking $q = 1$ for illustration, the ground-state energy decreases drastically but will always remain above the energy barrier. This drastic decrease is also observed for higher values of q, but when μ rises beyond a specific value namely $\mu_s = \sqrt{3/2}, \sqrt{3/4}$ and $\mu_s \simeq 0.717$ for $q = 2$, $q = 3$ and $q = 4$ respectively, the ground-state energy drops below the energy barrier and tends to a finite value i.e. $\epsilon_0(\mu \to \infty) = (3/4)a_0$

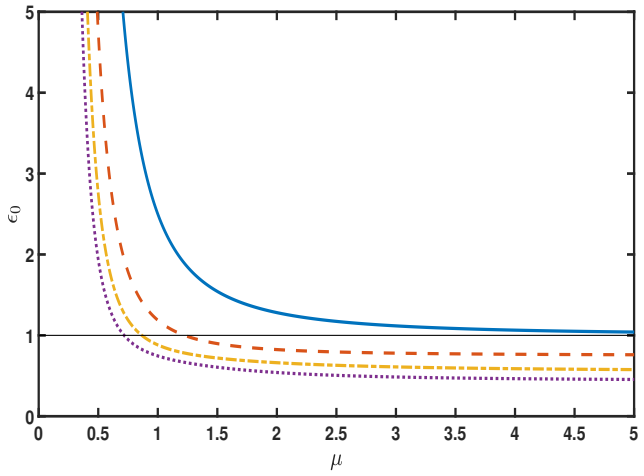

Figure 25: Variation of the ground-state energy ϵ_0 with the shape deformability parameter μ, for four different values of q (corresponding to four different temperatures) namely: $q = 1$ (Solid line), $q = 2$ (Dashed line), $q = 3$ (Dash-dotted line), $q = 4$ (Dotted line). The horizontal line stands for the energy barrier a_0 here fixed as $a_0 = 1$.

for $q = 2$, $\epsilon_0(\mu \to \infty) = (5/9)a_0$ for $q = 3$ and $\epsilon_0(\mu \to \infty) = (7/16)a_0$ for $q = 4$. Moreover for a fixed value of μ, lower energy levels are obtained by increasing the temperature order q

III.4.3 Probability density function

Having obtained the analytical expressions of the exact ground-state wavefunctions and energy eigenvalues at several temperatures for arbitrary values of the deformability parameter μ, quantities such as the probability density which are relevant in the formulation of correlation functions and correlation lengths at low temperatures, turn out to be easy to obtain. In effect, the probability density associated with the classical field u is nothing but the square of the normalized ground-state wavefunction. For this reason, we expect the shape deformability μ to affect the probability density the same way it qualitatively affects the ground-state wavefunction. The ground-state wavefunctions (unnormalized) for four different temperatures are plotted in Fig. **??**, considering different values of the shape deformability parameter μ. To have more insight on Fig.**??**, it was necessary to associate the general properties of probability densities for bistable systems with the feature related to the deformability of each parametrized DWP. We recall from Fig.**??** that the ground state energies correspond to the high temperature regime for small μ, as they were found to be greater than the energy barrier. Hence in this regime the pseudoparticle in the four potentials holds sufficient energy to escape from one well to another and move freely as if trapped instead by a single-well potential. The whole space becomes probable as the full state

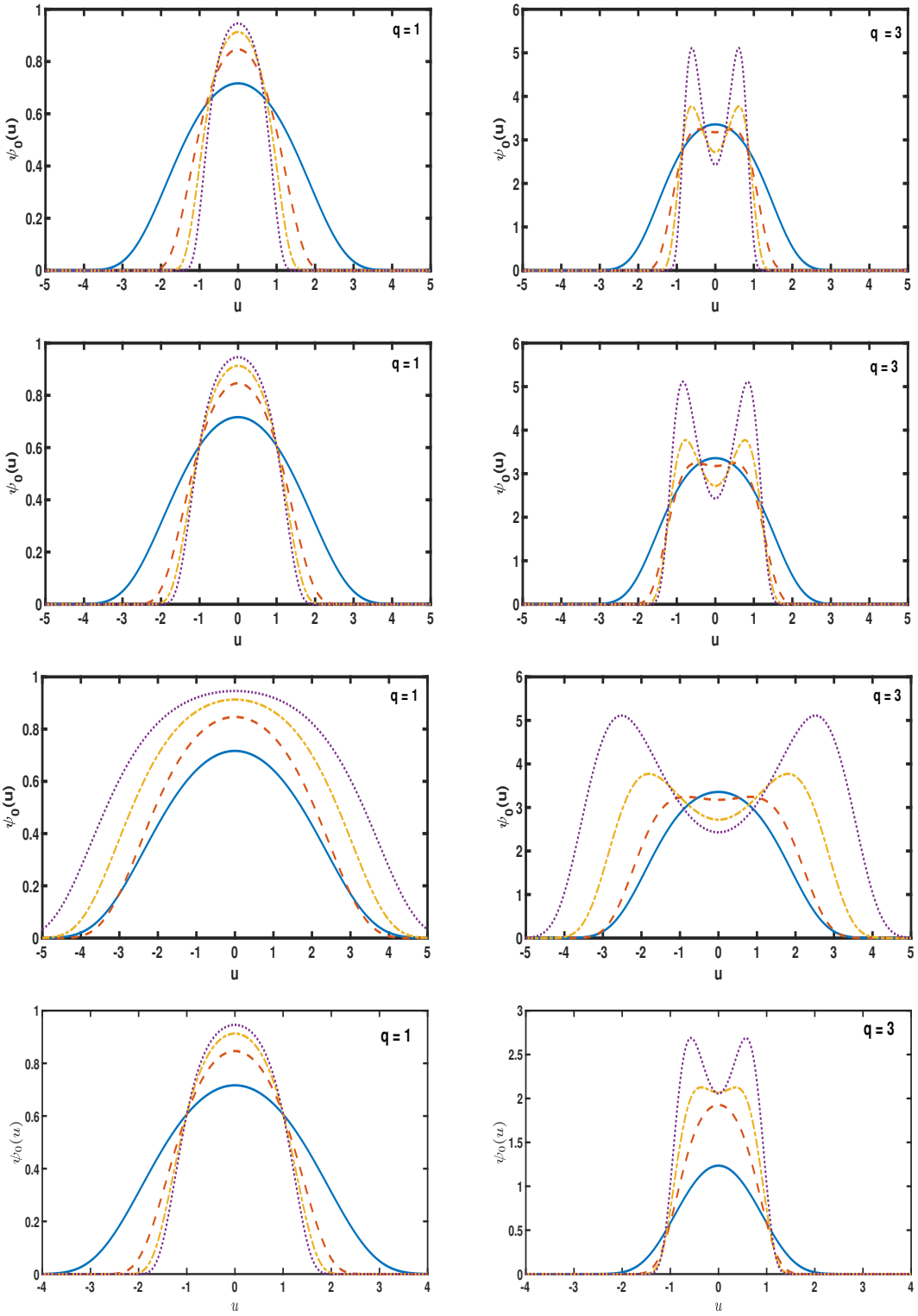

Figure 26: Ground state wavefunctions in position space at three temperature, for $\mu = 0.5$, for four different values of q(corresponding to four different temperatures) namely: $\mu = 0.5$ (Solid line),$\mu = 1$ (Dashed line), $\mu = 1.5$ (Dash-dotted line), $\mu = 2$ (Dotted line). From left to right: model with variable position of minima, model with variable barrier height, model with variable barrier height and position of minima

space is covered with power-law tails, with a maximum probability density at the barrier peak. As μ increases, the probability density at the three temperature in the four models experiences increase in the amplitude, but while showing decrease in width in model 1, model 2 and model 4, the probability density width instead increases in model 3. A rise of μ in model 1, model 2 and model 4 will decrease respectively the barrier width, the barrier height, and the wells width of the potential. In the four models the deformation will also strengthen the steepness of the reflective walls and then restricts the attainable space to the region covered by just the valleys and the energy barrier. In model 3, the barrier rises with its width gradually increasing as the degenerate minima move far from each other, increasing μ will consequently widen the attainable space covered by the energy barrier. The ground state being high in the four models, the energy barrier remains the most probable. It is important the associate the choice of q when discussing the variation of the shape deformability parameter in the four models, as this will yield remarkable change in the probability density. E.g. Taking $q = 1$, the ground state energy levels always stay, freely from μ, higher than the energy barrier. Increasing μ may lower the temperature, but a probability density with a single peak located at the barrier will still be obtained (left graphes in Fig.**??**. Though this behavior is observed for choices of q greater than one, it is valid only in the range $\mu < \mu_s$. As μ rises beyond μ_s, the ground state energy levels descend below the barrier height and the transitions from one well to another become less frequent as the temperature decreases lower than the transition temperature. The pseudoparticles stay much longer, confined in the potential wells, so that the valleys become more probable. This trend is illustrated in Fig.**??** by the probability density in all models exhibiting a double-peak shape, each peak located in the vicinity of the degenerate minima of the potentials. To enrich our understanding of the temperature dependence of the probability density for a fixed μ, but at different temperatures, in Fig. **??** we represented the ground-state probability density for $\mu = 2$ and for three distinct temperatures at which the quasi-exactly solvable condition holds. We note a continuous shift from a single peak feature to a two-peak feature, with decreasing temperature. Remark that the change in the peak width with temperature is different from that of the ϕ^4 model. Instructively the exact probability densities, are superimposed with those obtained from numerical simulations of the following additive-noise Fokker-Planck equation associated to the model:

$$\partial_{tt}^2 u - \partial_{xx}^2 u + \eta \partial_t u + dV(u, \mu)/du = F(x, t), \tag{179}$$

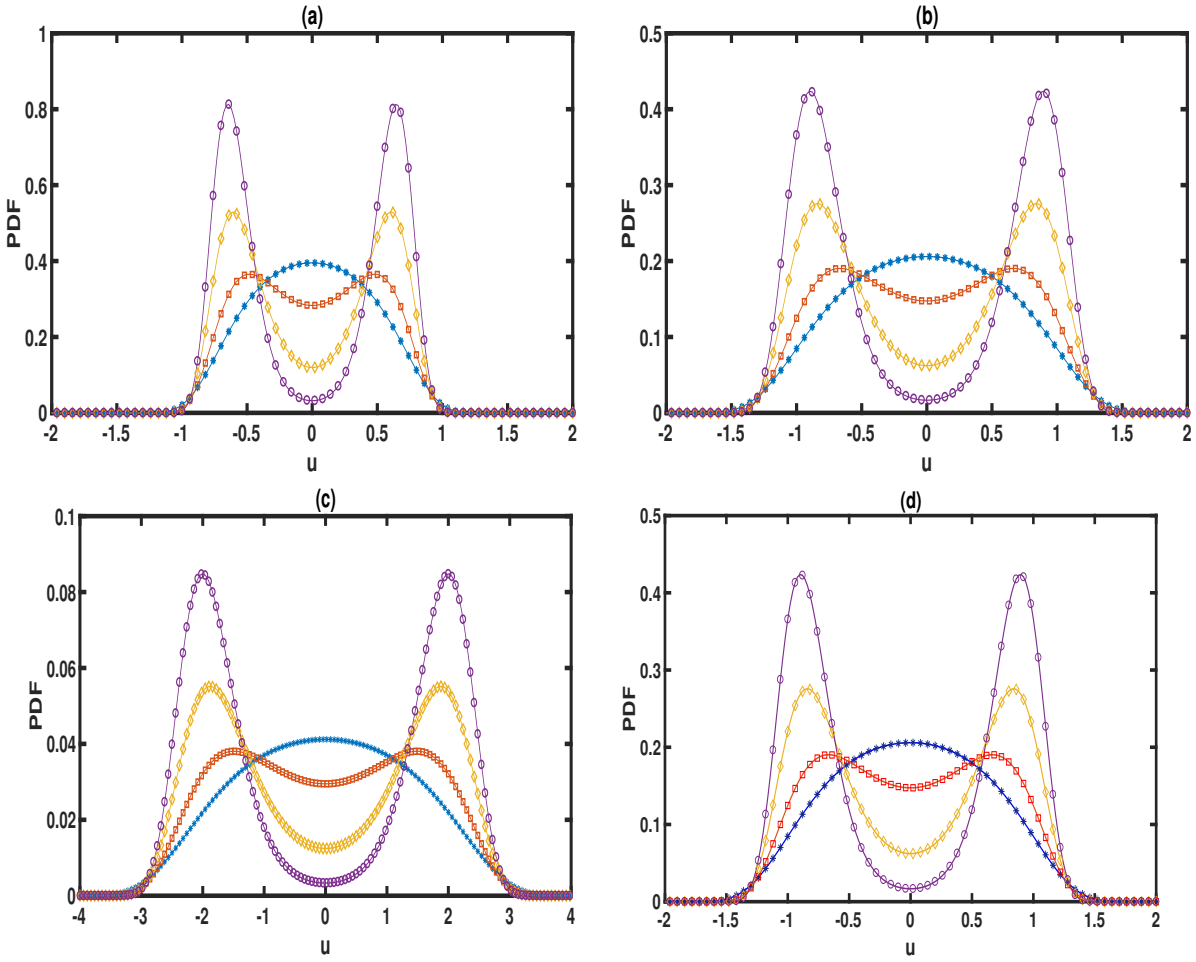

Figure 27: Comparaison of the exact (Solid Line) probability density and the results from Langevin simulations, for $\mu = 2$ and for values of β obtained for $q = 1$ (stars), $q = 2$ (squares), $q = 3$ (diamonds), and $q = 4$ (circles), in (a) model 1, (b) model 2, (c) model 3, and (d) model 4. Note the excellent agreement.

where the Gaussian white noise $F(x,t)$, and the viscosity η, are related by the fluctuation-dissipation theorem:

$$\langle F(x,t)F(x',t')\rangle = 2\eta\beta^{-1}\delta(x-x')\delta(t-t'). \tag{180}$$

We used standard techniques [**?**] to solve the discrete version of the above Fokker-Planck equation, and sampled the results in time to obtain time-averaged probability densities after arbitrary initial conditions had been driven to equilibrium. In the simulations we employed both an Euler and Runge-Kutta schemes (presented in chapter **??**, with a lattice size of typically 350.000 points taking a lattice spacing of $d = 0.02$ and a time step of $h = 0.001$. As evidenced by Fig. **??**, the exact (i.e. analytical) probability density and the results from numerical simulations, show excellent agreement. This agreement between the analytical and numerical results suggests that the ground-state energies can be numerically computed using the corresponding probability densities, at any temperature where quasi-exactly solvable condition holds for a wide range of values of the shape deformability parameter μ. A relevant implication of this is the possibility to compute exactly, thermodynamic quantities such as enthalpy, internal energy, entropy and so on.

III.5 Kink-antikink scattering-induced breathing bound states and oscillons in the parametrized DW model

As Refs. [**?**] already presents the influence of the deformability of the DK family members in the context of kink-antikink scattering, in this section we will just present the result only accounting for the newly proposed parametric DWP defined by (**??**) and (**??**).

III.5.1 kink-phonon scattering spectrum

We consider the Hamiltonian (**??**) (in the dimensionless form)

$$H = \int dx \left[\frac{1}{2}\pi^2 + \frac{1}{2}(\partial_x u)^2 + V(u,\mu)\right], \tag{181}$$

where the generic bistable potential $V(u)$ is replaced by $V(u,\mu)$ defined by (**??**), while considering the model specified by equations (**??**). The solitary-wave solution to the equation of motion, i.e.:

$$\frac{\partial^2 u}{\partial t^2} - \frac{\partial^2 u}{\partial x^2} + V(u,\mu) = 0, \tag{182}$$

derived from the Hamilonian (**??**), can be shown to express:

$$\begin{aligned} u_{K,\bar{K}}(s) &= \pm\frac{1}{\alpha(\mu)}\tanh^{-1}\left[\frac{\mu}{\sqrt{1+\mu^2}}\tanh\frac{s}{d(\mu)}\right], \\ s &= x-vt, \end{aligned} \tag{183}$$

where:

$$d(\mu)=\frac{2\mu\sqrt{2a(\mu)}}{\alpha(\mu)\sqrt{(1+\mu^2)}}. \tag{184}$$

The solution with "+" sign stands for a kink $u_K(x)$, while the solution with "-" sign stands for an antikink $u_{\bar{K}}(x)$ of width $d(\mu)$. In the static regime, the characteristic energy (or rest mass) associated with the static kink and static antikink solution eq. (**??**) is obtained by using the general expression:

$$E_K=\int_{-\infty}^{+\infty}\rho_\mu(x)dx, \tag{185}$$

with:

$$\rho_\mu(x)=\frac{1}{2}\left(\frac{\partial u}{\partial x}\right)^2+V(u,\mu) \tag{186}$$

the kink energy density. Substituting the solitary-wave solution eq. (**??**) obtained in formula (**??**) yields:

$$E_K=\frac{\sqrt{2a(\mu)}}{2\alpha(\mu)\mu^2}\left[2\alpha(\mu)(1+2\mu^2)-sinh(2\mu)\right]. \tag{187}$$

In Fig. **??**, shape profiles of the static kink solution $u_K(x)$ (a) and of the kink energy density $\rho_\mu(x)$ (b), are plotted versus the spatial coordinate x for some values of the deformability parameter μ. The bottom graph in the figure, i.e. graph (c), represents the variation of the kink rest energy as a function of the deformability parameter μ. One sees that as the deformability parameter μ increases, the asymptotic values of $u_K(x)$ as $|x|\to\infty$ remains the same but a decrease in the kink width is noticeable. On the other hand, an increase of μ leaves the maximum of the energy density unaffected but affects the width of the energy density in the region covered by the barrier and the potential wells. Remarkably the energy density seems to decrease with μ as we go far in the region covered by the repulsive walls of the potential, such that in this region the kink is expected to become more localized.

Fig. **??**c depicts the kink rest energy as a monotonically increasing function of the shape

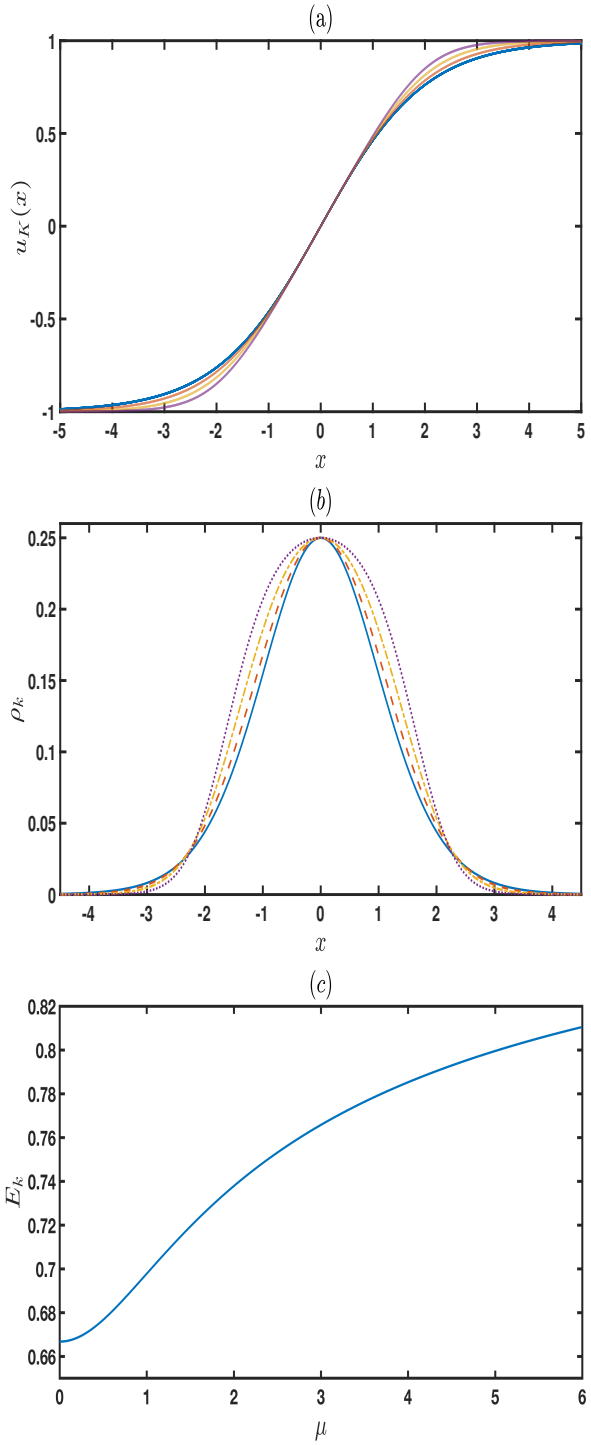

Figure 28: (Color online) (a) Shape of the kink $u_K(x)$ and (b) of the energy density $\rho_\mu(x)$ as a function of x, for: $\mu = 0$ (Solid line), $\mu = 2.0$ (Dashed line), $\mu = 4.0$ (Dot-dashed line) and $\mu = 8.0$ (Dotted line). (c) Variation of the kink creation energy E_K, as a function of μ. The plots are obtained taking $a_0 = 1/8$.

deformability parameter. In other words, an increase in μ will enhance the kink stability and hence the sharpness of the kink profile.

Most of the processes from the kink-antikink collisions arise as a consequence of vibrational modes inherent to the kink scattering excitation spectrum. Usually a perturbation theory is utilized to derive the spectrum of localized excitations around a kink [**?**, **?**]. To this last point, perturbing linearly the scalar field $u(x,t)$ around one kink solution $u_K(x)$ i.e. $u(x,t) = u_K(x) + \eta(x)\exp(-i\omega t)$, yields the following Schrödinger-like eigenvalue problem [**?**, **?**]:

$$\left[-\frac{\partial^2}{\partial x^2} + V_{sch}(x,\mu)\right]\eta = \omega^2\eta. \tag{188}$$

In this eigenvalue equation the quantity $V_{sch}(x,\mu) = \frac{d^2V}{du^2}$ is the scattering potential in the picture of the Schrödinger-like eigenvalue problem, which in the present case is given by:

$$\begin{aligned} V_{sch}(x,\mu) &= a_0\frac{\left[\mu^2\tanh^4\left(\frac{x}{d(\mu)}\right) + 3\tanh^2\left(\frac{x}{d(\mu)}\right) - c(\mu)\right]}{\left[d(\mu)\left(\mu^2\tanh^2\left(\frac{x}{d(\mu)}\right) - c(\mu)\right)\right]^2}, \\ c(\mu) &= 1+\mu^2. \end{aligned} \tag{189}$$

Note that this scattering potential determines the kink stability upon scattering with phonons [**?**, **?**]. Instructively an identical expression for $V_{sch}(x,\mu)$ is obtained by taking a linear perturbation around an antikink solution.

Distinct profiles of the scattering potential $V_{sch}(x,\mu)$, for different values of the deformability parameter μ, are represented in Fig. **??**. One sees that as μ increases, the scattering potential has its width that gradually decreases and its asymptotic limit growing drastically higher. In the range $0 < \mu \lesssim 1.2$, the potential possesses a global minimum located at $x = 0$, which transforms into a local maximum together with the appearance of two degenerate minima in the potential as the value of μ rises larger than 1.2.

The same way as the scattering potential, the occurrence of bound states holds a key importance in grasping some relevant features of the scattering structure of the system [**?**, **?**]. In particular a resonance mechanism for the exchange of energy between the translational mode and a vibrational mode, may result in rich consequences in the spectral features of the system [**?**]. To gain insight onto this last feature, we solved the eigenvalue eq. (**??**) for μ and the results emphasizing the influence of the parametrization on the appearance of bound states, are shown

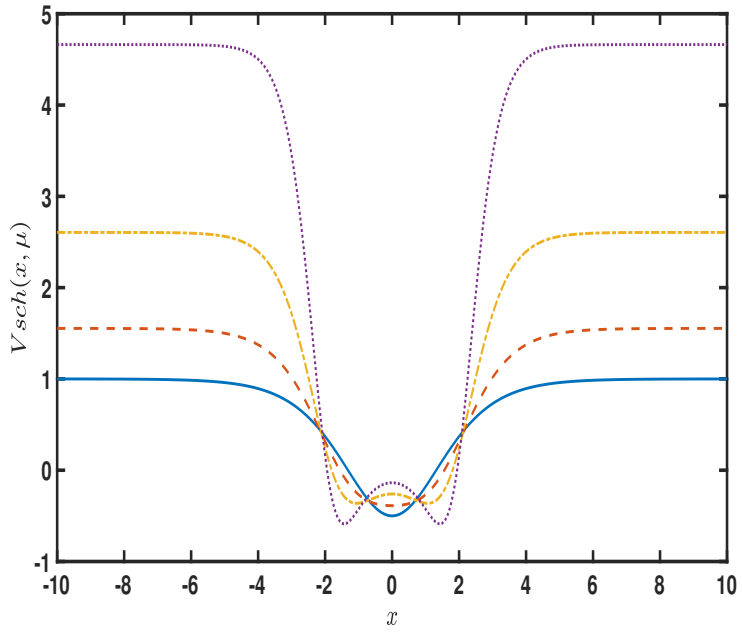

Figure 29: Plot of the scattering potential $V_{sch}(x,\mu)$ as a function of x, for $\mu = 0$ (Solid line), $\mu = 1.0$ (Dashed line), $\mu = 2.0$ (Dot-dashed line) and $\mu = 3.0$ (Dotted line). Here $a_0 = 1/8$.

in Fig. **??**. We note the presence of a zero-mode for all the values of the shape deformability parameter, moreover the appearance of new bound states is observed as μ rises. For instance, as μ lies in the range $0.55 \lesssim \mu \lesssim 1.8$ we notice the presence of two vibrational states, and in the ranges $1.8 \lesssim \mu \lesssim 4.0$ and $\mu \gtrsim 4$ a third and a fourth bound state emerge respectively. Furthermore the lower vibrational has its frequency increasing as μ grows to a specific value, then decreasing while the frequencies of higher vibrational states are monotonically increasing functions of the deformability parameter.

III.5.2 Analysis of kink-antikink collisions

The dynamical equation pertaining to colliding kink-antikink pairs will be solved numerically in this section, with the aim to explore some characteristic spectral features of kink-antikink scatterings and identify vibrational models associated with the collisions. To this end, eq. (**??**) is discretized on a spacial grid with periodic boundary conditions, with a potential barrier height taken as $a_0 = 1/8$. The grid is divided into N nodes such that zone widths δx in the simulations have fixed size, with the location of the $n-th$ point on the grid given by $x_n = n\Delta x$. The scalar field is then defined by $u_n(t) = u(x_n, t)$ for $n = 1, 2, ..., N$. The second-order spatial derivative is approximated using a fourth-order central-difference scheme [**?**], which leads to a set of N

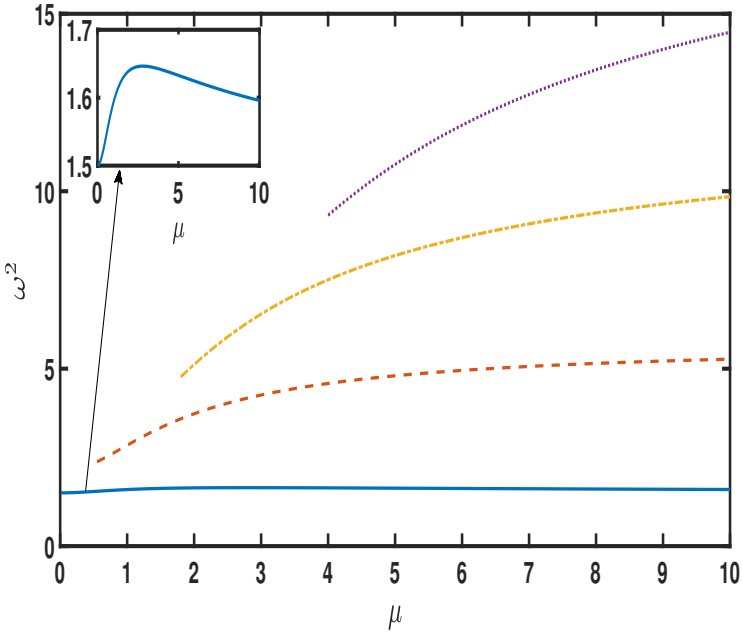

Figure 30: Plot of the squared frequencies ω^2 of the vibrational states, as a function of μ. Here $a_0 = 1/8$.

coupled second-order ordinary differential equations in u_n i.e.:

$$\frac{\partial^2 u_n}{\partial t^2} = \frac{1}{12(\Delta x)^2}(-u_{n-2} + 16u_{n-1} - 30u_n \\ +16u_{n+1} - u_{n+2}) - \frac{dV(u_n, \mu)}{du_n}, \tag{190}$$

which is solved numerically using a fourth-order Runge-Kutta scheme with fixed step. The accuracy of our algorithm stands with errors that scale as $(\Delta x)^2$ and $(\Delta t)^4$.

The initial data used in our simulations represent a kink and antikink centered at the points $x = -x_0$ and $x = x_0$ respectively, and moving forward each other with initial velocities v in the laboratory frame. The definition of the starting function can therefore be expressed:

$$u(x, 0) = u_K(x + x_0, v, 0) - u_K(x - x_0, -v, 0) - u_m, \tag{191}$$

where $u_m = \pm 1$ stands for the kink-antikink and antikink-kink initial configurations, respectively. We set the grid to be sufficiently large, with left and right boundaries respectively at $x_l = -400$ and $x_r = +400$, and the separation distance to be $2x_0 = 24$. The choice of a large grid

together with periodic boundary conditions, was to avoid the reflected kink forms to travel to the boundary, and also to prevent any radiation emitted during the collision process to eventually find itself back to interact with the kinks. The grid is discretized with $N = 10^5$ nodes and all simulations were run with a temporal step size $\Delta t = 0.7(\Delta x)$, found to be a good consensus between the costly computational time and the production of results form high-resolution runs.

Several outputs obtained from numerical simulations at some different initial velocities are now discussed. For weak velocities, the kink and antikink are expected to bound upon collision and have enough time to radiate sufficient energy forming a bion state. This is shown in figs. **??**(a) and **??**(e), where we plotted the evolution of the center of mass $u(x = 0, t)$ of the kink-antikink pair, for some values of the shape deformability parameter for which the system has just one vibrational mode. Irrespective of the barrier deformation, the kink-antikink pair moving with an initial velocity lower than a critical velocity v_c settles to an erratically oscillating bion state. But for large velocities $v > v_c$, the kink-antikink pair does not have enough time to radiate sufficient energy to form a bion state. Thus the kink and antikink will once collide and permanently reflect each other during the scattering process. This is represented in figs. **??**(b) and **??**(f). For all the considered values of μ one can note the appearance of a spike illustrating the collision, followed by a leveling off at $u = +1$ implying that the kink and antikink have reflected and traveled far from each other. Still, the transition between the bion state and the reflection state is not smooth as the initial velocities increase. There are regions of values of v for which these two states alternate. This regions were reported in several works as "windows" [**?**, **?**, **?**, **?**, **?**]. For instance, in figs. **??**(c) and **??**(g), we note two spikes in the evolution of the center of mass implying that the kink and antikink collide and reflect, then return to collide again before receding to a permanent reflection. Referring to the number of collisions before the last and permanent reflection, the sets of contiguous initial velocities leading to this state can be identified as forming a two-bounce window. The presence of a three-bounce window is evidenced in figs. **??**(d) and **??**(h), the velocities lying in the three-bounce windows are found on the edge of the two-bounce regions. When values of the deformability parameter μ are located in the range where there exists only one vibrational mode, the system presents a similar fractal structure as the one observed from the scattering process in the ϕ^4 model. For example we can note the existence of a four-bounce window in Fig. **??**. The appearance of n-bounce windows is also expected to be observed for this range of shape deformability parameter values. To further understand

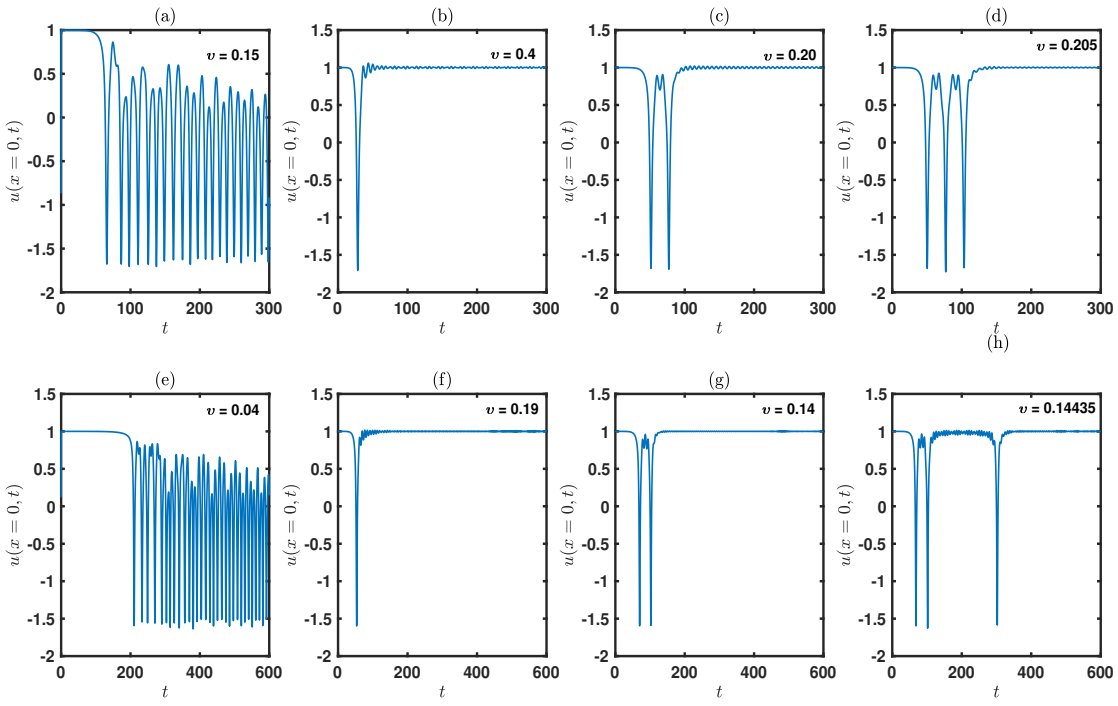

Figure 31: Possible results for a kink-antikink collision at several initial velocities, considering two values of the shape deformability parameter μ. $\mu = 0$: (a), (b),(c) and (d). $\mu = 0.5$: (e), (f),(g) and (h). Values of μ were chosen such that only one vibrational mode appears in the excitation spectrum.

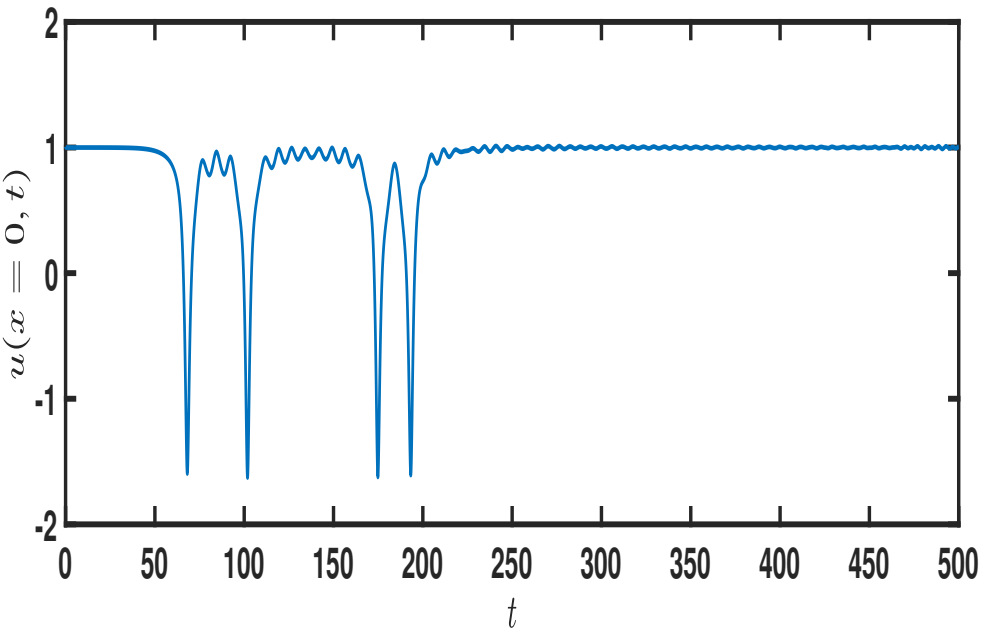

Figure 32: A four-bounce window taking $\mu = 0.5$ is evidenced by plotting $u(x = 0, t)$ for $v = 0.1445$. Note the presence of four large spikes illustrating collision after which the kink and antikink reflect and recede from each other forming a two-soliton state.

the structure of scattering in the system, in Fig. **??** we plotted the time of the three bounces as a function of the initial velocity. The intervals in which the time for the third collisions diverges, range in the two-bounce windows. A case with only one vibrational mode is illustrated in Fig. **??**(a), which shows plot of the collision times for $\mu = 0.5$ (compare with figs. **??**(e), **??**(f), **??**(g) and **??**(h)). We can note that bion states are formed for $v < v_c \sim 0.183$ while for $v > v_c$, the collision results in an inelastic scattering between the pair corresponding to one-bounce around one vacuum. Moreover, the figure captures the complete set of two-bounce windows of which the width continuously decreases and accumulates around v_c. The scattering times in the presence of several vibrational modes are plotted in Fig. **??**(b) where we considered the shape of the potential for $\mu = 5$. We first see that v_c grows larger with μ. From our simulations we observed that the variation of the critical velocities is not a monotonic function of the shape deformability parameter, we first observed a decrease of v_c as μ increases till $\mu \sim 1$ then recedes to an increasing behavior (this result is not presented here). This reflects that the attraction between the kink and antikink lessens as the system is deformed departing from the ϕ^4 model, but the attractive interaction gets stronger and stronger as $\mu \gtrsim 1$. Suppression of two-bounce windows is also observed in Fig. **??**(b). This is justified by the presence of several vibrational modes complicating the energy transfer from the translational mode to just one vibrational mode to achieve resonance conditions.

One of our main point of focus in this section is the possible production of oscillons. For relatively small values of the deformability parameter μ, for which only one vibrational mode is generated in the excitation spectrum, oscillon structures cannot appear, the kink-antikink collisions with initial velocities lower than the critical velocity can only result in bion and n-bounce states. The ϕ^4 model being an asymptotic limit of the parametrized DW model in this range of values of μ, this agrees with the ϕ^4 model showing no evidence for the formation of oscillons as a result of the scattering process. We see from Fig. **??** that for larger values of μ, the presence of more than one vibrational mode favors the production of oscillons. At some velocities of the colliding kink, lower than the critical velocities, the bion is formed and travels with oscillons which can oscillate around each other, or escape to infinities. We can compare the appearance of one bion and two oscillons travelling together with a large flux of emitted radiation in Fig. **??**(a), and the appearance of one bion and four oscillons in Fig. **??**(b), travelling with quite no radiation and a larger degree of harmonicity. Note that the larger the shape deformability parameter the

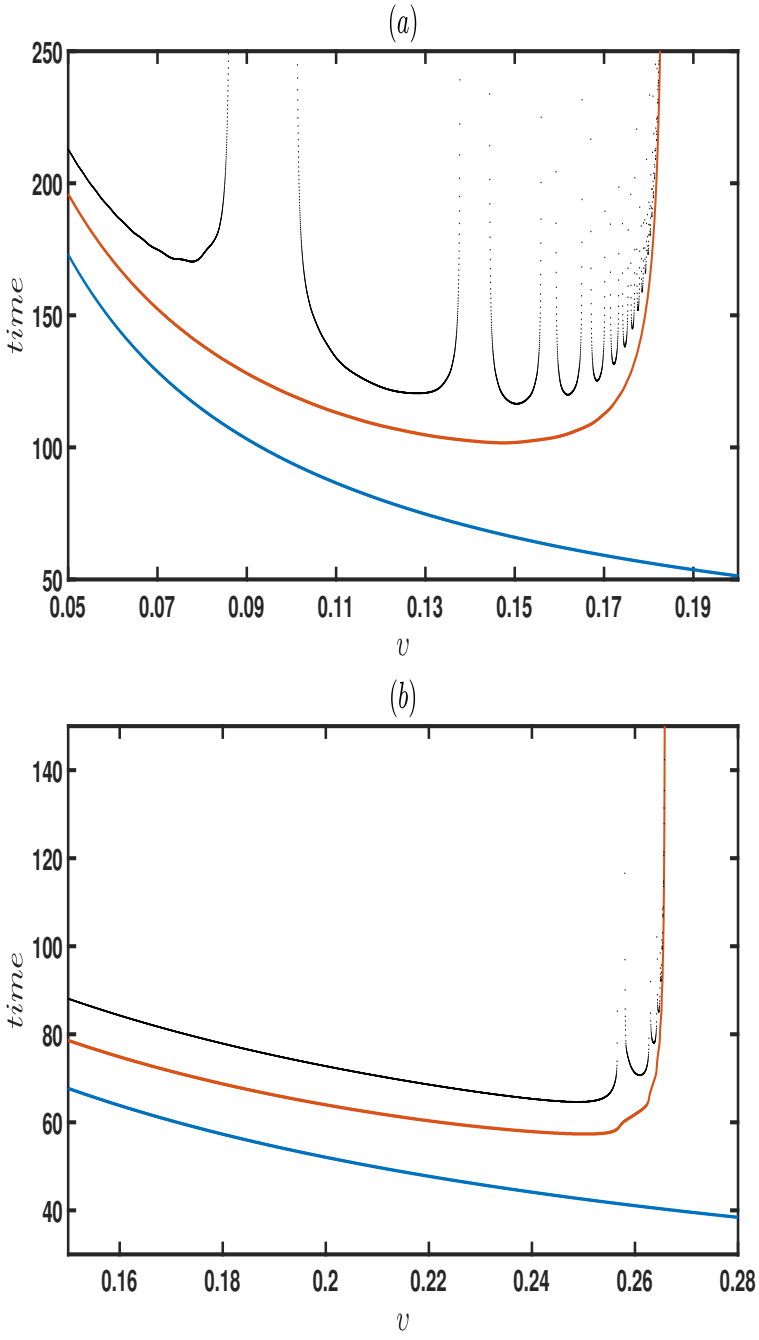

Figure 33: Kink-antikink collision times to first (blue), second (red) and third (dotted-black) bounces, as a function of initial velocity for (a) $\mu = 0.5$ and (b) $\mu = 5.0$.

greater the number of created oscillons.

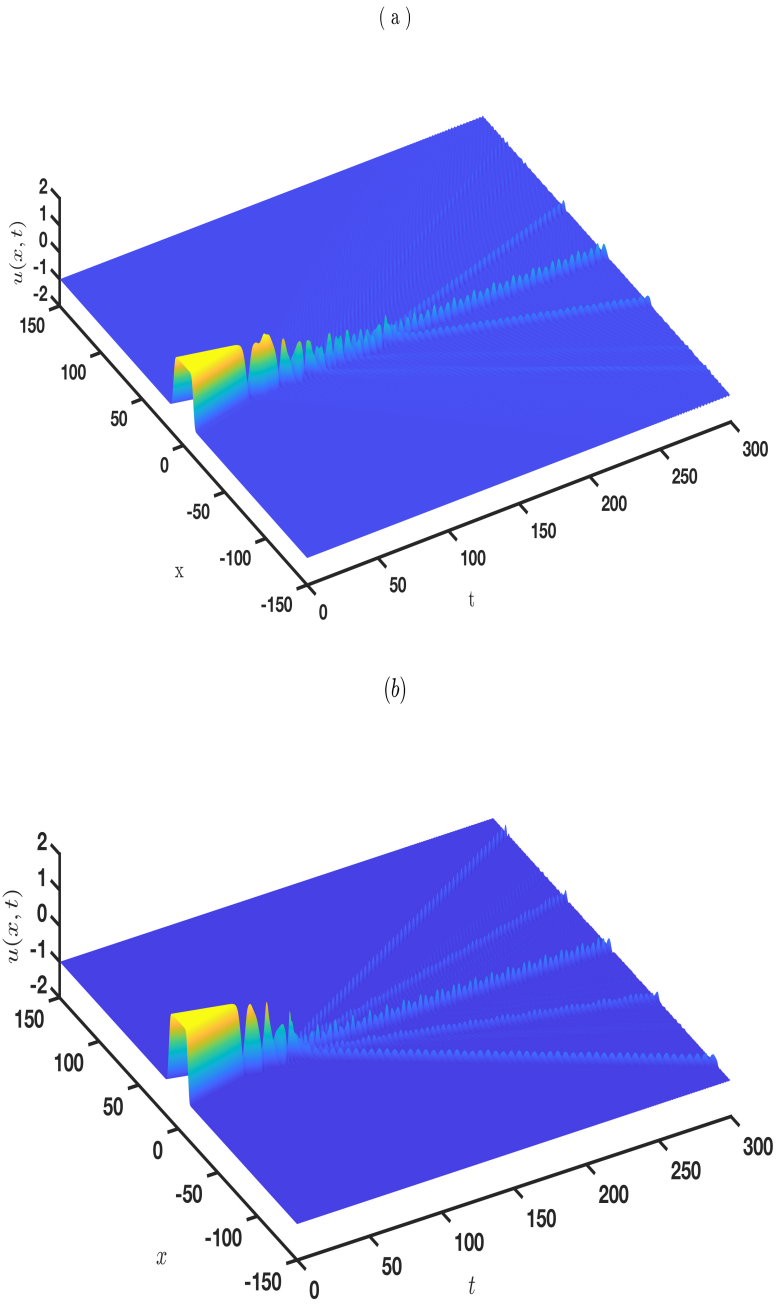

Figure 34: Oscillons resulting from kink-antikink collisions: (a) $\mu = 3.0$ and $\upsilon = 0.23$ ($\upsilon_c = 0.245$) showing one bion and two oscillons, (b) $\mu = 5.0$ and $\upsilon = 0.236$ ($\upsilon_c = 0.27$) showing one bion and four oscillons.

III.6 Conclusion

In this chapter, we have presented the analytical and numerical results obtained from the theoretical treatment of bistable systems presented in Chapter **??**, considering the four parametric

DWPs having the ϕ^4 potential as their asymptotic limit. First of all, we have shown numerically and analytically that the order of the transitions the quantum tunneling to the classical crossover is linked to the shape of the system. For small values of the shape parameter these transitions are only of the second order, but we obtained a critical value μ_c above which first-order transitions can also occur. Later on, it was found that under a certain condition, the statistical mechanics of the systems could be exactly analyzed at some temperatures. For any non null value of the shape parameter we derived the exact formulation of the ground states for at least four temperatures. The influence of the deformability on the probability density function have been discussed. At last, we studied numerically the kink-antikink scattering in one specific case of our set of potentials. We found that the collision of the pair could result in bound states or display $n-$bounce windows before separation. But as the shape parameter increases, the system becomes more favorable to the generation of oscillons.

General Conclusion

In this thesis, we have investigated the influence of shape deformability on the occurrence and orders of transitions in quantum tunneling, on kink-antikink scattering-induced phenomena, and on the statistical mechanics of a deformable bistable system, taking the particular case a family of Dikané-Kofané potentials. Some generalities and literature review, together with the definition of the concept of bistability are presenetd in Chapter I. Chapter II presents the general model and the methods we used for our investigations, and our results a discussed in Chapter III.

At first, using three criteria to determine the order of phase transitions, we investigated the transition from the quantum tunneling regime to the classical crossover regime for our potentials. The type of transition depends on the potential parameter. We have established the existence of a critical value of the shape deformability parameter μ above which a first-order transition in quantum tunneling would occur, besides the second-order transition inherent to the Ginzburg-Landau feature of the DW potential energy. We found that the critical value obtained is not affected by a the barrier height or the position of the degenerated minima, but by the deformability addressing only a variation of the curvature shape of the barrier. We then concluded that the flatness of the barrier is an important factor favoring the occurence of first-order phase transitions. Potential barriers with a strongly flat curvature shape suppress the thermally assisted tunneling, inducing the thermal activation to compete directly with the ground-state tunneling, leading to a sharp first-order transition.

We later on explored the possibility to study the statistical mechanics of the system via the transfer-integral operator method, with emphasis on conditions for quasi-exact solvability of the associated pseudoparticle's Schrödinger equation. We first applied the transfer-integral formalism and obtained the Schrödinger equation governing the states of the system. We determined the conditions for which the latter equation was solvable, at least to obtain some states of the pseudoparticle. With the help of the Sommerfeld method it was possible to derive the exact formulations of ground-state wavefunctions and their corresponding eigenenergies for some

temperatures determined by the quasi-exact solvability condition. Knowing just the low-lying eigenvalues and eigenfunctions is sufficient to obtain almost complete information regarding the classical thermodynamics of the field theoretic system. Concerning the dependence of these wavefunctions and eigenenergies on the shape deformability parameter, we found that for each value of μ the quasi-exact solvability of the model allows the exact computation of the eigenstates at various temperatures. These temperatures were obtained above and below the transition temperature, depending on the values of the shape deformability parameter. It was established that the QES property of our models holds only at a discrete set of temperatures. The strategy was then to tune system parameters so as to straddle an interesting region in temperature space which, for this thesis, we have taken to be the region around the short-range order ('kink') transition point. Then, the influence of shape deformability on the probability density was examined. Another important result in this study is the validation of numerical techniques. Recent advances in large scale computations have made it possible to calculate quantities such as the PDF using Langevin dynamics to a very high accuracy. The PDF is the probability distribution of field values average over the total system volume. Alternatively, it is equal to the square of the ground state wavefunction of the transfer operator at a given temperature. All the thermodynamics information can be shown to reside in the PDF. Our analytical results for the PDF showed a striking agreement with large-scale Langevin simulations at the temperatures we obtained from the solvability condition, implying that the study of probability density-based thermodynamics via Langevin simulations is feasible for bistable systems with the family of potentials we considered in this study. The advantage of such simulations is that representative field configurations are available and can be analyzed to compute such quantities as the kink density, finite temperature kink profile, the spatial kink distribution, kink transport and nucleation, etc. This sort of analysis is not possible with the Monte Carlo techniques.

Oscillons are breather-like bound states generated by self-interactions of kink-antikink pairs that exist in some scalar-field models, [**?**, **?**, **?**, **?**, **?**] in the context of cosmology their built-in mechanism suggests that they can affect the standard picture of scalar ultra-light dark matter. To determine more exactly which of the characteristic features introduced by the potential deformability effectively controls the oscillon production, in this thesis we revisited the study made in literature by considering the newly proposed member of the DK family of potentials. The DW potential has fixed potential minima and fixed barrier height. However, the steepness of the po-

tential walls, and hence the flatness it the barrier top, can be tuned by varying a deformability parameter. Examining the kink-antikink scattering processes, we found that the parametrized bistable model inherits some of the general features of the ϕ^4 model that is the possibility of formation of bion states, reflected states and also n-bounce windows. However, the appearance of additional modes in the scattering spectrum, as the DWP deformation becomes predominant in our model, suggests the possibility of suppression of the two-bounce windows due to a kind of interference, as was already detailed in some other works [**?**, **?**] . Long-lived, quasi-harmonic and low-amplitude structures called oscillons were shown to form after kink-antikink collisions with some initial velocities less than a critical velocity. This is not observed for low values of μ, where the model has only one vibrational state and is more close to the ϕ^4 model. The rising number of vibrational states as μ increases yields to an intricate situation where the realization of the mechanism of resonant energy exchange between the translational and one vibrational mode becomes more difficult. The appearance of oscillons is thus favored by the deformation in our model. In the works of Bazeia et al., reporting the appearance of oscillons in hyperbolic models [**?**] for two members of our family of DWPs, they showed that the production of oscillons is boosted by applying the conformational changes from those potentials deformability such as reducing the distance between the minima keeping the barrier height fixed, or decreasing the barrier height while keeping the minima fixed. They pointed out that the factor unifying the two contexts is the lowering of the kink energy by the deformability in the two models. The scattering dynamics at the center of mass in our newly proposed model are roughly the same as the one in the work of Refs. [**?**] and [**?**], however the increase of the kink energy in our new model disagrees with a tentative idea to extend the consideration of kink energy being a determinant unifying factor to a more general case. The deformation in our model is manifested through an increase of the steepness of the potential walls, with the barrier top becoming flattened hence imposing an anharmonic shape to the potential barrier. This trend can also be observed as an implicit result of the deformation in the two models considered by Bazeia et al. in Ref. [**?**], and also in the sinh-deformed ϕ^4 model in Ref. [**?**] shown to allow the creation of oscillons. Bistable systems modeled by potentials with anharmonic barrier are thus suggested to be good candidates to observe the formation of oscillons in kink-scattering processes.

Investigations in the above contexts led to results that curiously apply to all known and still unknown members of the family of parametric DWPs considered in this study:

- The transition from quantum tunneling regime to the classical crossover regime depends on the potential parameter. The transition is of the first-order and occur in all the potential models for $\mu > \sqrt{3/2}$.

- All the members of the class possess the QES property provided a particular condition. The exact formulation of eigenstates can be made for at least four temperatures both above and below symmetry breaking temperature, these temperatures are closely related to the potential shape. The fact that the potential are smoothly varying DWPs allowing quasi-exact solvability with energy eigenvalues obtained are simple functions, conversely to the numerous known QES DWPs, is to be mentioned.

- The possibility of generation of oscillons will be favored as far as the member will display an increase of the flatness of the potential barrier as a consequence of a change in the deformability.

These features commonly shared by these potentials are of great interest for the study of complex physical systems in the deformable landscape.

In this thesis, despite the consideration of a general form for bistable potentials modeling the system, it is to be recalled that we proposed a new parametric deformable system addressing a new type of deformability, appearing only implicitly in the existing deformable DWPs in litterature. From our results, it is obvious that the deformability modeled by our potential is a factor justifying the observation of some interesting phenomena. The proposed potential is bistable and also possesses reflective wall. It is then suitable to model the interactions in hydrogen bonds, and It would then be relevant to study the impact of the deformability it triggers on proton-transfer in hydrogen bonds. Also, the proposed potential show an increase of the confinements strength of its well together with a flattening of its barrier as the shape deformability parameter increases. As the influence of confinement strength was already shown in literature to be critical in the context of stochastic resonance, it would be interesting to investigate the influence of the rise of the ahnarmonicity of the barrier in the context of thermally activated escape and also stochastic resonance. indeed, the shape of the barrier could impose consideration of the inter and intra-well dynamics while invalidating the two-state approximation and, on the other hand, have a noticeable influence on the residence time of the particles in the potential well.

Appendix

Exact solutions to the eigenvalue problem (equation **??**):

$$\frac{\partial^2}{\partial z^2}\psi_j + q^2\left[E_j - (\xi\cosh(2z)-1)^2\right]\psi_j = 0, \tag{192}$$

where $z = \alpha(\mu)u$, $\xi = (1+2\mu^2)^{-1}$, $E_j = 4\mu^4\xi^2\epsilon_j/a(\mu)$ and

$$q^2 = \frac{a(\mu)}{2\mu^4(\alpha(\mu)\xi)^2}\beta^2. \tag{193}$$

Here, we are interested in solutions which vanish in the limit $z \to \pm\infty$. In this respect, we can readily define:

$$\psi(z) = r(z)\exp\left[-z_0\cosh(2z)\right], \tag{194}$$

where the function $r(z)$ is a polynomial expressed as a linear combination of $\cosh m_p z$ or $\sinh m_p z$ and their powers, with z_0 and m_p ($p = 0, 1, 2, ...$) being constant quantities to be determined. Applying the Sommerfeld method (see Sec. **??**), the exact expressions for the wavefunctions, and of the associated energy eigenvalues, are found and listed below

Taking $q = 1$:

$$\psi_0(z) = \exp\left[-\frac{\xi}{2}\cosh(2z)\right], \quad E_0 = 1+\xi^2$$

Next for $q = 2$ the solutions are:

$$\psi_0(z) = \cosh(z)\exp\left[-\xi\cosh(2z)\right], \quad E_0 = \xi^2 - \xi + \frac{3}{4},$$

and

$$\psi_1(z) = \sinh(z)\exp\left[-\xi cosh(2z)\right], \quad E_1 = \xi^2 + \xi + \frac{3}{4}.$$

Note that $E_1 - E_0 = 2\xi$.

For $q = 3$ we have:

$$\begin{aligned} \psi_0(z) &= \left[6\xi + \left(1 + \sqrt{1+36\xi^2}\right)\cosh(2z)\right]\exp\left[-\frac{3\xi}{2}\cosh(2z)\right], \\ E_0 &= \xi^2 - \frac{2}{9}\sqrt{1+36\xi^2} + \frac{7}{9} \end{aligned}$$

$$\begin{aligned} \psi_1(z) &= \sinh(2z)\exp\left[-\frac{3\xi}{2}\cosh(2z)\right], \\ E_1 &= \xi^2 + \frac{5}{9}. \end{aligned}$$

$$\begin{aligned} \psi_2(z) &= \left[6\xi + \left(-1 + \sqrt{1+36\xi^2}\right)\cosh(2z)\right]\exp\left[-\frac{3\xi}{2}\cosh(2z)\right], \\ E_2 &= \xi^2 + \frac{2}{9}\sqrt{1+36\xi^2} + \frac{7}{9}. \end{aligned}$$

Note that

$$E_1 - E_0 = \frac{2}{9}\sqrt{1+36\xi^2} - \frac{1}{9}, \quad E_2 - E_1 = \frac{4}{9}\sqrt{1+36\xi^2}$$

For $q = 4$ we have:

$$\begin{aligned} \psi_0(z) &= \left[12\xi cosh(z) + \left(2 - 4\xi + 2\sqrt{1-4\xi+16\xi^2}\right)cosh(3z)\right]\exp\left[-2\xi cosh(2z)\right], \\ E_0 &= \frac{1}{16}\left(16\xi^2 - 4\sqrt{1-4\xi+16\xi^2} - 8\xi + 11\right). \end{aligned}$$

$$\begin{aligned} \psi_1(z) &= \left[12\xi sinh(z) + \left(2 + 4\xi + 2\sqrt{1+4\xi+16\xi^2}\right)sinh(3z)\right]\exp\left[-2\xi cosh(2z)\right], \\ E_1 &= \frac{1}{16}\left(16\xi^2 - 4\sqrt{1-4\xi+16\xi^2} + 8\xi + 11\right). \end{aligned}$$

$$\begin{aligned} \psi_2(z) &= \left[12\xi cosh(z) + \left(2 - 4\xi - 2\sqrt{1-4\xi+16\xi^2}\right)cosh(3z)\right]\exp\left[-2\xi cosh(2z)\right], \\ E_2 &= \frac{1}{16}\left(16\xi^2 + 4\sqrt{1-4\xi+16\xi^2} - 8\xi + 11\right). \end{aligned}$$

Note that

$$E_1 - E_0 \quad = \quad \xi + \frac{1}{4}\sqrt{1 - 4\xi + 16\xi^2} - \frac{1}{4}\sqrt{1 + 4\xi + 16\xi^2}$$

and

$$E_2 - E_0 = \frac{1}{2}\sqrt{1 - 4\xi + 16\xi^2} \tag{195}$$

List of Publications

1. **F. Naha Nzoupe**, A. M. Dikandé and C. Tchawoua, *Phase transition in quantum tunneling and exact statistical mechanics for a model of parameterized double-well potential*, Math. Meth. Appl. Sci, 1 (2020).

2. **F. Naha Nzoupe**, A. M. Dikandé and C. Tchawoua, *Kink-antikink scattering-induced breathing bound states and oscillons in a parametrized ϕ^4 model*, Mod. Phys. Lett. A 36, 2150015-1 (2021).

Received: 19 June 2020

DOI: 10.1002/mma.6965

SPECIAL ISSUE PAPER

WILEY

Phase transition in quantum tunneling and exact statistical mechanics for a model of parameterized double-well potential

Fernand Naha Nzoupe[1] | **Alain Moíse Dikandé**[2] | **Clement Tchawoua**[1]

[1]Laboratory of Mechanics, Department of Physics, Faculty of Science, University of Yaoundé, Yaoundé, Cameroon

[2]Laboratory of Research on Advanced Materials and Nonlinear Sciences (LaRAMaNS), Department of Physics, Faculty of Science, University of Buea, Buea, Cameroon

Correspondence
Alain Moíse Dikandé, Laboratory of Research on Advanced Materials and Nonlinear Sciences (LaRAMaNS), Department of Physics, Faculty of Science, University of Buea P.O. Box 63 Buea, Cameroon.
Email: dikande.alain@ubuea.cm

Communicated by: D. Alexandrov

A model for one-dimensional bistable systems characterized by a deformable double-well energy landscape is introduced in order to investigate the effect of shape deformability on the order of phase transition in quantum tunneling and on the quasi-exact integrability of the classical statistical mechanics of these systems. The deformable double-well energy landscape is modeled by a parameterized double-well potential possessing two fixed degenerate minima and a constant barrier height, but a tunable shape of its walls which affects the confinement of the two wells. It is found that unlike bistable models involving the standard ϕ^4-field model for which the transition in quantum tunneling is predicted to be strictly of second order, a parameterization of the double-well potential also favors a first-order transition occurring above a universal critical value of the shape deformability parameter. The partition function of the model is constructed within the framework of the transfer integral formalism, with emphasis on low-lying eigenstates of the transfer integral operator. Criteria for quasi-exact integrability of the partition function were formulated, in terms of the condition for possible existence of exact eigenstates of the transfer integral operator. The quasi-exact solvability condition is obtained analytically, and from this, some exact eigenstates are derived at several temperatures. The exact probability densities obtained from the analytical expressions of the ground state wavefunctions at different temperatures are found to be in excellent agreement with the probability density obtained from numerical simulations of the Fokker–Planck equation.

KEYWORDS

bistable systems, Fokker-Planck equation, quantum equilibrium statistical mechanics, quantum field theory, related classical field theories, solitons, transition in quantum tunneling

MSC CLASSIFICATION

37J05; 35Q84; 37K40; 81T28; 82B10

1 | INTRODUCTION

In systems with multiple equilibrium states, the transition between metastable states separated by energy barriers arises either in the classical regime via thermal activation, or in the quantum regime via tunneling processes. At high

temperature, thermal activation governs the transition which usually occurs as a hopping over the potential barrier. However, at low enough temperature (i.e., near quantum criticality $T \rightarrow 0$), the transition is governed by quantum tunnelings through the potential barrier. In this second context, the system dynamics is characterized by classical configurations called instantons,[1,2] which are expected to dominate the thermal rate at low temperature.[3,4] As the temperature increases, the thermally induced crossover becomes more and more important, and at some critical temperature, a phenomenon known as 'phase transition in quantum tunneling'[5] can take place. This phenomenon has recently attracted a great deal of interest; in particular, it was demonstrated that some physical systems can exhibit not only a smooth second-order transition at a critical temperature T_0 but also a first-order transition[6-12] at some different temperature.

Another aspect of interest in the study of displacive elementary excitations in condensed matter physics is their dominant contribution in the low-temperature statistical mechanics of the systems.[13-17] In the early 1980s, a soliton gas phenomenology was proposed[15] to address the problem of low-temperature statistical mechanics of condensed matter systems admitting kin and solitary wave solutions in general. This phenomenology, then called transfer integral formalism, was later generalized to kink-bearing systems for which kink–phonon interactions lead to reflectionless scattering potentials.[18] The transfer integral formalism has gained a constantly growing attention over the four last years, because of the universal framework it offers in the study of a wide range of thermodynamics-based processes including in quantum systems.[19-23] In kinetic theory, the formalism has been used to develop nontrivial (i.e., quasi-exact) approaches to escape rate problems in both classical and quantum regimes[24,25] and so on.

The above-mentioned studies, however, rest mainly on the assumption of two universal models, namely, the sine-Gordon[26,27] model, assumed to describe systems with periodic one-site potentials, and the ϕ^4[28,29] model intended for systems with double-well (DW) energy landscapes. Yet real physical systems to which these models and studies address are actually far more complex, sometimes also displaying a rich diversity with unique structural features. For instance, the sine-Gordon and ϕ^4 potentials both have fixed extrema, in addition to their shape profiles that are rigid and hence restrict their applications to only very few physical contexts. Nonetheless, it has been shown that these weaknesses can be overcome by envisaging a parameterization of these two universal models. Indeed, the sine-Gordon model was generalized by Remoissenet and Peyrard[3,30,31] into a parameterized periodic potential (the so-called Remoissenet–Peyrard potential),[30-32] and the ϕ^4 potential was parameterized[33-36] into a DW potential model with a tunable shape profile. It is worthwhile to stress that although some other parametric DW potentials exist in the literature,[37-39] the family of DW potentials proposed in other studies[33-36] is peculiar in that it groups three different classes with distinct shape deformability features, but the three classes admit the ϕ^4 potential as a specific limit.

The importance of shape deformability in the context of bistable systems lies in two issues related to their structural properties. The first issue is linked with the problem of symmetry breaking, for which the ϕ^4 model predicts the transition in quantum tunneling to be strictly of second order.[9-12] The second issue is related to observations[13,15] that the transfer integral formalism always reduces the classical statistical mechanics of a one-dimensional (1D) ϕ^4-field theory, to a time-dependent quantum mechanical problem for which no exact solution exists. The first issue was recently addressed by Zhou et al,[40] who formulated the problem of transitions in quantum tunneling for one[34] among the three existing classes of parameterized DW potentials.[33-36] Thus, Zhou et al[40] obtained that due to the extra degree of freedom accounting for shape deformability, bistable systems which can be described by the parameterized DW potential could exhibit a first-order transition occurring at a finite critical value of the shape deformability parameter, besides the second-order transition predicted by the ϕ^4 model. As for the second issue, given that the classical statistical mechanics of a field theoretical system can be fully analyzed with just the knowledge of its low-lying eigenstates, parameterized DW models are quite likely to introduce the possibility for quasi-exactly solvable (QES) systems in field theory.[41-46]

In the work of Zhou et al,[40] the parameterized DW potential was one for which the height of the potential barrier could be varied continuously by varying a shape deformability parameter, leaving unchanged the positions of the two degenerate minima.[34] In the present work we wish to examine the possible occurrence of a first-order transition in quantum tunneling, for a new family of DW potential which is parameterized in such a way that the barrier height and positions of the two minima are always fixed, but the steepness of the potential walls can be tuned which affects the confinement of the two potential wells. We shall see that this model also leads to a first-order transition in quantum tunneling, besides the second-order transition predicted within the framework of the ϕ^4 theory. We will also discuss the issue of exact integrability of the statistical–mechanical problem for this new parameterized DW model. For this purpose, the low-temperature partition function will be expressed in terms of a transfer integral operator eigenvalue problem,[18] for which exact low-lying eigenstates will be shown to exist provided under a specific condition. Analytical expressions of some exact low-lying eigenfunctions, together with the corresponding energy eigenvalues, will be derived and results for the probability density

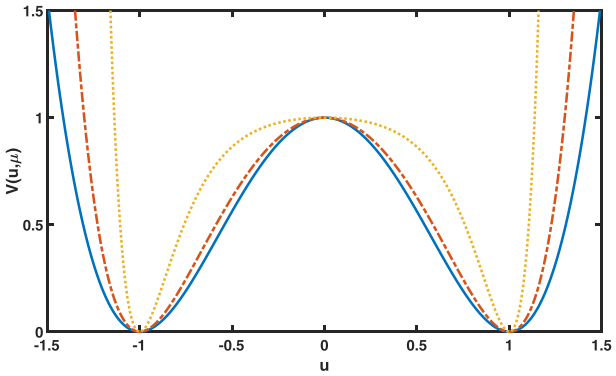

FIGURE 1 (Color online) Profiles of the parameterized double-well potential $V(u,\ \mu)$ for different values of the shape deformability parameter μ: $\mu \rightarrow 0$ (solid line), $\mu = 1.0$ (dot-dashed line), and $\mu = 4.0$ (dotted line). $a_0 = 1$ [Colour figure can be viewed at wileyonlinelibrary.com]

functions discussed analytically. Note that these probability density functions can also be obtained numerically following modern stochastic approaches to noise-driven dynamical transitions of quantum oscillators in bistable systems (see e.g., other studies[47-51]). In the present context, we choose to solve numerically the Fokker–Planck equation associated with the system with a deformable bistable shape profile, assuming a Gaussian white noise.

2 | THE MODEL OF PARAMETERIZED DW POTENTIAL

We are interested in 1D systems for which the bistable energy landscape is represented by a DW potential of the general form

$$V(u,\mu) = a(\mu)\left[\frac{\sinh^2(\alpha(\mu)u)}{\mu^2} - 1\right]^2, \mu > 0, \tag{1}$$

where $a(\mu) > 0$ and $\alpha(\mu)$ are two functions of the shape deformability parameter μ. From a general standpoint, the variable u is a one-component dimensionless field defined on a one-dimensional lattice of points; in the context of phenomenological theory for second-order phase transition, this variable plays the role of order parameter. In physical systems such as one-dimensional atomic and molecular chains, the variable u can be associated with the coordinate of an atom or a molecule relative to a stable equilibrium position along the chain.

$V(u,\ \mu)$ given by (1) belongs to a family of parametric DW potentials[33-36] whose shape profiles can be tuned differently, but which admit a common asymptotic limit which is the ϕ^4 potential when $\mu \rightarrow 0$. For the new member, the two functions $a(\mu)$ and $\alpha(\mu)$ are defined as

$$\alpha(\mu) = sinh^{-1}\mu, a(\mu) = a_0, \tag{2}$$

in which case $V(u,\ \mu)$ is a DW potential with two degenerate minima fixed at $u = \pm 1$ and a barrier height also fixed at a constant value a_0. However, a variation of μ changes the steepness of the potential walls and consequently the sharpness (or confinement) of the potential wells. In Figure 1, $V(u,\ \mu)$ is sketched for some arbitrary values of μ. When μ tends to zero, the parameterized DW potential reduces to $V(u) = a_0\left(u^2 - 1\right)^2$.[13,15] When μ is varied, the slope of the potential walls gets steeper. Hence, the narrowest part of the potential barrier broadens while the flatness of the barrier top becomes more pronounced, resulting in an enhancement of the confinement of the potential wells. Quite instructively, a variation of the barrier shape observed in Figure 1 is consistent with the experimentally observed rates and experimentally observed kinetic isotope effects, when studying vibrationally assisted hydrogen tunneling in enzyme-catalyzed reactions.[52] Indeed, in these biophysical processes, the effect of the catalyzer becoming less efficient results in a progressive broadening of the narrowest part of the barrier, with the shoulder shape of the barrier peak becoming increasingly less pronounced. The parameterized DW potential (Equations 1 and 2) is infinite at the boundaries of the final interval and therefore is suitable for modeling hydrogen bonds in enzyme-catalyzed reactions. Also worthwhile to note, for significant values of the shape deformability parameter μ, the DW potential (Equations 1 and 2) displays features similar to the double-Morse potential, used[39] to describe proton motion in the hydrogen bond O–H$\cdots$O in KDP ferroelectrics. In these specific materials,[39] the one-body proton potential rises steeply in the vicinity of the oxygen atoms, with a gentler slope at the sides of the potential barrier. The parametric DW potential (Equations 1 and 2) can reproduce some of these peculiar features, namely, by taking the proton displacement u from the center of the hydrogen bond and using μ to mimic the rate of variation of the O–O bond distance. Last but not least, a confinement of potential wells in bistable systems has recently been shown to play a crucial role in the occurrence of stochastic resonance in these systems.[53]

3 | FIRST-ORDER TRANSITION IN QUANTUM TUNNELING

Consider a 1D quantum system with a Euclidean action (in dimensionless form):

$$S = \int d\tau \left(\frac{1}{2} \left(\frac{du}{d\tau} \right)^2 + V(u, \mu) \right), \tag{3}$$

where u is a scalar field in one time and zero space dimension, $\tau = it$ is the imaginary time, and $V(u,\ \mu)$ is the parameterized DW potential energy. The integral is taken over the period τ_p of the path. In statistical mechanics, this period is related to temperature T through the relation $\tau_p = \hbar/(k_B T)$, where k_B is the Boltzmann constant. Without loss of generalities, we will take $\hbar \equiv 1$.

The decay rate of the system in the semiclassical limit is of the form

$$\Gamma \sim \exp^{-F_{min}/T}, \tag{4}$$

where F_{min} is the minimum of the effective 'free energy'[10] $F \equiv E + TS(E) - E_{min}$. E is the energy of a classical pseudo-particle in the system, while $E_{min} = 0$ corresponds to the bottom of the potential. The minimum of the effective Euclidean action (i.e., S_{min}) is obtained by minimizing (3) along the trajectories $\phi(\tau)$ satisfying the energy integral equation:

$$\left(\frac{du_c}{dt} \right)^2 = 2\left(V(u_c, \mu) - E\right). \tag{5}$$

When $E = 0$, corresponding to $\tau_p = \infty$ and $T = 0$, the particle is at rest at the bottom of one of the two degenerate potential wells. The solution to Equation (5) in this case is a regular vacuum instanton (kink soliton) given by

$$u_c(\tau) \to \frac{1}{\alpha(\mu)} \tanh^{-1} \left[\frac{\mu}{\sqrt{1+\mu^2}} \tanh \frac{\tau}{\sqrt{2} d(\mu)} \right], \tag{6}$$

where $d(\mu) = \mu \left[a_0 \alpha^2(\mu)(1+\mu^2) \right]^{-1/2}$ is the kink width. Imposing periodic boundary conditions, with τ_p the period of motion, leads instead to the following expression for the trajectory $u_c(\tau)$ with energy $E \geq 0$:

$$u_c(\tau) = \frac{1}{\alpha(\mu)} \tanh^{-1} \left[C_1 \cdot sn\left(C_2 \tau, \kappa\right) \right], \tag{7}$$

with $sn(\tau,\ \kappa)$ a Jacobi elliptic function,[54] with the modulus κ of which is given by

$$\kappa = \sqrt{\frac{\left(1 - \sqrt{E/a_0}\right)\left[1 + \mu^2\left(1 + \sqrt{E/a_0}\right)\right]}{\left(1 + \sqrt{E/a_0}\right)\left[1 + \mu^2\left(1 - \sqrt{E/a_0}\right)\right]}}. \tag{8}$$

The two parameters C_1 and C_2 appearing in formula (7) were defined as

$$C_1 = \sqrt{\frac{\mu^2\left(1 - \sqrt{E/a_0}\right)}{1 + \mu^2\left(1 - \sqrt{E/a_0}\right)}}, \tag{9}$$

$$C_2 = \frac{\alpha(\mu)}{\mu} \sqrt{2a_0 \left(1 + \sqrt{\frac{E}{a_0}}\right)\left[1 + \mu^2\left(1 - \sqrt{\frac{E}{a_0}}\right)\right]}. \tag{10}$$

The trajectory (7) possesses real periods for values of its argument equal to $4m\mathcal{K}(\kappa)$, where m is an integer and $\mathcal{K}(\kappa)$ is the quarter period determined by the complete elliptic integral of the first kind.[54] Equation (7) therefore describes a

periodic trajectory which we can refer to as periodon,[55-57] the period of which is ($m = 1$):

$$\tau_p = \frac{4}{C_2}\mathcal{K}(\kappa). \tag{11}$$

The classical action corresponding to the periodon (Equation 7) is obtained as

$$S_p(E) = E\tau_p + W\left(u_c(\tau_p)/2, E\right), \tag{12}$$

where

$$W\left(u_c(\tau_p)/2, E\right) = \frac{2C_2}{(\alpha(\mu)C_1)^2}[(C_1^4 - \kappa^2)\Pi(C_1, \kappa) + \kappa^2\mathcal{K}(\kappa) + C_1^2(\mathcal{K}(\kappa) - \mathcal{E}(\kappa))].$$

$\mathcal{E}(\kappa)$ and $\Pi(C_1, \kappa)$ in the last formula are the complete elliptic integrals of the second and third kinds, respectively.[54] At $E = a_0$, which corresponds to the top of the potential barrier, the solution to Equation (5) is the trivial configuration $u_c(\tau) = 0$. This trajectory is a sphaleron[58] and its action is the thermodynamic action, namely,

$$S_0(\mu) = a_0\tau. \tag{13}$$

For the sphaleron, the escape rate has the Boltzmann signature, characteristic of a pure thermal activation, that is,

$$\Gamma_c \sim \exp\left(-a(\mu)\tau_p\right) = \exp\left(-a(\mu)/k_BT\right). \tag{14}$$

From the above results, we can conclude that a periodon interpolates between the sphaleron $u_c(\tau) = 0$ and the instanton given by Equation (6). Hence, the escape rate in the preriodon sector will be

$$\Gamma \sim \exp\left(-S_{min}(E)\right), \tag{15}$$

where $S_{min}(E) = min\left\{S_0, S_p(E)\right\}$.

To examine the possible occurrence and characteristic features of the transition(s) in quantum tunneling, for the 1D quantum system with the action given by formula (3), it is useful to start with the remark that for periodic problems in classical statistical mechanics, the derivative of the action with respect to the energy is equivalent to the oscillation time τ of the system with this energy. Since the oscillation time τ is proportional to the inverse temperature, with the action corresponding to motion in the periodon sector, we can readily define the period of motion as

$$\tau_p(E) = \frac{1}{k_BT} = \frac{dS_p(E)}{dE}, \frac{dS_0}{d\tau_p} = a(\mu). \tag{16}$$

Taking (16) together with (11) and (12), it is possible to analyze the influence of the shape deformability parameter μ on the temperature dependence of S_{min}, based upon the energy dependence of the period of periodon $\tau_p(E)$. In particular, these equations will help us obtain the critical value of μ at which a first-order transition from quantum to thermal regime can be expected.

Two well-established criteria are known[5,8] which determine conditions for occurrence of transitions in quantum tunnelings, in the general problem of decay of a metastable state.[5,8-10,59] The first criterion states that the transition will be of first order if the period $\tau_p(E)$ decreases to a minimum and next increases again when E increases from the potential bottom to the barrier height. If $\tau_p(E)$ instead decreases monotonically with increasing E, the transition will be of second order. The second criterion states that if at some critical temperature, the first derivative of $S_{min}(T)$ is discontinuous and an abrupt change is observed in the temperature dependence of the action, then the transition from quantum to thermal regime is a first-order transition in temperature. The first criterion is equivalent to solving the equation

$$\frac{d}{dE}\tau_p(E) = 0, \tag{17}$$

TABLE 1 Numerical computation of critical values of E_1

μ^2	Energy E_1 at minimun of $\tau_p(E)$	$E_0 = a_0$ (barrier height)
9	0.1503	0.5
4	0.2278	0.5
2	0.3817	0.5
1.6	0.4691	0.5
1.501	0.4994	0.5

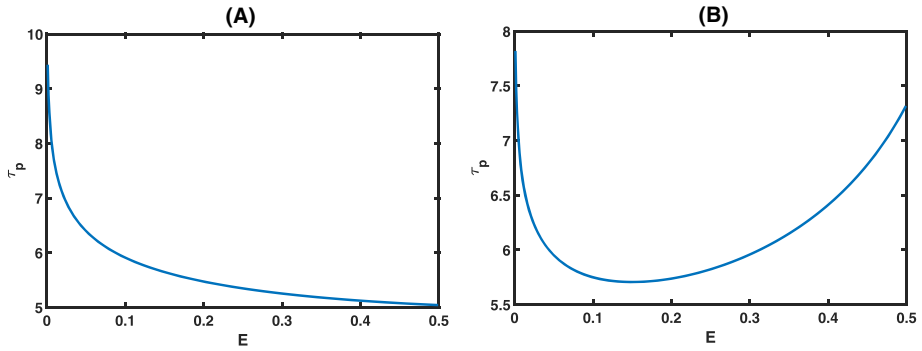

FIGURE 2 (Color online) Variation of the instanton period with the energy E for (a) $\mu = 1$ and (b) $\mu = 3$. Here, $a_0 = 0.5$ [Colour figure can be viewed at wileyonlinelibrary.com]

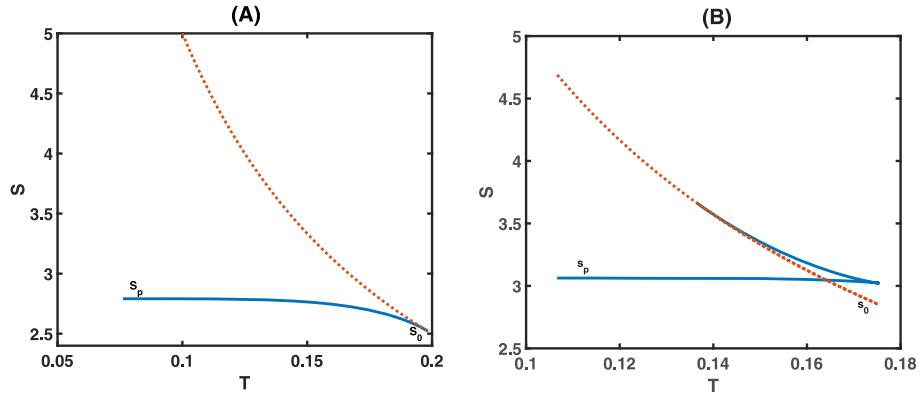

FIGURE 3 (Color online) Plots of the action versus temperature. The dashed line corresponds to the thermodynamic action and the solid line to the periodon action: (a) $\mu = 1$, second-order transition from quantum to thermal regimes. (b) $\mu = 3$, first-order transition from quantum to thermal regimes [Colour figure can be viewed at wileyonlinelibrary.com]

where one seeks for nontrivial solutions with the temperature dependence of $\tau_p(E)$ given by (16). We solved the last equation numerically by setting $a_0 = 1/2$ and evaluated the energy E_1 corresponding to the minimum of $\tau_p(E)$ for some values of μ. Results are shown in Table 1.

The table indicates the quantity E_1 approaching the maximum energy E_0, when μ tends to $\sqrt{3/2}$. Therefore, the critical value of μ for a transition in quantum tunneling would be $\mu_c = \sqrt{3/2}$, and smaller values of μ should correspond to unphysical values of the energy E. Clearly, a first-order quantum–classical transition will occur in the parameterized DW model when the deformability parameter lies in the range $\mu > \sqrt{3/2}$. For values of μ far above the critical threshold μ_c, we should have $E_1 \approx 0$ and $E_1 \to E_0$ as μ decreases to μ_c. So to say, increasing the deformability parameter above, the critical value μ_c should result in a sharper first-order transition in quantum tunneling.[60]

Figure 2 represents the energy dependence of the period τ_p of periodon for two values of the shape deformability parameter μ, selected respectively below and above the critical value μ_c. Figure 2a suggests a monotonic decrease of the periodon period with increasing energy, for $\mu = 1$ lower than μ_c. However, for $\mu = 3$, which is a value greater than μ_c, the period has a re-entrant behavior after decreasing until a critical value of the energy as evidenced in Figure 2b. This re-entrant behavior of the period actually reflects a favorable condition for a first-order transition. The physical behaviors just discussed and emerging from Figure 2 can also be observed in the corresponding plots of the periodon and thermodynamic actions shown in Figure 3, here also for $\mu = 1$ and $\mu = 3$, respectively. When the temperature increases, we observe a smooth change from S_p to S_0 in Figure 3a, characteristic of a second-order transition. In Figure 3b, the change from quantum to classical regime is seen to be abrupt, which is in agreement with the second criterion proposed by Chudnovsky[8] for a first-order phase transition in temperature.

It can be useful to be able to determine analytically the critical value μ_c of μ for a first-order transition; in this respect, we exploit the proposal of Liang et al,[11] who extended the criteria for determining the order of transition in quantum

tunneling, to the dependence of the Euclidean action with the instanton period. Indeed, the authors postulated that when the period $\tau_p(E \rightarrow V_0)$ of the periodon close to the barrier peak is accessible, the condition $\tau_p(E \rightarrow V_0) - \tau_s < 0$ or $\omega^2 - \omega_s^2 > 0$ will be sufficient for a first-order transition. Here, V_0 and τ_s denote respectively the barrier height and period of small oscillations around the sphaleron and ω and ω_s are the corresponding frequencies. In our context, the last criterion translates to

$$V''''(u_{sph}, \mu) - \frac{5\left[V'''(u_{sph}, \mu)\right]^2}{3V''(u_{sph}, \mu)} < 0, \tag{18}$$

where $u_{sph} = 0$ corresponds to position of the sphaleron solution. Since the potential is symmetric, we must have $V'''(0, \mu) = 0$, such that the criterion reduces to $V''''(0, \mu) < 0$. Using the general expression of the potential given by formula (1), the criteria can be expressed more generally as

$$4\left(\frac{3}{\mu^2} - 2\right)\frac{\alpha(\mu)^4 a(\mu)}{\mu^2} < 0, \tag{19}$$

which suggests a critical value of $\mu_c^2 = 3/2$ irrespective of the specific forms of $\alpha(\mu)$ and $a(\mu)$. This is in agreement with the results of Zhou et al,[40] where the phase transition in quantum tunneling was investigated with different forms of $a(\mu)$ and $\alpha(\mu)$ corresponding to the complete hierarchy of Dikandé–Kofané DW potentials.

To close this section, we wish to underline that the parameterized DW potential considered in this study is member of the family of potentials changing slowly near the top and the bottom, which were recently designated to stand for ideal candidates for a first-order transition.[46] When $\mu \rightarrow 0$, the parameterized DW potential reduces to the ϕ^4 model that can account only for second-order transition. As μ increases, the concave shoulders of the barrier become less pronounced and the narrowest part of the barrier enlarges progressively. Therefore, as the shape deformability parameter approaches a critical value μ_c, the barrier top becomes similar to that of a rectangular barrier and the probability of thermally assisted tunneling, just below the top of the barrier, decreases gradually due to the increase of the tunneling distance. In the region $\mu > \mu_c$, this tunneling becomes unfavorable, and a first-order transition occurs as a consequence of a direct competition between the ground state tunneling and thermal activation. The independence of μ_c on the barrier height highlights the critical role of the shape of the top of the potential barrier, in the occurrence and the nature of the transition from quantum to thermal regime.

4 | STATISTICAL MECHANICS AND QUASI-EXACT SOLVABILITY CONDITION

We now turn to the low-temperature statistical mechanics of the parameterized DW potential model given in (1) and (2), paying attention to the canonical partition function using the transfer integral formalism.[14-18] The (dimensionless) Hamiltonian governing the continuum dynamics of the system reads

$$H = \int dx \left[\frac{1}{2}\pi^2 + \frac{1}{2}(\partial_x u)^2 + V(u, \mu)\right], \tag{20}$$

where π is the momentum conjugate to the displacement field u. The solitary wave solution to the equation of motion, that is,

$$\frac{\partial^2 u}{\partial t^2} - \frac{\partial^2 u}{\partial x^2} + V(u, \mu) = 0, \tag{21}$$

derived from the Hamilonian (20), can be shown to express

$$u_c(s, \mu) = \pm\frac{1}{\alpha(\mu)}\tanh^{-1}\left[\frac{\mu}{\sqrt{1+\mu^2}}\tanh\frac{s}{\sqrt{2}d(\mu)}\right], \tag{22}$$
$$s = x - vt,$$

and corresponds to the vacuum instanton already obtained in formula (6). This solution describes a kink (+) or an antikink (−) with a rest mass

$$M_0(\mu) = \frac{\sqrt{2a(\mu)}}{2\alpha(\mu)\mu^2}\left[2\alpha(\mu)(1+\mu^2) - sinh(2\mu)\right]. \tag{23}$$

For the low-temperature statistical mechanics, we apply the transfer integral formalism, and with the Hamiltonian given in Equation (20), we find a Schrödinger-like equation for eigenstates of the transfer integral operator:

$$-\frac{1}{2\beta^2}\frac{\partial^2}{\partial u^2}\psi_j + a(\mu)\left(\frac{\sinh^2(\alpha(\mu)u)}{\mu^2} - 1\right)^2 \psi_j = \epsilon_j \psi_j. \tag{24}$$

In the thermodynamic limit, the lowest eigenstate with energy ϵ_0 brings the most relevant contribution to the partition function. In this context, Z can readily reduce to the classical partition function:

$$Z_c = (2\pi/\beta h)^N \exp\left(-\beta N \epsilon_0\right), \tag{25}$$

where $\beta = (k_B T)^{-1}$ and $N\,(\to \infty)$ is the total number of particles in the system.

Most generally, finding exact values of the partition function Z depends on the solvability of the eigenvalue problem (24). To transform this eigenvalue problem into a form for which the exact solvability is established,[38,61,62] we use the variable change $z = \alpha(\mu)u$ and introduce $\xi = (1+2\mu^2)^{-1}$, $E_j = 4\mu^4\xi^2\epsilon_j/a(\mu)$. With these new variables, the eigenvalue problem (24) becomes

$$\frac{1}{2\beta^2}\frac{\partial^2}{\partial z^2}\psi_j + \frac{a(\mu)}{4\mu^4(\alpha(\mu)\xi)^2}\left[E_j - (\xi\cosh(2z) - 1)^2\right]\psi_j = 0. \tag{26}$$

Remark that by taking $2\beta = 1$ and rescaling the parameter $E_j \to E_j/\eta^2$ with $\eta = \sqrt{a(\mu)}/[2\mu^2\alpha(\mu)\xi] = n+1$, $n = 0, 1, 2, \ldots$, the eigenvalue problem (26) turns exactly to the equation treated in Konwent.[38] In this last work, the author obtained exact expressions of eigenfunctions and energy eigenvalues of the corresponding eigenvalue problem, for some energy levels n. By following a similar idea in our context, this will mean taking one energy level at a fixed temperature which yields the value of μ for which the system is QES. However, what we really want is instead to obtain eigenstates at different temperatures for each value of μ. This is possible by considering a distinct picture in which the temperature is related to the shape deformability parameter through

$$\beta^2 = \frac{2\mu^4(\alpha(\mu)\xi)^2}{a(\mu)}q^2, \tag{27}$$

where q is a positive integer hereafter referred to as 'temperature order'. Substituting (27) into (26), we obtain

$$\frac{\partial^2}{\partial z^2}\psi_j + q^2\left[E_j - (\xi\cosh(2z) - 1)^2\right]\psi_j = 0. \tag{28}$$

Equation (28) describes a QES system similar to the one studied in other studies,[38,61,62] for the energy level $n = 1$. We are interested in solutions which vanish in the limit $z \to \pm\infty$; in this respect, we can readily define

$$\psi(z) = r(z)\exp\left[-z_0\cosh(2z)\right], \tag{29}$$

where the function $r(z)$ is a polynomial expressed as a linear combination of $\cosh m_p z$ or $\sinh m_p z$ and their powers, with z_0 and m_p ($p = 0, 1, 2, \ldots$) being constant quantities to be determined.

The exact expressions for the (unnormalized) ground state wavefunctions, and of the associated energy eigenvalues, are found for the first four values of q and are

$q = 1$:

$$\begin{aligned}\psi_0(u) &= \exp\left[-\frac{\cosh(2\alpha(\mu)u)}{2(1+2\mu^2)}\right],\\ \epsilon_0 &= \frac{a(\mu)}{4\mu^4}\left[1 + (1+2\mu^2)^2\right].\end{aligned} \tag{30}$$

$q = 2$:

$$\begin{aligned}\psi_0(u) &= \cosh(\alpha(\mu)u)\exp\left[-\frac{\cosh(2\alpha(\mu)u)}{1+2\mu^2}\right],\\ \epsilon_0 &= \frac{a(\mu)}{16\mu^4}\left[3(1+2\mu^2)^2 - 8\mu^2\right].\end{aligned} \tag{31}$$

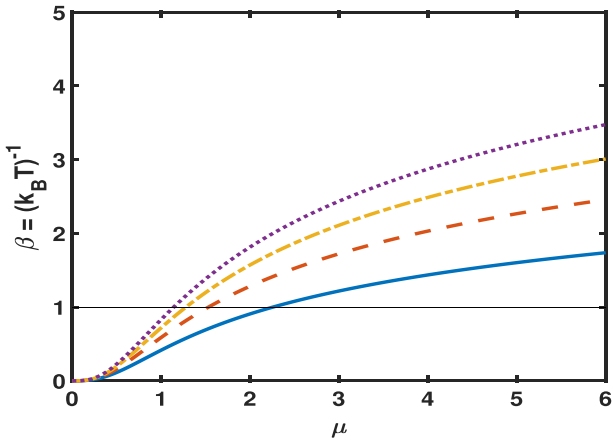

FIGURE 4 (Color online) Variation of the inverse temperature β as a function of the shape deformability parameter μ, for four different values of q according to the quasi-exact solvability condition (27): $q = 1$ (solid line), $q = 2$ (dashed line), $q = 3$ (dash-dotted line), and $q = 4$ (dotted line). The horizontal line stands for the energy barrier taken to be $a_0 = 1$ [Colour figure can be viewed at wileyonlinelibrary.com]

$q = 3$:

$$\begin{aligned}\psi_0(u) &= [\frac{6}{1+2\mu^2} + \left(1 + \sqrt{1 + \frac{36}{(1+2\mu^2)^2}}\right)\cosh(2\alpha(\mu)u)]\exp\left[-\frac{3\cosh(2\alpha(\mu)u)}{2(1+2\mu^2)}\right],\\ \epsilon_0 &= \frac{a(\mu)}{36\mu^4}[9 - 2(1+2\mu^2)\sqrt{(1+2\mu^2)^2+36} + 7(1+2\mu^2)^2].\end{aligned} \tag{32}$$

$q = 4$:

$$\begin{aligned}\psi_0(u) &= 2[\frac{6\cosh(\alpha(\mu)u)}{1+2\mu^2} + \left(2\mu^2 - 1 + \sqrt{12 - 8\mu^2 + (1+2\mu^2)^2}\right)\frac{\cosh(3\alpha(\mu)u)}{1+2\mu^2}]\\ &\quad\times\exp\left[-\frac{2\cosh(2\alpha(\mu)u)}{1+2\mu^2}\right],\\ \epsilon_0 &= \frac{a(\mu)}{16\mu^4}[2 - 4\mu^2 - (1+2\mu^2)\sqrt{(1+2\mu^2)^2 - 8\mu^2 + 12} + \frac{11}{4}(1+2\mu^2)^2].\end{aligned} \tag{33}$$

Eigenfunctions and eigenvalues for some higher energy levels are given in Appendix C1.

The condition for quasi-exact solvability of the system at several temperatures is defined by relation (28). This relation sets the dependence of the temperature (in unit of the Boltzmann constant) on the shape deformability parameter μ and is illustrated in Figure 4. It is particularly remarkable that in the limit $\mu \to 0$, the quasi-exact solvability condition requires $T \to \infty$. This is in excellent agreement with the transfer operator prediction relative to the absence of exact solutions at finite temperatures, for the ϕ^4 model. We can also conclude from Figure 4 that for small values of μ, the four temperatures are far greater than the energy barrier a_0. As μ gradually increases, the temperatures obtained from the largest to the lowest q steadily decrease and go far below the energy barrier. For sufficiently large values of μ, the exact solvability condition thus holds at four temperatures lying below the symmetry-breaking temperature.

The free energy is strongly related to the ground state energy. Influence of μ on the ground state energies and on their relative positions with respect to the energy barrier is illustrated in Figure 5. The ground state energies are infinitely large for $\mu \to 0$ and decrease with an increase of μ irrespective of q. However, combining the influence of μ together with the choice of q affects the position of the energy level with respect to the energy barrier. Taking $q = 1$ for illustration, the ground state energy decreases drastically but will always remain above the energy barrier. This drastic decrease is also observed for higher values of q, but when μ rises beyond a specific value, namely, $\mu_s = \sqrt{3/2}$, $\sqrt{3/4}$ and $\mu_s \simeq 0.717$ for $q = 2$, $q = 3$, and $q = 4$, respectively, the ground state energy drops below the energy barrier and tends to a finite value, that is, $\epsilon_0(\mu \to \infty) = (3/4)a_0$ for $q = 2$, $\epsilon_0(\mu \to \infty) = (5/9)a_0$ for $q = 3$, and $\epsilon_0(\mu \to \infty) = (7/16)a_0$ for $q = 4$. Moreover, for a fixed value of μ, lower energy levels are obtained by increasing the temperature order q.

Having obtained the analytical expressions of the exact ground state wavefunctions and energy eigenvalues at several temperatures for arbitrary values of the deformability parameter μ, quantities such as the probability density, which are relevant in the formulation of correlation functions and correlation lengths at low temperatures, turn out to be easy to obtain. In effect, the probability density associated with the classical field u is nothing but the square of the normalized ground state wavefunction. For this reason, we expect the shape deformability μ to affect the probability density the same way it qualitatively affects the ground state wavefunction. The ground state wavefunctions (unnormalized), for four different temperatures, are plotted in Figure 6 considering different values of the shape deformability parameter μ. To capture the physics lying in the difference in profiles of the probability density which emerges from Figure 6, it is useful to

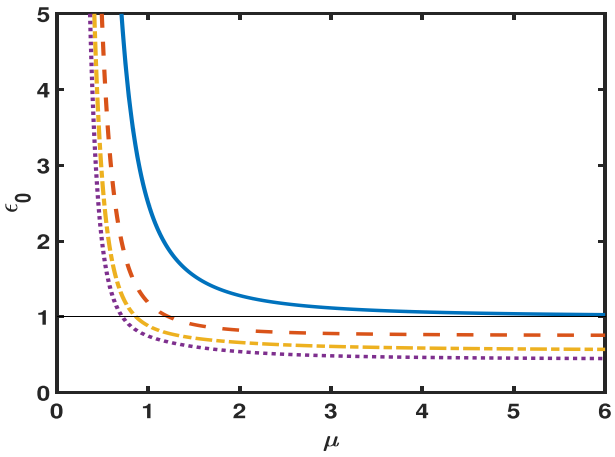

FIGURE 5 (Color online) Variation of the ground state energy ϵ_0 with the shape deformability parameter μ, for four different values of q (corresponding to four different temperatures), namely, $q = 1$ (solid line), $q = 2$ (dashed line), $q = 3$ (dash-dotted line), and $q = 4$ (dotted line). The horizontal line stands for the energy barrier a_0 here fixed as $a_0 = 1$ [Colour figure can be viewed at wileyonlinelibrary.com]

combine features related to the deformability and general properties of probability densities for bistable systems. To this last point, in Figure 5, we have seen that for small values of μ, the ground state energies were higher than the energy barrier a_0 and hence correspond to a high-temperature regime. Thus, in this regime, the Schrödinger pseudo-particles have sufficient energy to cross the energy barrier and move freely from one well to another, behaving as if they were trapped in a single-well potential. The full state space is then covered with power law and the whole space has a finite probability, with a maximum probability density at the barrier peak. As μ increases, the probability density at the four temperatures increases in amplitude and decreases in width, but is still dominated by a single peak. This is actually justified by the fact that an increase of μ enhances the potential confinement by strengthening the steepness of the reflective walls, thus restricting the attainable space to the region covered by just the valleys and the energy barrier. The ground state energy being high, the energy barrier remains the most probable state. For $q = 1$, the ground state energy lies above the energy barrier independently of μ. It turns out that even a lowering of temperature by increase in μ will still yield a probability density with a single peak located at the barrier (top graph in Figure 6). However, for choices of q greater than one, this behavior is observed only for $\mu \leq \mu_S$. When μ increases in the range $\mu > \mu_S$, the ground state energy falls below the energy barrier a_0 and a decrease in temperature below the transition temperature restricts the transitions from one well to the other well. The pseudo-particles are consequently more confined in the potential wells, such that the valleys become more probable. In Figure 6, this is illustrated by the probability density showing two peaks, each located in the neighborhood of the degenerate minima of the parameterized DW potential. To enrich our understanding of the temperature dependence of the probability density for a fixed μ, but at different temperatures, in Figure 7, we represented the ground state probability density for $\mu = 2$ and for three distinct temperatures at which the QES condition holds. We note a continuous shift from a single peak feature to a two-peak feature with decreasing temperature. Remark that the change in the peak width with temperature is different from that of the ϕ^4 model. Instructively, the exact probability densities are superimposed with those obtained from numerical simulations of the following additive-noise Fokker–Planck equation associated to the model:

$$\partial_{tt}^2 u - \partial_{xx}^2 u + \eta \partial_t u + dV(u, \mu)/du = F(x, t), \tag{34}$$

where the Gaussian white noise $F(x,\ t)$ and the viscosity η are related by the fluctuation–dissipation theorem:

$$\langle F(x,t)F(x',t')\rangle = 2\eta\beta^{-1}\delta(x-x')\delta(t-t'). \tag{35}$$

We used standard techniques[63] to solve the discrete version of the above Langevin equation and sampled the results in time to obtain time-averaged probability densities after arbitrary initial conditions had been driven to equilibrium. In the simulations, we employed both Euler and Runge–Kutta schemes, with a lattice size of typically 350 K points taking a lattice spacing of $d = 0.02$ and a time step of $h = 0.001$. As evidenced by Figure 7, the exact (i.e., analytical) probability density and the results from numerical simulations show excellent agreement. This agreement between the analytical and numerical results suggests that the ground state energies can be numerically computed using the corresponding probability densities, at any temperature where QES condition holds for a wide range of values of the shape deformability parameter μ. A relevant implication of this is the possibility to compute exactly thermodynamic quantities such as the enthalpy, the internal energy, and the entropy.

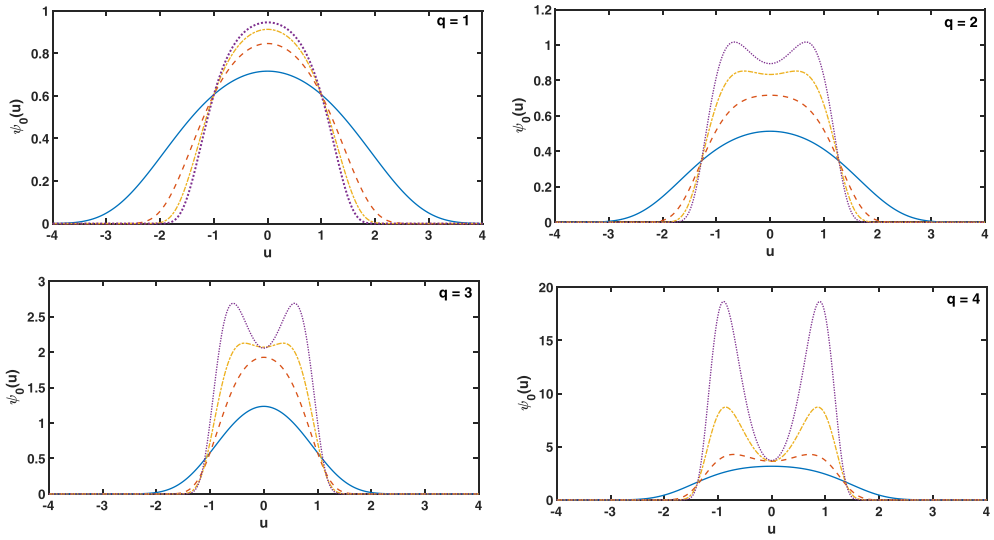

FIGURE 6 (Color online) Ground state wavefunctions in position space at four different temperatures, for $\mu = 0.5$ (solid line), $\mu = 1$ (dashed line), $\mu = 1.5$ (dot-dashed line), and $\mu = 2$ (dashed line) [Colour figure can be viewed at wileyonlinelibrary.com]

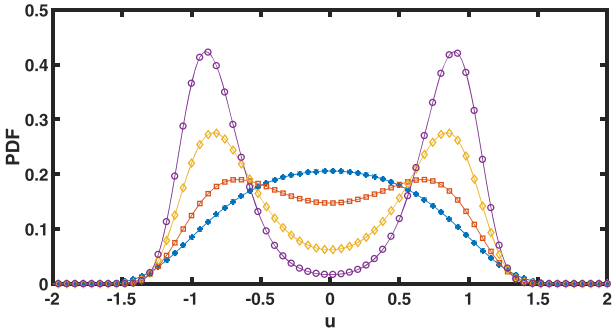

FIGURE 7 (Color online) Comparison of the exact (solid Line) probability density function (PDF) and the results from numerical simulations of he Langevin equation, for $\mu = 2$ and for values of β obtained for $q = 1$ (stars), $q = 2$ (squares), $q = 3$ (diamonds), and $q = 4$ (circles). Note the excellent agreement between exact PDFs and numerical simulations [Colour figure can be viewed at wileyonlinelibrary.com]

5 | CONCLUSION

We have investigated the influence of shape deformability on the occurrence and orders of transitions in quantum tunneling and on the statistical mechanics of a bistable system characterized by a parameterized DW potential. Systems with this feature abound in nature, ranging from biology to soft matters such as lipid membranes,[64] linear polymer chains, molecular crystals, and hydrogen-bonded ferroelectrics and antiferroelectrics. In these systems, chemical processes such as the effects of catalyzers or solvants, isotopic substitutions, or simply the intrinsic structure of molecular chains (e.g., flexible chain backbones and soft interactions) can favor changes in bond lengths and characteristic parameters of the DW energy landscape as for instance the height of the potential barrier, positions of the potential wells, and the steepness of the potential walls. These characteristic parameters are well known to govern symmetry-breaking instabilities in low-dimensional systems.

We have established the existence of a critical value of the shape deformability parameter μ above which a first-order transition in quantum tunneling would occur, besides the second-order transition inherent to the Ginzburg–Landau feature of the DW potential energy. We explored the possibility to study the statistical mechanics of the system via the transfer integral operator method, with emphasis on conditions for quasi-exact solvability of the associated pseudo-particle's Schrödinger equation. We determined the condition and obtained ground state eigenfunctions and the corresponding energy eigenvalues for temperatures determined by the quasi-exact solvability condition. Concerning the dependence of these wavefunctions and energy eigenvalues on the shape deformability parameter, we found that for each value of μ, the quasi-exact solvability of the model allows exact computation of the eigenstates at various temperatures. These temperatures were obtained above and below the transition temperature, depending on values of the shape deformability parameter. The influence of shape deformability on the probability density was also examined. Analytical results showed a striking agreement with large-scale simulations of the Fokker–Planck equation, implying that the study of probability density-based thermodynamics via Langevin simulations is feasible for bistable systems with the parameterized DW potential.

AUTHOR CONTRIBUTIONS

F. Naha Nzoupe carried out the analytical calculations and the numerical simulations; Alain M. Dikandé proposed the topic, assisted in the simulations, and drafted the manuscript; and C. Tchawoua contributed in the analytical calculations and in the write up of the manuscript.

FINANCIAL DISCLOSURE

None reported.

CONFLICT OF INTEREST

The authors declare no potential conflict of interests.

ORCID

Alain Moïse Dikandé https://orcid.org/0000-0002-3910-5163

REFERENCES

1. Andreassen A, Farhi D, Frost W, Schwartz MD. Direct approach to quantum tunneling. *Phys Rev Lett*. 1601;117(23):2016.
2. Kar S. An instanton approach to quantum tunnelling for a particle on a rotating circle. *Phys Lett A*. 1992;168:179-186.
3. Remoissenet M. *Waves Called Solitons: Concept and Experiments*2^{nd}. 2nd ed.: Springer-Verlag; 1999.
4. Eilenberger G. *Solitons: Mathematical Methods for Physicists*, Vol. 19: Springer-Berlin; 1981.
5. Müller-Kirsten HJW, Park DK, Rana JMS. First-order phase transitions in quantum-mechanical tunneling models. *Phys Rev B*. 1999;60:6662-6667.
6. Linde AD. Fate of the false vacuum at finite temperature: theory and applications. *Phys Lett B*. 1981;100:37-40.
7. Affleck I. Quantum-statistical metastability. *Rev Phys Lett*. 1981;46:388-391.
8. Chudnovsky EM. Phase transitions in the problem of the decay of a metastable state. *Phys Rev A*. 1992;46:8011-8014.
9. Garanin DA, Chudnovsky EM. Thermally activated resonant magnetization tunneling in molecular magnets: $mn_{12}ac$ and others. *Phys Rev B*. 1997;56:11102-11118.
10. Chudnovsky EM, Garanin DA. First- and second-order transitions between quantum and classical regimes for the escape rate of a spin system. *Phys Rev Lett*. 1997;79:4469-4472.
11. Liang JQ, Müller-Kirsten HJW, Park DK, Zimmerschied F. Periodic instantons and quantum–classical transitions in spin systems. *Phys Rev Lett*. 1998;81:216-219.
12. Lee SY, Müller-Kirsten HJW, Park DK, Zimmerschied F. Quantum tunneling and phase transitions in spin systems with an applied magnetic field. *Phys Rev B*. 1998;58:5554-5562.
13. Krumhansl JA, Schrieffer JR. Dynamics and statistical mechanics of a one-dimensional model Hamiltonian for structural phase transitions. *Phys Rev B*. 1975;11:3535-3545.
14. Currie JF, Sarker S, Bishop AR, Trullinger SE. Statistical mechanics of one-dimensional complex scalar fields with phase anisotropy. *Phys Rev A*. 1979;20:2213-2224.
15. Currie JF, Krumhansl JA, Bishop AR, Trullinger SE. Statistical mechanics of one-dimensional solitary-wave-bearing scalar fields Exact results and ideal-gas phenomenology. *Phys Rev B*. 1980;22:477-496.
16. DeLeonardis RM, Trullinger SE. Exact kink-gas phenomenology at low temperatures. *Phys Rev B*. 1980;22:4558-4561.
17. Dikandé AM, Kofané TC. Nonlinear dynamics and thermodynamics of two-component scalar field systems at low temperatures. *Physica A*. 1995;215:104-122.
18. Trullinger SE, Deleonardis RM. Statistical mechanics of the double-quadratic chain: exact results and ideal-gas phenomenology for nonreflectionless solitary waves. *Phys Rev A*. 1979;20:2225-2234.
19. Wang Q, Juarez-Perez EJ, Jiang S, et al. Approaching isotropic transfer integrals in crystalline organic semiconductors, 4; 2020.
20. Pâtu OI, Klümper A, Foerster A. Quantum critical behavior and thermodynamics of the repulsive one-dimensional Hubbard model in a magnetic field. *Phys Rev B*. 2020;101:035149.
21. Nava A, Giuliano R, Campagnano G, Giuliano D. Transfer matrix approach to the persistent current in quantum rings: application to hybrid normal-superconducting rings. *Phys Rev B*. 2016;94:205125.
22. Walker JS, Gathright J. Exploring one-dimensional quantum mechanics with transfer matrices. *Amer Jour Phys*. 1994;62:408.
23. Ãlvarez-Estrada RF, Calvo GF, Serrano H. A transfer integral technique for solving a class of linear integral equations: convergence and applications to DNA. *J Comput Appl Math*. 2012;236:3561-3571.
24. Dong JJ, Yang Y. Functional field integral approach to quantum work. *Phys Rev B*. 2019;100:035124.
25. Risken H. *The Fokker–Planck Equation: Methods of Solution and Applications*. 3rd: Springer; 1996.
26. Perring JK, Skyrme THR. A model unified field equation. *Nucl Phys*. 1962;31:550-555.

27. Rubinstein J. Sine-Gordon Equation. *J Math Phys*. 1970;11:258.
28. Landau LD, Lifschitz EM. *Statistical Physics*. Oxford: Pergamon; 1955.
29. Landau LD. *Collected Papers*. Oxford: Pergamon; 1965.
30. Remoissenet M, Peyrard MJ. A new simple model of a kink bearing Hamiltonian. *Phys C Solid State Phys*. 1981;14:L481.
31. Peyrard M, Remoissenet M. Solitonlike excitations in a one-dimensional atomic chain with a nonlinear deformable substrate potential. *Phys Rev B*. 1982;26:2886-2899.
32. Braun OM, Dauxois T, Paliy MV, Peyrard M. Mobility and diffusivity in a generalized Frenkel–Kontorova model. *Phys Rev B*. 1997;54:321-331.
33. Dikandé AM, Kofané TC. Classical–statistical mechanics of kink-bearing deformable systems: continuum study and lattice discreteness corrections. *Solid State Commun*. 1994;89:283-288.
34. Kofané TC, Dikandé AM. Phonons response to nonlinear excitations in a new parametrized double-well one-site potential lattice. *Solid State Commun*. 1993;86:749-754.
35. Dikandé AM, Kofané TC. Exact kink solutions in a new non-linear hyperbolic double-well potential. *J Phys Condens Matter*. 1991;3:L5203.
36. Dikandé AM, Kofané TC. Class of deformable double-well potentials with exact kink solutions. *Solid State Commun*. 1994;89:559-561.
37. Konwent H, Machnikowski P, Magnuszewski P, Radosz A. Mathematical and general. Some properties of double-Morse potentials. *J Phys A*. 1998;31:7541.
38. Konwent H. One-dimensional Schrödinger equation with a new type double-well potential. *Phys Lett A*. 1986;118:467-470.
39. Lawrence MC, Robertson GN. Estimating the proton potential in KDP from infrared and crystallographic data. *Ferroelectrics*. 1981;34:179-186.
40. Zhou JB, Liang JQ, Pu FC. Phase transition in quantum tunneling for a parameterized double-well potential. *Phys Lett A*. 2001;278:243-248.
41. Ushverridze AG. Quasi-exactly solvable Models in Quantum Mechanics (Institute Of Physics Publishing); 1994.
42. Cooper F, Khare A, Sukhatme U. Supersymmetry and quantum mechanics. *Phys Rep*. 1995;251:267-385.
43. Razavy M. An exactly soluble Schrödinger equation with a bistable potential. *Am J Phys*. 1980;48:285.
44. Razavy M. *Quantum Theory of Tunneling*. New Jersey: World Scientific; 2003.
45. Downning CA. On a solution of the Schrödinger equation with a hyperbolic double-well potential. *J Math Phys*. 2101;54(07):2013.
46. Turbiner AV. One-dimensional quasi-exactly solvable Schrödinger equations. *Phys Rep*. 2016;642:1-72.
47. Magazzù L, Valenti D, Spagnolo B, Grifoni M. Dissipative dynamics in a quantum bistable system: crossover from weak to strong damping. *Phys Rev E*. 2015;92:0321231-03212320.
48. Valenti D, Magazzù L, Caldara P, Spagnolo B. Stabilization of quantum metastable states by dissipation. *Phys Rev B*. 2015;91:2354121-2354127.
49. Magazzù L, Hänggi P, Spagnolo B, Valenti D. Quantum resonant activation. *Phys Rev E*. 2017;95:0421041-04210413.
50. Magazzù L, Carollo A, Spagnolo B, Valenti D. Quantum dissipative dynamics of a bistable system in the sub-ohmic to super-ohmic regime. *J Stat Mech-Theory E*. 2015:054016.
51. Spagnolo B, Carollo A, Valenti D. Stabilization by dissipation and stochastic resonant activation in quantum metastable systems. *Eur Phys J Spec Top*. 2018;227:379-420.
52. Basran J, Patel S, Sutcliffe MJ, Scrutton NS. Importance of barrier shape in enzyme-catalyzed reactions. *J Biol Chem*. 2001;276:6234-6242.
53. Heinsalu E, Patriarca M, Marchesoni F. Stochastic resonance in bistable confining potentials. *Eur Phys J B*. 2009;69:19-22.
54. Magnus W, Oberhettinger F, Tricomi FG. *Handbook of Transcendental Functions*. New York: McGraw-Hill; 1953.
55. Magyari E. Kinks and periodons at a $T = 0$ first-order phase transition point in one-dimensional anharmonic lattices. *Z Phys B*. 1981;43:345-351.
56. Marais S, Heine V. The search for periodons. *J Phys Condens Mat*. 1990;2:2547-2557.
57. Riste T. *Nonlinear Phenomena at Phase Transitions and Instabilities*. New York: Plenum; 1981.
58. Liang JQ, Müller-Kirsten HJW. Periodic instantons and quantum-mechanical tunneling at high energy. *Phys Rev D*. 1992;46:4685-4690.
59. Garanin DA, Hidalgo XM, Chudnovsky EM. Quantum-classical transition of the escape rate of a uniaxial spin system in an arbitrarily directed field. *Phys Rev B*. 1998;57:13639-13654.
60. Gorokhov DA, Blatter G. Decay of metastable states: sharp transition from quantum to classical behavior. *Phys Rev B*. 1997;56:3130-3139.
61. Habib S, Khare A, Saxena A. Statistical mechanics of double sinh-Gordon kinks. *Physica D*. 1998;123:341-356.
62. Khare A, Habib S, Saxena A. Exact thermodynamics of the double sinh-Gordon theory in $1 + 1$ dimensions. *Phys Rev Lett*. 1997;79:3797-3800.
63. Griner A, Strittmatter W, Honerkamp J. Numerical integration of stochastic differential equations. *J Stat Phys*. 1988;51:95-108.
64. Bivas I, Tonchev NS. Membrane stretching elasticity and thermal shape fluctuations of nearly spherical lipid vesicles. *Phys Rev E*. 2416;100(02):2019.

How to cite this article: Naha Nzoupe F, Dikandé AM, Tchawoua C. Phase transition in quantum tunneling and exact statistical mechanics for a model of parameterized double-well potential. *Math Meth Appl Sci*. 2020;1-15. https://doi.org/10.1002/mma.6965

APPENDIX A: EXACT SOLUTIONS TO THE EIGENVALUE PROBLEM (EQUATION 28)

1. $q = 1$:

$$\psi_0(\phi) = \exp\left[-\frac{\cosh(2\alpha(\mu)\phi)}{2(1+2\mu^2)}\right], \qquad \epsilon_0 = \frac{a(\mu)}{4\mu^4}\left[1+(1+2\mu^2)^2\right] \tag{A1}$$

2. $q = 2$:

$$\psi_0(\phi) = \cosh(\alpha(\mu)\phi)\exp\left[-\frac{\cosh(2\alpha(\mu)\phi)}{1+2\mu^2}\right], \qquad \epsilon_0 = \frac{a(\mu)}{16\mu^4}\left[3(1+2\mu^2)^2 - 8\mu^2\right]. \tag{A2}$$

$$\psi_1(\phi) = \sinh(\alpha(\mu)\phi)\exp\left[-\frac{\cosh(2\alpha(\mu)\phi)}{1+2\mu^2}\right], \qquad \epsilon_1 = \frac{a(\mu)}{16\mu^4}\left[3(1+2\mu^2)^2 + 8(1+\mu^2)\right], \tag{A3}$$

with $\epsilon_1 - \epsilon_0 = \frac{a(\mu)}{4\mu^4}(1+2\mu^2)$.

3. $q = 3$:

$$\psi_0(\phi) = \left[\frac{6}{1+2\mu^2} + \left(1+\sqrt{1+\frac{36}{(1+2\mu^2)^2}}\right)\cosh(2\alpha(\mu)\phi)\right]\exp\left[-\frac{3\cosh(2\alpha(\mu)\phi)}{2(1+2\mu^2)}\right], \qquad \epsilon_0 = \frac{a(\mu)}{36\mu^4}[9 - 2(1+2\mu^2)\sqrt{(1+2\mu^2)^2+36} + 7(1+2\mu^2)^2]. \tag{A4}$$

$$\psi_1(\phi) = \sinh(2\alpha(\mu)\phi)\exp\left[-\frac{3\cosh(2\alpha(\mu)\phi)}{2(1+2\mu^2)}\right], \qquad \epsilon_1 = \frac{a(\mu)}{36\mu^4}\left[9 + 5(1+2\mu^2)^2\right]. \tag{A5}$$

$$\psi_2(\phi) = \left[\frac{6}{1+2\mu^2} - \left(\sqrt{1+\frac{36}{(1+2\mu^2)^2}} - 1\right)\cosh(2\alpha(\mu)\phi)\right]\exp\left[-\frac{3\cosh(2\alpha(\mu)\phi)}{2(1+2\mu^2)}\right], \qquad \epsilon_2 = \frac{a(\mu)}{36\mu^4}[9 + 2(1+2\mu^2)\sqrt{(1+2\mu^2)^2+36} + 7(1+2\mu^2)^2], \tag{A6}$$

with:

$$\epsilon_1 - \epsilon_0 = \frac{a(\mu)}{18\mu^4}\left[(1+2\mu^2)\sqrt{(1+2\mu^2)^2+36} - 2(1+2\mu^2)^2\right], \tag{A7}$$

and:

$$\epsilon_2 - \epsilon_0 = \frac{a(\mu)}{9\mu^4}\left[(1+2\mu^2)\sqrt{(1+2\mu^2)^2+36}\right]. \tag{A8}$$

4. $q = 4$:

$$\psi_0(\phi) = 2\left[\frac{6\cosh(\alpha(\mu)\phi)}{1+2\mu^2} + \left(2\mu^2 - 1 + \sqrt{12 - 8\mu^2 + (1+2\mu^2)^2}\right)\frac{\cosh(3\alpha(\mu)\phi)}{1+2\mu^2}\right] \times \exp\left[-\frac{2\cosh(2\alpha(\mu)\phi)}{1+2\mu^2}\right], \tag{A9}$$

$$\epsilon_0 = \frac{a(\mu)}{16\mu^4}\left[2 - 4\mu^2 - (1+2\mu^2)\sqrt{(1+2\mu^2)^2 - 8\mu^2 + 12} + \frac{11}{4}(1+2\mu^2)^2\right].$$

$$\psi_1(\phi) = 2\left[\frac{6\sinh(\alpha(\mu)\phi)}{1+2\mu^2} + \left(2\mu^2 + 3 + \sqrt{20 + 8\mu^2 + (1+2\mu^2)^2}\right)\frac{\sinh(3\alpha(\mu)\phi)}{1+2\mu^2}\right] \times \exp\left[-\frac{2\cosh(2\alpha(\mu)\phi)}{1+2\mu^2}\right], \tag{A10}$$

$$\epsilon_1 = \frac{a(\mu)}{16\mu^4}\left[6 + 4\mu^2 - (1+2\mu^2)\sqrt{(1+2\mu^2)^2 + 8\mu^2 + 20} + \frac{11}{4}(1+2\mu^2)^2\right].$$

$$\psi_2(\phi) = 2[\frac{6\cosh(\alpha(\mu)\phi)}{1+2\mu^2} + \left(2\mu^2 - 1 - \sqrt{12 - 8\mu^2 + (1+2\mu^2)^2}\right)\frac{\cosh(3\alpha(\mu)\phi)}{1+2\mu^2}] \times \exp\left[-\frac{2\cosh(2\alpha(\mu)\phi)}{1+2\mu^2}\right], \tag{A11}$$

$$\epsilon_2 = \frac{a(\mu)}{16\mu^4}[2 - 4\mu^2 + (1+2\mu^2)\sqrt{(1+2\mu^2)^2 - 8\mu^2 + 12} + \frac{11}{4}(1+2\mu^2)^2],$$

with:

$$\epsilon_1 - \epsilon_0 = \frac{a(\mu)}{16\mu^4}[4 + 8\mu^2 + (1+2\mu^2)\sqrt{(1+2\mu^2)^2 - 8\mu^2 + 12}] - \frac{a(\mu)}{16\mu^4}\left[(1+2\mu^2)\sqrt{(1+2\mu^2)^2 + 8\mu^2 + 20}\right], \tag{A12}$$

and:

$$\epsilon_2 - \epsilon_0 = \frac{a(\mu)}{8\mu^4}\left[(1+2\mu^2)\sqrt{(1+2\mu^2)^2 - 8\mu^2 + 12}\right]. \tag{A13}$$

Modern Physics Letters A
2150015 (14 pages)

DOI: 10.1142/S0217732321500152

World Scientific
www.worldscientific.com

Kink–antikink scattering-induced breathing bound states and oscillons in a parametrized ϕ^4 model

F. Naha Nzoupe

Laboratory of Mechanics, Department of Physics, Faculty of Science, University of Yaoundé I, P. O. Box 812 Yaoundé, Cameroon

Alain M. Dikandé*

Laboratory of Research on Advanced Materials and Nonlinear Science (LaRAMaNS), Department of Physics, Faculty of Science, University of Buea, P. O. Box 63 Buea, Cameroon
dikande.alain@ubuea.cm

C. Tchawoua

Laboratory of Mechanics, Department of Physics, Faculty of Science, University of Yaoundé I, P. O. Box 812 Yaoundé, Cameroon

Received 27 August 2020
Revised 10 November 2020
Accepted 11 November 2020
Published 18 December 2020

Recent studies have emphasized the important role that a shape deformability of scalar-field models pertaining to the same class with the standard ϕ^4 field, can play in controlling the production of a specific type of breathing bound states so-called oscillons. In the context of cosmology, the built-in mechanism of oscillons suggests that they can affect the standard picture of scalar ultra-light dark matter. In this paper, kink scatterings are investigated in a parametrized model of bistable system admitting the classical ϕ^4 field as an asymptotic limit, with focus on the formation of long-lived low-amplitude almost harmonic oscillations of the scalar field around a vacuum. The parametrized model is characterized by a double-well potential with a shape-deformation parameter that changes only the steepness of the potential walls, and hence the flatness of the hump of the potential barrier, leaving unaffected the two degenerate minima and the barrier height. It is found that the variation of the deformability parameter promotes several additional vibrational modes in the kink-phonon scattering potential, leading to suppression of the two-bounce windows in kink–antikink scatterings and the production of oscillons. Numerical results suggest that the anharmonicity of the potential barrier,

*Corresponding author.

characterized by a flat barrier hump, is the main determinant factor for the production of oscillons in double-well systems.

Keywords: Scalar field; parametrized ϕ^4 model; instantons; kink–antikink collision; oscillons.

PACS Nos.: 03.50.-z, 05.45.Yv, 11.10.St, 03.65.Nk

1. Introduction

The generation and interactions of solitary waves and solitons have attracted a great deal of interest over the past years, due to the fact that they can control many features related to the dynamics of natural systems ranging from biology and organic polymers, to classical and quantized fields in condensed-matter and high-energy physics.[1–6] The simplest localized solutions known in field theory are kink and antikink solitons, they display topological profiles in $(1 + 1)$ spacetime dimensions and can be generated in classical as well as quantum scalar field systems.

In non-integrable scalar field theories such as the ϕ^4 field,[4,7] scatterings of a kink–antikink pair usually give rise to a competition between a bion state and a two-soliton solution characterized by a fractal structure in the parameter space of scattering velocity.[8] For some impact velocities, the kink–antikink collision will give birth to a breather-like bound-state (bion) solution, that radiates progressively until a total annihilation of the pair. For other ranges of velocities, the pair performs an inelastic scattering with the solitons colliding once and separating thereafter. There also exist particular regions in velocity (n-bounce windows), where the scalar field at the center of mass can bounce several times (n times) before the final separation of the pair. The later n-bounce windows have been explained as the consequence of a resonance mechanism for the exchange of energy between the vibrational and translational modes, resulting from discrete eigenstates of the Schrödinger-like equation inherent to the stability analysis of the ϕ^4 kink.[8,9]

The last decade has witnessed a regain of interest in kink scatterings in non-integrable models, marked by intensive studies for instance of multi-kink collisions,[10–15] the interactions of a kink or an anti-kink with a boundary or a defect,[16,17] the scattering processes in models with generalized dynamics,[18] non-polynomial models,[19–22] polynomial models with one[16,23–32] and two[33–37] scalar fields and so on. However, all these studies involve mostly two universal models which are the sine-Gordon model,[1] assumed to describe systems with periodic one-site potentials, and the ϕ^4 model intended for physical systems with double-well (DW) potentials. Although the ϕ^4 kink for example has very recently been linked with topological excitations observed in buckled graphene nanoribbon,[38] real physical systems to which the two universal models address are actually rather quite diverse, and most often unique in some aspects of their physical features. Indeed, the ϕ^4 and sine-Gordon model have fixed extrema while their shape profiles, including their potential barriers, are rigid which confine their applicability to a very narrow class of physical

systems. To lift the shortcomings related to the rigidity of shape profiles, these two universal models have been parametrized leading to two hierarchies of deformable-shape one-site potentials i.e. the Remoissenet–Peyard periodic potential,[39–41] and the family of Dikandé–Kofané (DK) DW potentials.[41–43]

In two recent studies,[22,44] Bazeia *et al.* addressed the issue of the influence of shape deformability of DW potentials, on kink–antikink scatterings with production of oscillon bound states.[14,22,44] Thus they first applied the shape deformability procedure to the standard ϕ^4 by introducing a bistable model with non-polynomial potential, which they called sinh-deformed ϕ^4 potential.[22] Despite this new model showing similar features with the ϕ^4 model a new phenomenon was observed, indeed under certain conditions the kink–antikink pair in the new model was found to convert, after collision, into long-lived low amplitude and almost harmonic oscillations of the scalar field around one vacuum. They interpreted these almost harmonic oscillations as a bound state of individual oscillons.[45] Later on the authors investigated[44] kink–antikink collisions with production of oscillons, considering two members of the family of DK DW potentials.[42,43,46,47] One member was a DW potential with variable separation between the two degenerate minima but with fixed barrier height,[42] and the other member was the DW potential with variable barrier height but fixed positions of the two degenerate minima. The oscillons production in these two members of the family of DK DW potentials were established, and shown to occur when the distance between the minima gets smaller for the first member, and when the barrier height becomes lower for the second member. Based on their results with the two DK DW models, the authors concluded that the lowering of kink energy with increase of the shape deformability parameter was the determinant factor favoring the production of oscillons in the two models.

Stimulated by the studies of Bazeia *et al.*,[22,44] in this paper, we investigate kink–antikink collisions and the possible production of oscillons in a DW model with fixed barrier height and fixed separation between the two degenerate minima, but a variable curvature of the barrier hump. With this we wish to establish that parametrized DW models with increasing kink energy as a function of a deformability parameter, are also quite prone to production of oscillons upon kink–antikink collisions. In fact, we will show that the anharmonicity of the potential at its maximum, characterized by a flat barrier hump with increasing deformability parameter, is more likely to represent the unifying factor favoring the production of oscillons in the DK DW hierarchy. Proceeding with we shall introduce a new member to the family of DK DW potentials,[43] characterized by a parametrization that leaves unaffected the barrier height and positions of the two potential minima, but allows tuning the steepness (or the curvatures) of the potential walls causing the barrier hump to flatten out.

In Sec. 2, we introduce the member of parametrized DK DW potential with variable steepness, and formulate its field-theoretical dynamics. This enables us determine some associate characteristic quantities such as its kink and antikink

solutions and the kink creation energy. In Sec. 3, we examine the kink–antikink scatterings, with emphasis on the production of oscillons as the deformability parameter is varied. Section 4 is devoted to a summary of results and conclusion.

2. The Model, Kink Solution and Kink-Phonon Scattering Spectrum

Consider a field-theoretical model in $(1+1)$-dimensional spacetime, the dynamics of which is described by the Lagrangian:

$$L = \frac{1}{2}\left(\frac{\partial\varphi}{\partial t}\right)^2 - \frac{1}{2}\left(\frac{\partial\varphi}{\partial x}\right)^2 - V(\varphi,\mu), \tag{1}$$

where $\varphi(x,t)$ is a real scalar field in one space (x) and temporal (t) dimensions. $V(\varphi,\mu)$ is a one-body scalar potential which can be expressed more generally:[43]

$$V(\varphi,\mu) = \frac{1}{8}\left(\frac{\sinh^2(\alpha(\mu)\varphi)}{\mu^2} - 1\right)^2, \quad \mu > 0. \tag{2}$$

In the present study, we pick

$$\alpha(\mu) = a\sinh(\mu), \tag{3}$$

which is a function of a real parameter μ assumed to control shape profile of the DW potential. For arbitrary values of the shape deformability parameter μ, the scalar potential $V(\varphi,\mu)$ is a bistable function symmetric around a potential barrier located at the equilibrium state $\varphi = 0$. The potential possesses two degenerate vacuum states at $\varphi = \pm 1$. Thus, unlike the two members of the DK DW potential discussed by Bazeia *et al.* in Ref. 44, the barrier height and minima positions of the parametrized DW potential (2) are always fix. However, on Fig. 1, where $V(\varphi,\mu)$ is sketched for some values of μ, one sees that the variation of μ influences the steepness of the potential walls. Quite interestingly, Fig. 1 suggests that the change in steepness of the potential walls, caused by a variation of the deformability parameter μ, has the consequence of rendering the top of the potential barrier either

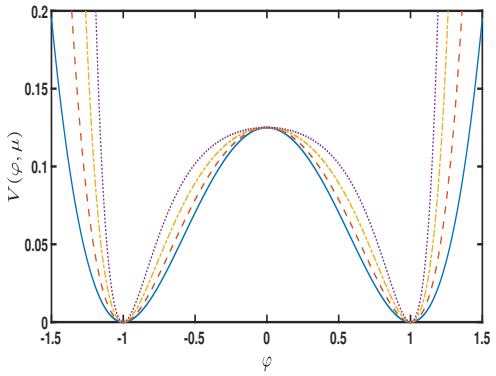

Fig. 1. Plot of the double-well potential $V(\varphi,\mu)$, for some values of μ: $\mu = 0$ (solid line), $\mu = 2.0$ (dashed line), $\mu = 4.0$ (dot-dashed line), $\mu = 8.0$ (dotted line).

flat or sharp. Indeed, when μ tends to zero the parametrized DW potential (2) reduces exactly to the standard ϕ^4 potential:[48,49]

$$V(u) = \frac{1}{8}(u^2 - 1)^2. \tag{4}$$

As μ increases the minima positions and the barrier height remain unchanged, but the slope of the potential walls gets steeper: the narrowest part of the potential barrier broadens while the flatness (i.e. the anharmonicity) of the barrier hump (or top) becomes more pronounced, resulting in an enhancement of the confinement of the two potential wells.

The Lagrangian in formula (1) leads to the following equation of motion for the field φ:

$$\frac{\partial^2\varphi}{\partial t^2} - \frac{\partial^2\varphi}{\partial x^2} + \frac{d}{d\varphi}V(\varphi, \mu) = 0. \tag{5}$$

In the static regime, the solitary-wave solution to this equation is given by

$$\varphi_{K,\bar{K}}(x) = \pm\frac{1}{\alpha(\mu)} \tanh^{-1}\left[\frac{\mu}{\sqrt{1+\mu^2}} \tanh\frac{\sqrt{2}x}{d(\mu)}\right], \tag{6}$$

where

$$d(\mu) = \frac{2\mu}{\alpha(\mu)\sqrt{(1+\mu^2)}}. \tag{7}$$

The solution with "+" sign stands for a kink $\varphi_K(x)$, while the solution with "−" sign stands for an antikink $\varphi_{\bar{K}}(x)$ of width $d(\mu)$. The characteristic energy (or rest mass) associated with the static kink and static antikink solution (Eq. (6)) is obtained by using the general expression:

$$E_K = \int_{-\infty}^{+\infty} \rho_\mu(x)dx, \tag{8}$$

with

$$\rho_\mu(x) = \frac{1}{2}\left(\frac{\partial\varphi}{\partial x}\right)^2 + V(\varphi, \mu) \tag{9}$$

the kink energy density. Substituting the solitary-wave solution obtained in formula (6) this yields:

$$E_K = \frac{1}{4\alpha(\mu)\mu^2}[2\alpha(\mu)(1+\mu^2) - \sinh(2\alpha\mu))]. \tag{10}$$

In Fig. 2, shape profiles of the static kink solution $\varphi_K(x)$ (graph (a)) and of the kink energy density $\rho_\mu(x)$ (graph (b)), are plotted versus the spatial coordinate x for some values of the deformability parameter μ. The bottom figure (graph (c)), represents the variation of the kink rest energy as a function of the deformability parameter μ. One sees that as the deformability parameter μ increases, the asymptotic values of $\varphi_K(x)$ as $|x| \to \infty$ remains the same but a decrease in the kink width

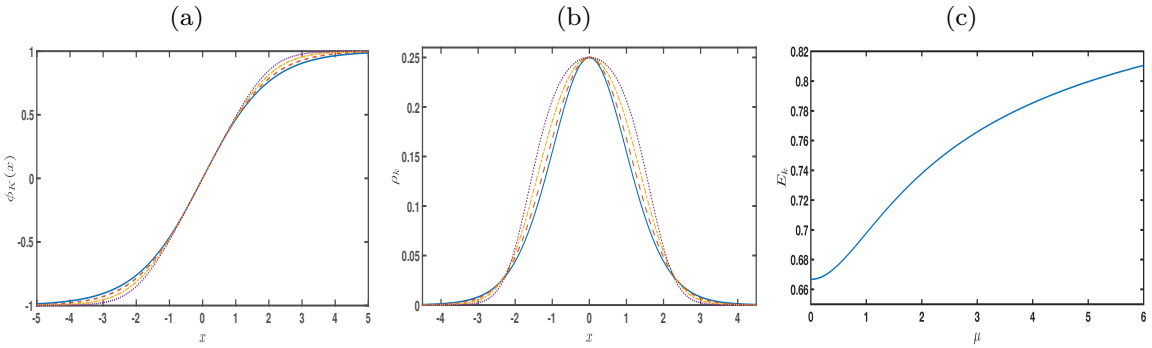

Fig. 2. (a) Shape of the kink $\varphi_K(x)$ and (b) of the energy density $\rho_\mu(x)$ as a function of x, for: $\mu = 0$ (solid line), $\mu = 2.0$ (dashed line), $\mu = 4.0$ (dot-dashed line) and $\mu = 8.0$ (dotted line). (c) Variation of the kink creation energy E_K, as a function of μ.

is noticeable. On the other hand, an increase of μ leaves the maximum of the energy density unaffected but affects the width of the energy density in the region covered by the barrier and the potential wells. Remarkably the energy density seems to decrease with μ as we go far in the region covered by the repulsive walls of the potential, such that in this region the kink is expected to become more localized.

Figure 2(c) depicts the kink rest energy as a monotonically increasing function of the shape deformability parameter. In other words, an increase in μ will enhance the kink stability and hence the sharpness of the kink profile.

Most of the processes from the kink–antikink collisions arise as a consequence of vibrational modes inherent to the kink scattering excitation spectrum. Usually a perturbation theory is utilized to derive the spectrum of localized excitations around a kink.[47,48] To this last point, perturbing linearly the scalar field $\varphi(x,t)$ around the one kink solution $\varphi_K(x)$ i.e. $\varphi(x,t) = \varphi_K(x) + \eta(x)\exp(-i\omega t)$, yields the following Schrödinger-like eigenvalue problem:[47,48]

$$\left[-\frac{\partial^2}{\partial x^2} + V_{\rm sch}(x,\mu)\right]\eta = \omega^2\eta. \tag{11}$$

In this eigenvalue equation, the quantity $V_{\rm sch}(x,\mu) = \frac{d^2V}{d\varphi^2}\big|_{\phi_K}$ is the scattering potential, which in the present case is given by:

$$V_{\rm sch}(x,\mu) = a_0\frac{\left[\mu^2\tanh^4\left(\frac{x}{d(\mu)}\right) + 3\tanh^2\left(\frac{x}{d(\mu)}\right) - c(\mu)\right]}{\left[d(\mu)\left(\mu^2\tanh^2\left(\frac{x}{d(\mu)}\right) - c(\mu)\right)\right]^2}, \quad c(\mu) = 1+\mu^2. \tag{12}$$

Note that this scattering potential determines the kink stability upon scattering with phonons.[47,48] Instructively an identical expression for $V_{\rm sch}(x,\mu)$ is obtained by taking a linear perturbation around an antikink solution.

Distinct profiles of the scattering potential $V_{\rm sch}(x,\mu)$, for different values of the deformability parameter μ, are represented in Fig. 3. One sees that as μ increases, the scattering potential has its width that gradually decreases and its asymptotic

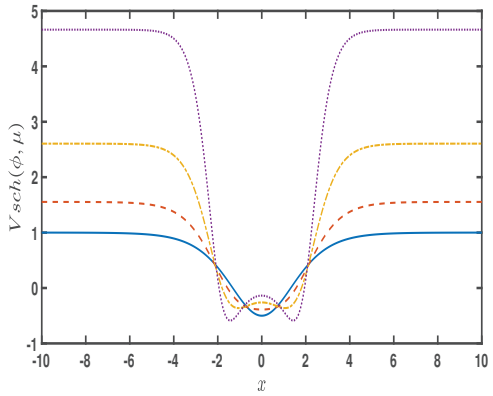

Fig. 3. Plot of the scattering potential $V_{sch}(x,\mu)$ as a function of x, for $\mu = 0$ (solid line), $\mu = 1.0$ (dashed line), $\mu = 2.0$ (dot-dashed line) and $\mu = 3.0$ (dotted line).

limit growing drastically higher. In the range $0 < \mu \lesssim 1.2$ the potential possesses a global minimum located at $x = 0$, which transforms into a local maximum together with the appearance of two degenerate minima in the potential as the value of μ rises larger than 1.2.

The same way as the scattering potential, the occurrence of bound states holds a key importance in grasping some relevant features of the scattering structure of the system.[22,44] In particular a resonance mechanism for the exchange of energy between the translational mode and a vibrational mode, may result in rich consequences in the spectral features of the system.[44] To gain insight onto this last feature, we solved the eigenvalue equation (11) for μ and results emphasizing the influence of the parametrization on the appearance of bound states, are shown in Fig. 4. We note the presence of a zero-mode for all the values of the shape deformability parameter, moreover the appearance of new bound states is observed as μ rises. For instance, as μ lies in the range $0.55 \lesssim \mu \lesssim 1.8$ we notice the presence of two vibrational states, and in the ranges $1.8 \lesssim \mu \lesssim 4.0$ and $\mu \gtrsim 4$ a third and a fourth bound state emerge, respectively. Furthermore, the lower vibrational has its frequency increasing as μ grows to a specific value, then decreasing while the

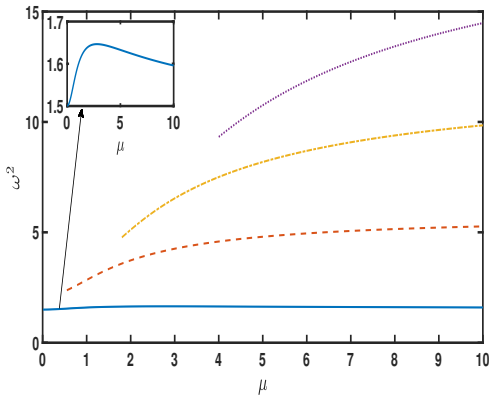

Fig. 4. Plot of the squared frequencies ω^2 of the vibrational states, as a function of μ.

frequencies of higher vibrational states are monotonically increasing functions of the deformability parameter.

3. Analysis of Kink–Antikink Collisions

The dynamical equation pertaining to colliding kink–antikink pairs will be solved numerically in this section, with the aim to explore some characteristic spectral features of kink–antikink scatterings and identify vibrational models associated with the collisions. To this end, Eq. (5) is discretized on a spatial grid with periodic boundary conditions. The grid is divided into N nodes such that zone widths δx in the simulations have fixed size, with the location of the nth point on the grid given by $x_n = n\Delta x$. The scalar field is then defined by $\varphi_n(t) = \varphi(x_n, t)$ for $n = 1, 2, \ldots, N$. The second-order spatial derivative is approximated using a fourth-order central-difference scheme,[50] which leads to a set of N coupled second-order ordinary differential equations in φ_n i.e.:

$$\frac{\partial^2 \varphi_n}{\partial t^2} = \frac{1}{12(\Delta x)^2}(-\varphi_{n-2} + 16\varphi_{n-1} - 30\varphi_n + 16\varphi_{n+1} - \varphi_{n+2}) - \frac{dV(\varphi_n, \mu)}{d\varphi_n}, \tag{13}$$

which is solved numerically using a fourth-order Runge-Kutta scheme with fixed step. The accuracy of our algorithm stands with errors that scale as $(\Delta x)^2$ and $(\Delta t)^4$.

The initial data used in our simulations represent a kink and antikink centered at the points $x = -x_0$ and $x = x_0$ respectively, and moving forward each other with initial velocities v in the laboratory frame. The definition of the starting function can therefore be expressed as

$$\varphi(x, 0) = \varphi_K(x + x_0, v, 0) - \varphi_K(x - x_0, -v, 0) - \varphi_m, \tag{14}$$

where $\varphi_m = \pm 1$ for the kink–antikink and the antikink–kink initial configurations, respectively. We set the grid to be sufficiently large, with left and right boundaries respectively at $x_l = -400$ and $x_r = +400$, and the separation distance to be $2x_0 = 24$. The choice of a large grid together with periodic boundary conditions, was to avoid the reflected kink forms to travel to the boundary, and also to prevent any radiation emitted during the collision process to eventually find itself back to interact with the kinks. The grid is discretized with $N = 10^5$ nodes and all simulations were run with a temporal step size $\Delta t = 0.7(\Delta x)$, found to be a good consensus between the costly computational time and the production of results from high-resolution runs.

Several outputs obtained from numerical simulations at some different initial velocities are now discussed. For weak velocities, the kink and antikink are expected to bound upon collision and have enough time to radiate sufficient energy forming a bion state. This is shown in Figs. 5(a) and 5(e), where we plotted the evolution

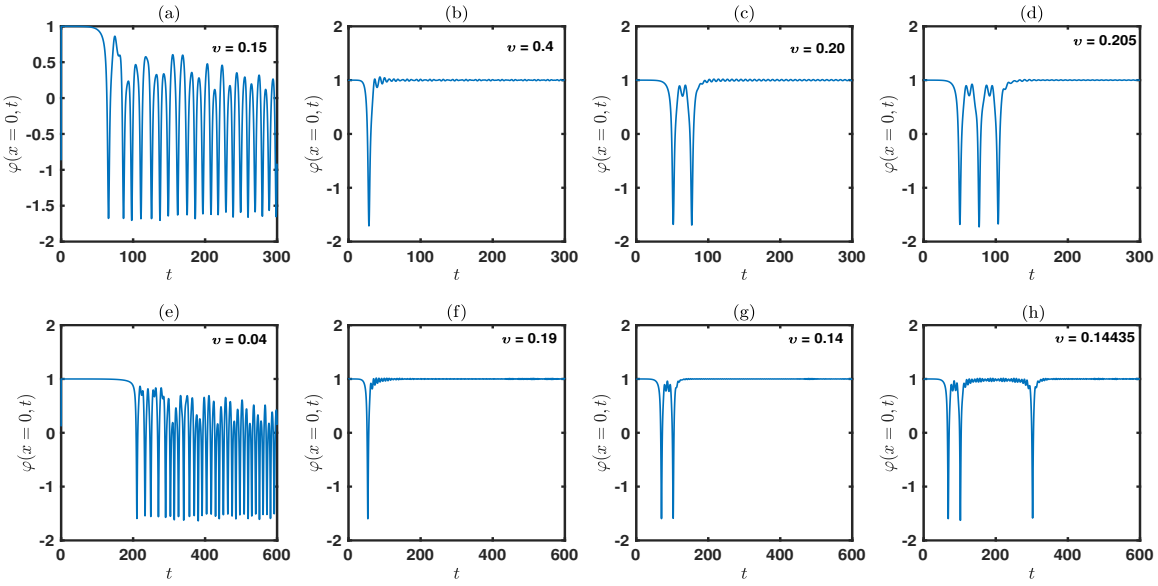

Fig. 5. Possible results for a kink–antikink collision at several initial velocities, considering two values of the shape deformability parameter μ. $\mu = 0$: (a), (b), (c) and (d). $\mu = 0.5$: (e), (f),(g) and (h). Values of μ were chosen such that only one vibrational mode appears in the excitation spectrum.

of the center of mass $\varphi(x = 0, t)$ of the kink–antikink pair, for some values of the shape deformability parameter for which the system has just one vibrational mode. Irrespective of the barrier deformation, the kink–antikink pair moving with an initial velocity lower than a critical velocity v_c settles to an erratically oscillating bion state. But for large velocities $v > v_c$, the kink–antikink pair does not have enough time to radiate sufficient energy to form a bion state. Thus the kink and antikink will once collide and permanently reflect each other during the scattering process. This is represented in Figs. 5(b) and 5(f). For all the considered values of μ one can note the appearance of a spike illustrating the collision, followed by a leveling off at $\varphi = +1$ implying that the kink and antikink have reflected and traveled far from each other. Still, the transition between the bion state and the reflection state is not smooth as the initial velocities increase. There are regions of values of v for which these two states alternate. This regions were reported in several works as "windows".[8,9,24,25,44] For instance, in Figs. 5(c) and 5(g), we note two spikes in the evolution of the center of mass implying that the kink and antikink collide and reflect, then return to collide again before receding to a permanent reflection. Referring to the number of collisions before the last and permanent reflection, the sets of contiguous initial velocities leading to this state can be identified as forming a two-bounce window. The presence of a three-bounce window is evidenced in Figs. 5(d) and 5(h), the velocities lying in the three-bounce windows are found on the edge of the two-bounce regions. When values of the deformability parameter μ are located in the range where there exists only one vibrational mode, the system presents a similar fractal structure as the one observed from the scattering process in the ϕ^4 model. For example we can note the existence of a four-bounce window

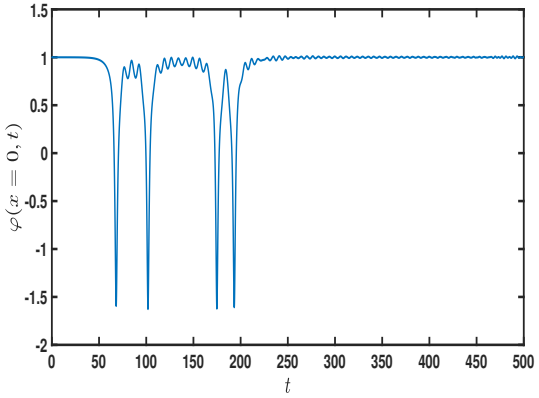

Fig. 6. A four-bounce window taking $\mu = 0.5$ is evidenced by plotting $\varphi(x = 0, t)$ for $v = 0.1445$. Note the presence of four large spikes illustrating collision after which the kink and antikink reflect and recede from each other forming a two-soliton state.

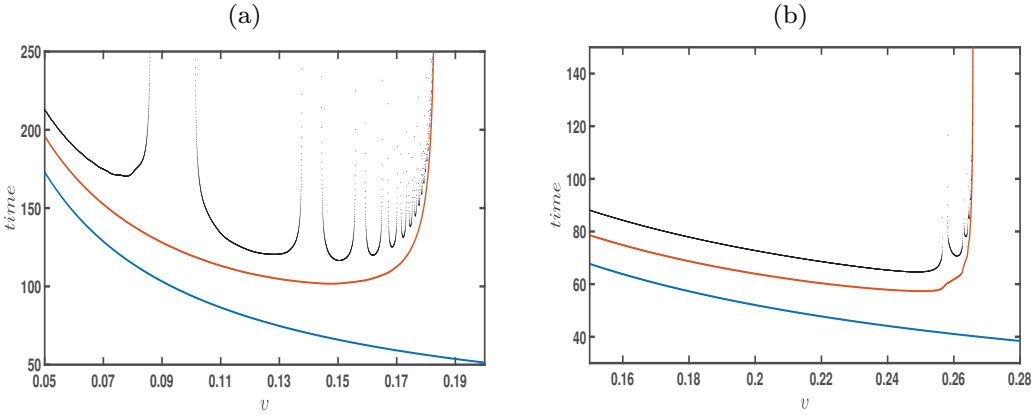

Fig. 7. (Color online) Kink–antikink collision times to first (blue), second (red) and third (dotted-black) bounces, as a function of initial velocity for (a) $\mu = 0.5$ and (b) $\mu = 5.0$.

in Fig. 6. The appearance of n-bounce windows is also expected to be observed for this range of shape deformability parameter values. To further understand the structure of scattering in the system, in Fig. 7, we plotted the time of the three bounces as a function of the initial velocity. The intervals in which the time for the third collisions diverges, range in the two-bounce windows. A case with only one vibrational mode is illustrated in Fig. 7(a), which shows plot of the collision times for $\mu = 0.5$ (compare with Figs. 5(e)–5(h)). We can note that bion states are formed for $v < v_c \sim 0.183$ while for $v > v_c$, the collision results in an inelastic scattering between the pair corresponding to one-bounce around one vacuum. Moreover, the figure captures the complete set of two-bounce windows of which the width continuously decreases and accumulates around v_c. The scattering times in the presence of several vibrational modes are plotted in Fig. 7(b) where we considered the shape of the potential for $\mu = 5$. We first see that v_c grows larger with μ. From our simulations, we observed that the variation of the critical velocities is not a monotonic function of the shape deformability parameter, we first observed

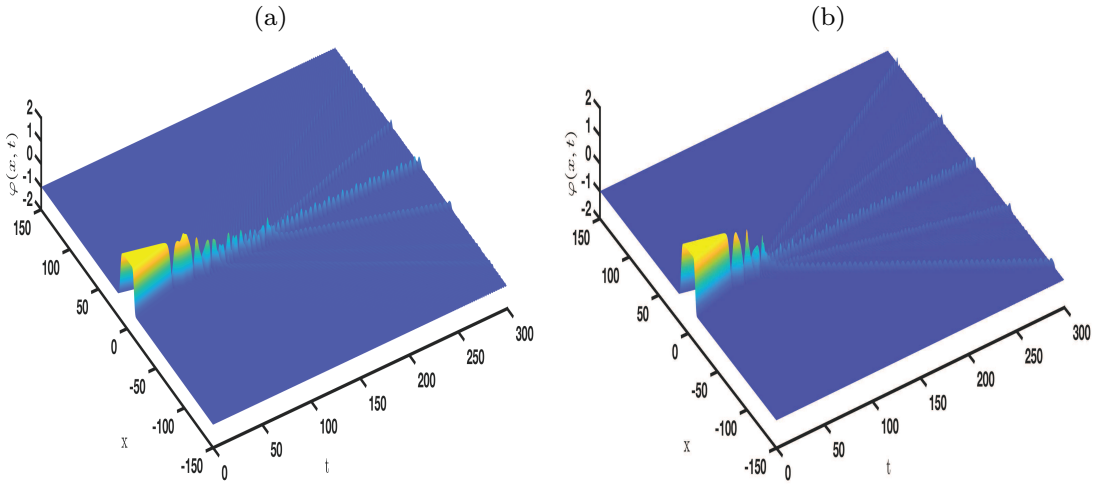

Fig. 8. Oscillons resulting from kink–antikink collisions: (a) $\mu = 3.0$ and $v = 0.23\,(v_c = 0.245)$ showing one bion and two oscillons, (b) $\mu = 5.0$ and $v = 0.236\,(v_c = 0.27)$ showing one bion and four oscillons.

a decrease of v_c as μ increases till $\mu \sim 1$ then recedes to an increasing behavior (this result is not presented here). This reflects that the attraction between the kink and antikink lessens as the system is deformed departing from the ϕ^4 model, but the attractive interaction gets stronger and stronger as $\mu \gtrsim 1$. Suppression of two-bounce windows is also observed in Fig. 7(b). This is justified by the presence of several vibrational modes complicating the energy transfer from the translational mode to just one vibrational mode to achieve resonance conditions.

One of our main point of focus in this paper is the possible production of oscillons. For relatively small values of the deformability parameter μ, for which only one vibrational mode is generated in the excitation spectrum, oscillon structures cannot appear, the kink–antikink collisions with initial velocities lower than the critical velocity can only result in bion and n-bounce states. The ϕ^4 model being an asymptotic limit of the parametrized DW model in this range of values of μ, this agrees with the ϕ^4 model showing no evidence for the formation of oscillons as a result of the scattering process. We see from Fig. 8 that for larger values of μ, the presence of more than one vibrational mode favors the production of oscillons. At some velocities of the colliding kink, lower than the critical velocities, the bion is formed and travels with oscillons which can oscillate around each other, or escape to infinities. We can compare the appearance of one bion and two oscillons traveling together with a large flux of emitted radiation in Fig. 8(a), and the appearance of one bion and four oscillons in Fig. 8(b), traveling with quite no radiation and a larger degree of harmonicity. Note that the larger the shape deformability parameter the greater the number of created oscillons.

4. Conclusion

Oscillons are breather-like bound states generated by self-interactions of kink–antikink pairs that exist in some scalar-field models,[51–55] in the context of cosmology

their built-in mechanism suggests that they can affect the standard picture of scalar ultra-light dark matter. In two recent studies[22,44] the generation of oscillons in bistable systems, characterized by a parametrized double-well potential, was discussed with emphasis on the influence of the shape deformability on the oscillon production. First[22] the authors considered a deformable ϕ^4 potential represented by an hyperbolic double-well potential, and established that the deformability favors the emergence of oscillon modes from kink–antikink collisions and for well selected initial velocities of the colliding kinks. Later on[44] they extended the study to two members of the family of Dikandé–Kofané DW potentials. One of these members has its double-well minima fixed but a variable height of the potential barrier, whereas the other member has fixed barrier height but a variable separation between the two potential minima.

To determine more exactly which of the characteristic features introduced by the potential deformability, i.e. the variable positions of potential minima, or the variable height of the potential barrier, effectively controls the oscillon production, in this paper we revisited the study by considering a parametrized DW potential with fixed potential minima and fixed barrier height fixed. However, the steepness of the potential walls, and hence the flatness of the barrier top, can be tuned by varying a deformability parameter. The parametrized DW potential has the particularity to reduce to a ϕ^4 potential, just the same as with the already known family of DW potentials proposed in Refs. 42, 43, 47 and referred to as Dikandé–Kofané potential. Examining the kink–antikink scattering processes, we found that the parametrized bistable model inherits some of the general features of the ϕ^4 model that is the possibility of formation of bion states, reflected states and also n-bounce windows. However, the appearance of additional modes in the scattering spectrum, as the DW potential deformation becomes predominant in our model, suggests the possibility of suppression of the two-bounce windows due to a kind of interference, as was already detailed in some other works.[25,44] Long-lived, quasi-harmonic and low-amplitude structures called oscillons were shown to form after kink–antikink collisions with some initial velocities less than a critical velocity. This is not observed for low values of μ, where the model has only one vibrational state and is more close to the ϕ^4 model. The rising number of vibrational states as μ increases yields to an intricate situation where the realization of the mechanism of resonant energy exchange between the translational and one vibrational more becomes more difficult. The appearance of oscillons is thus favored by the deformation in our model.

In the works of Bazeia *et al.*, reporting the appearance of oscillons in hyperbolic models[44] for two deformable double-well potentials, they showed that the production of oscillons is boosted by applying the conformational changes from those potentials' deformability such as reducing the distance between the minima keeping the barrier height fixed, or decreasing the barrier height while keeping the minima fixed. They pointed out that the factor unifying the two contexts is the lowering of the kink energy by the deformability in the two models. The scattering

dynamics at the center of mass in our present model are roughly the same as the one in the work of Refs. 22 and44, however the increase of the kink energy in our model disagrees with a tentative idea to extend the consideration of kink energy being a determinant unifying factor to a more general case. The deformation in our model is manifest through an increase of the steepness of the potential walls, with the barrier top becoming flattened hence imposing an anharmonic shape to the potential barrier. This trend can also be observed as an implicit result of the deformation in the two models considered by Bazeia *et al.*,[44] and also in the sinh-deformed ϕ^4 model[22] shown to allow the creation of oscillons. Bistable systems modeled by potentials with anharmonic barrier are thus suggested to be good candidates to observe the formation of oscillons in kink-scattering processes.

Acknowledgment

The work of A. M. Dikandé is supported by the Alexander von Humboldt (AvH) Foundation.

References

1. Eds. A. R. Bishop and T. Schneider, Solitons and condensed matter physics, in *Proc. of the Symposium on Nonlinear* (*Soliton*) *Structure and Dynamics in Condensed Matter*, June 27–29, 1978, Oxford, England.
2. R. Rajaraman, *Solitons and Instantons*: *An Introduction to Solitons and Instantons in Quantum Field Theory* (North-Holland, 1982).
3. A. Vilenkin and E. P. S. Shellard, *Cosmic Strings and Other Topological Defects* (Cambridge Univ. Press, 2000).
4. T. Vachaspati, *Kinks and Domain Walls*: *An Introduction to Classical and Quantum Solitons* (Cambridge Univ. Press, 2006).
5. N. Manton and P. Sutcliffe, *Topological Solitons* (Cambridge Univ. Press, 2004).
6. J. Liu, Z.-K. Guo, R.-G. Cai and G. Shiu, *Phys. Rev. D* **99**, 103506 (2019).
7. Eds. P. G. Kevrekidis and J. Cuevas-Maraver, *A Dynamical Perspective on the ϕ^4 Model*: *Past*, *Present and Future* (Springer, 2019).
8. P. Anninos, S. Olivera and R. A. Matzner, *Phys. Rev. D* **44**, 1147 (1991).
9. D. K. Campbell, J. S. Schonfeld and C. A. Wintage, *Physica D* **9**, 1 (1983).
10. A. M. Marjaneh, V. A. Gani, D. Saadatmand, S. V. Dmitriev and K. Javidan, *JHEP* **07**, 028 (2017).
11. A. M. Marjaneh, A. Askari, D. Saadatmand and S. V. Dmitriev, *Eur. Phys. J. B* **91**, 22 (2018).
12. D. Saadatmand, S. V. Dmitriev and P. G. Kevrekidis, *Phys. Rev. D* **92**, 056005 (2015).
13. A. M. Marjaneh, D. Saadatmand, K. Zhou, S. V. Dmitriev and M. E. Zomorrodian, *Commun. Nonlinear Sci. Numer. Simul.* **49**, 30 (2017).
14. V. A. Gani, A. M. Marjaneh and D. Saadatmand, *Eur. Phys. J. C* **79**, 620 (2019).
15. J. T. Giblin, L. Hui, E. A. Lim and I. S. Yang, *Phys. Rev. D* **82**, 045019 (2010).
16. P. Dorey, A. Halavanau, J. Mercer, T. Romanczukiewicz and Y. Shnir, *JHEP* **1705**, 107 (2017).
17. R. Arthur, P. Dorey and R. Parini, *J. Phys. A* **49**, 165205 (2016).
18. A. R. Gomes, R. Menezes, K. Z. Nobera and F. C. Simas, *Phys. Rev. D* **90**, 065022 (2014).

19. F. C. Simas, A. R. Gomes and K. Z. Nobera, *Phys. Lett. B* **775**, 290 (2017).
20. V. A. Gani, A. M. Marjaneh, A. Askari, E. Belendryasova and D. Saadatmand, *Eur. Phys. J. C* **78**, 345 (2018).
21. D. Bazeia, E. Belendryasova and V. A. Gani, *J. Phys. Conf. Ser.* **934**, 012032 (2017).
22. D. Bazeia, E. Belendryasova and V. A. Gani, *Eur. Phys. J. C* **78**, 340 (2018).
23. F. C. Lima, F. C. Simas, K. Z. Nobrega and A. R. Gomes, *JHEP* **2019**, 147 (2019).
24. P. Dorey and T. Romanczukiewicz, *Phys. Lett. B* **779**, 117 (2018).
25. F. C. Simas, A. R. Gomes, K. Z. Nobera and J. C. R. E. Oliveira, *JHEP* **1609**, 104 (2016).
26. A. Demirkaya, R. Decker, P. G. Kevrekidis, I. C. Christov and A. Saxena, *JHEP* **12**, 071 (2017).
27. V. A. Gani, A. E. Kudryavtsev and M. A. Lizunova, *Phys. Rev. D* **89**, 125009 (2014).
28. H. Weigel, *J. Phys. Conf. Ser.* **482**, 012045 (2014).
29. T. Romanczukiewicz, *Phys. Lett. B* **773**, 295 (2017).
30. E. Belendryasova and V. A. Gani, *J. Phys. Conf. Ser.* **934**, 012059 (2017).
31. V. A. Gani, V. Lensky and M. A. Lizunova, *JHEP* **08**, 147 (2015).
32. E. Belendryasova and V. A. Gani, *Commun. Nonlinear Sci. Numer. Simul.* **67**, 414 (2019).
33. A. Halavanau, T. Romanczukiewicz and Y. Shnir, *Phys. Rev. D* **86**, 085027 (2012).
34. A. Alonso-Izquierdo, *Phys. Rev. D* **97**, 045016 (2018).
35. A. Alonso-Izquierdo, *Physica D* **365**, 12 (2018).
36. V. A. Gani, A. A. Kirillov and S. G. Rubin, *J. Phys. Conf. Ser.* **934**, 012046 (2017).
37. V. A. Gani, A. A. Kirillov and S. G. Rubin, *J. Cosmol. Astropart. Phys.* **04**, 042 (2018).
38. R. D. Yamaletdinov, V. A. Slipko and Y. V. Pershin, *Phys. Rev. B* **96**, 094306 (2017).
39. M. Remoissenet and M. Peyrard, *J. Phys. C* **14**, L481 (1981).
40. M. Remoissenet and M. Peyrard, *Phys. Rev. B* **29**, 3153 (1984).
41. M. Remoissenet, *Waves Called Solitons*: *Concepts and Experiments* (Springer, 1994).
42. A. M. Dikandé and T. C. Kofane, *J. Phys.*: *Condens. Matter* **3**, L5203 (1991).
43. A. M. Dikandé and T. C. Kofané, *Solid State Commun.* **89**, 559 (1994).
44. D. Bazeia, A. R. Gomes, K. Z. Nobrega and F. C. Simas, *Phys. Lett. B* **803**, 135291 (2020).
45. M. Gleiser, *Int. J. Mod. Phys. D* **16**, 219 (2007).
46. A. M. Dikandé and T. C. Kofané, *Solid State Commun.* **89**, 283 (1994).
47. T. C. Kofané and A. M. Dikandé, *Solid State Commun.* **86**, 749 (1993).
48. J. F. Currie, J. A. Krumhansl, A. R. Bishop and S. E. Trullinger, *Phys. Rev. B* **22**, 477 (1980).
49. J. A. Krumhansl and J. R. Schrieffer, *Phys. Rev. B* **11**, 3535 (1975).
50. R. W. Hornbeck, *Numerical Methods* (Prentice-Hall, 1975).
51. G. Fodor, P. Forgàcs, P. Grandclément and I. Ràcz, *Phys. Rev. D* **74**, 124003 (2006).
52. J. Sakstein and M. Trodden, *Phys. Rev. D* **98**, 123512 (2018).
53. G. Fodor, P. Forgàcs, Z. Horvàth and Á. Lukàcs, *Phys. Rev. D* **78**, 025003 (2008).
54. M. Hindmarsh and P. Salmi, *Phys. Rev. D* **77**, 105025 (2008).
55. C. Adam, K. Oles, T. Romanczukiewicz and A. Wereszczynski, *Phys. Rev. D* **101**, 105021 (2020).